Characterization of natural killer cell metabolic and functional responses following cancer surgery

Marlena Scaffidi

Thesis submitted to the University of Ottawa
in partial fulfillment of the requirements for the
Ph.D. in Microbiology and Immunology

Department of Biochemistry, Microbiology, and Immunology
Faculty of Medicine
University of Ottawa

Abstract

Surgery undeniably offers cancer patients the best chance of cure. Despite the benefits of surgical intervention, an unintended consequence of surgical stress is profound natural killer (NK) cell suppression. Due to their anti-tumour activity, NK cell dysfunction is a key driver of postoperative metastasis. NK cell activity is closely regulated by metabolic reprogramming in response to stimulation. Here we show that isolated NK cells display widespread intrinsic impairment across their various modes of effector function. We characterized the metabolism of NK cells on postoperative day 1 (POD1) at the pinnacle of their dysfunctional state. The most significant metabolic deficiency was in their ability to perform oxidative phosphorylation (OxPhos), more specifically their maximal respiration and spare respiratory capacity, two major indicators of their ability to respond to a high energetic demand. Their function could not be rescued through nutrient supplementation nor metabolic modulation for more efficient ATP generation. Of the metabolic interventions tested here, feeder cell-based *ex vivo* expansion was the only approach that partially overcame postoperative suppression, suggesting that comprehensively reprogramming NK cell metabolism before surgery is more effective than attempting to rescue it afterwards. In all, POD1 NK cells demonstrate a profound bioenergetic deficiency, corresponding to an impaired ability to efficiently uptake, metabolize, and channel the corresponding energy produced towards effector function. Given the important role that NK cells play in the anti-tumour immune response, this work addresses a largely unmet need to intervene during this critical window to circumvent postoperative NK cell suppression and ultimately improve outcomes for surgical cancer patients.

Acknowledgements

First, I would like to thank my supervisor Dr. Rebecca Auer for giving me the privilege of training in her lab. Thank you as well to Dr. Rafeah Alam for her support throughout this project. I would also like to thank my thesis advisory committee members Dr. Mary-Ellen Harper, Dr. Michele Ardolino, and Dr. Tommy Alain for their guidance and mentorship.

A very special thank you goes out to all the cancer patients who provided their blood samples at an incredibly difficult time in their lives, as well as the nurses and clerks who facilitated blood draws. Without them, this work would not have been possible.

I had the pleasure of working alongside some incredible people in the South Wing and making some wonderful friends along the way. Thank you to Henna, Riana, Sophie, Taylor, Agrima, Reagan, Ola, Chris, Priyoshi, Rafeah, Edita and Val for your friendship and support. A special thank you goes to Henna for being by my side since day one. I couldn't have done this without her. Henna - you're an amazing scientist, and I'm so excited to see where you are headed next. Outside of the lab, thank you to Lisa, Emma, Racheal, and Anne-Marie for being the best friends I could ask for.

I would like to thank my fiancé John for his patience, love, and support throughout this process. John – doing this degree brought me to you, and I am so grateful that we found each other. Thank you for always believing in me and pushing me to just keep moving forward. I love you and cannot wait to marry you this year.

Most of all, I would like to thank my parents, Fred and Rosalia. Mom and Dad - I would not have been able to complete my PhD without your love and support. You've always helped with anything I needed, at any time of the day (or night). Thank you for always believing in me and giving me a solid foundation to stand on. This degree is yours as much as it is mine.

Dedication

This thesis is dedicated to my grandparents, whom I love and miss dearly

Table of Contents

List of Abbreviations

Acetyl-CoA: acetyl coenzyme A
ACTH: adrenocorticotropic hormone
ADCC: antibody-dependent cell-mediated cytotoxicity
αMEM: alpha Minimum Essential Medium
APC: antigen presenting cell
ARG1: arginase-1
ATP: adenosine triphosphate
BL: baseline
BSA: bovine serum albumin
CD: cluster of differentiation
CFSE: carboxyfluorescein succinimidyl ester
CIML: cytokine-induced memory-like
CIS: cytokine-inducible SH2-containing protein
COX2: cyclooxygenase 2
CP450: cell proliferation dye eFluor 450
CTC: circulating tumour cell
DAMP: damage-associated molecular pattern
DAP10: DNAX-activating protein
DCA: sodium dichloroacetate
2-DG: 2-deoxyglucose
2-DG6P: 2-deoxyglucose-6-phosphate
DISC: death-inducing signaling complex
DMEM: Dulbecco's Modified Eagle Medium
DMSO: dimethyl sulfoxide
DRP1: dynamin-related protein 1
4EBP1: eukaryotic translation initiation factor 4E-binding protein 1
ECAR: extracellular acidification rate
EDTA: ethylenediaminetetraacetic acid
EGFR: epidermal growth factor receptor
ETC: electron transport chain
exNK cell: *ex vivo* expanded natural killer cell
FACS: fluorescence-activated cell sorting
FasL: fas ligand
FBS: fetal bovine serum
FCCP: carbonyl cyanide-4 (trifluoromethoxy) phenylhydrazone
FcγR: Fc gamma receptor
G6P: glucose-6-phosphate
GLUT1: glucose transporter 1
GSEA: gene set enrichment analysis
HD: healthy donor
HEPES: 4-(2-hydroxyethyl)-1-piperazineethanesulfonic acid
HER2: human epidermal growth factor receptor 2
HIF1α: hypoxia inducible factor 1-alpha
HLA: human leukocyte antigen

HMGB1: high mobility group box 1
HPA axis: hypothalamic-pituitary-adrenal
IFN-γ: interferon gamma
IL: interleukin
ip: intraperitoneal
iPSC: induced pluripotent stem cell
ITAM: immunoreceptor tyrosine-based activation motif
ITIM: immunoreceptor tyrosine-based inhibition motif
iNOS: inducible nitric oxide synthase
JAK: Janus kinase
KIR: killer cell Ig-like receptor
LFA-1: lymphocyte function-associated antigen
Mdivi-1: mitochondrial division inhibitor 1
MDSC: myeloid-derived suppressor cell
MHC: major histocompatibility complex
MICA/B: MHC class I chain related proteins A and B
mitoROS: mitochondrial reactive oxygen species
MMP: mitochondrial membrane potential
MRAS: metabolic reaction activity scores
MTOC: microtubule organizing centre
mTORC1: mechanistic target of rapamycin complex I
NADH: Nicotinamide adenine dinucleotide (reduced)
NADPH: nicotinamide adenine dinucleotide phosphate
NCR: natural cytotoxicity receptor
NCG: NOD-Prkdc^{em26Cd52}Il2rg^{em26Cd22}/NjuCrl
NK: natural killer
NKG2D: natural killer group 2, member D
NO: nitric oxide
OCR: Oxygen consumption rate
OHRI: Ottawa Hospital Research Institute
OPA-1: optic atrophy 1
OPP: O-propargylpuromycin
OxPhos: oxidative phosphorylation
PBMC: peripheral blood mononuclear cell
PBS: phosphate-buffered saline
PDH: pyruvate dehydrogenase
PDK: pyruvate dehydrogenase kinase
PFA: paraformaldehyde
PGC1α: PPARγ coactivator 1α
PGE2: prostaglandin E2
PI3K: phosphoinositide 3-kinase
PMN: polymorphonuclear
POD: postoperative day
PRR: pattern recognition receptor
PPARγ: peroxisome activator receptor gamma
P/S: penicillin/streptomycin

RBC: red blood cell
ROI: region of interest
ROS: reactive oxygen species
RPMI: Roswell Park Memorial Institute
RT: room temperature
SCENITH: Single cell energetic metabolism by profiling translation inhibition
SEM: standard error of the mean
SLC: solute carrier
SOCS: suppressor of cytokine signaling
SRC: spare respiratory capacity
STAT: signal transducer and activator of transcription
sxMDSC: surgery-induced myeloid-derived suppressor cell
TAA: tumour-associated antigen
TCA: tricarboxylic acid
TCE: tumour cell emboli
THPTA: tris-hydroxypropyltriazolylmethylamine
TME: tumour microenvironment
TMRM: tetramethylrhodamine
TNFα: tumour necrosis factor alpha
TGF-β: Transforming growth factor beta
TRAIL: tumour necrosis factor-related apoptosis-inducing ligand
ULBP: unique long 16-binding protein
VEGF: vascular endothelial growth factor

Significant Contributions

All NK cell cytotoxicity assays presented in Figure 3.8 were performed together with Henna Mistry and are included in a manuscript accepted in Cancer Immunology, Immunotherapy.

Dr. Mary-Ellen Harper from the University of Ottawa Faculty of Medicine provided use of the Seahorse XFe96 extracellular flux analyzer and corresponding reagents/materials. Dr. Claire-Fong McMaster and Dr. Mary-Ellen Harper assisted with troubleshooting and data interpretation.

Dr. Shama Naz and Dassine Azouaoui from the University of Ottawa Metabolomics core facility performed LC-MS on aqueous extracts from NK cells and downstream analysis of the raw data. Dr. Naz also assisted with the methods description for the metabolomics portion of this thesis.

Dr. Miroslava Cuperlovic-Culf from the National Research Council Canada assisted with analysis and interpretation of the metabolomics dataset and generated Figures 4.12C and 4.14.

Dr. Sarah Nersesian (OHRI) performed the METAFlux analysis. The corresponding data is presented in Figures 4.11 and 4.13.

Dr. Morgan Fullerton and Tyler Smith (University of Ottawa) assisted with SCENITH data interpretation. Dr. Sarah Nersesian also provided guidance for SCENITH.

Christiano Tanese de Souza performed all murine surgeries and injections for the *in vivo* experiments shown in Figures 5.8 - 5.10. IVIS imaging, peritoneal washes and associated data analysis were a joint effort with Henna Mistry and Christiano Tanese de Souza.

Henna Mistry designed and optimized the whole blood co-culture used in Chapter 5 to evaluate the function of *ex vivo* expanded NK cells under surgical stress.

List of Figures

Main Text:

Supplemental:

List of Tables

Main Text:

Supplemental:

Chapter 1: Introduction

1.1 Surgical stress and metastasis

1.1.1 The unintended consequence of cancer resection surgery

Surgical resection is part of the treatment plan for many cancer patients diagnosed with a solid tumour and offers patients the best chance of cure[1–8]. Despite the necessity of surgical intervention, the stress that surgery places on the body creates an opportune environment for residual tumour growth and metastasis to take place[8–11]. This was famously reported by Halsted in the early 1900s who found that breast cancer patients who underwent surgical resection of their tumour did not survive as long as those who did not receive surgery[12]. Demicheli et al conducted a retrospective study of breast cancer patients and found increased mortality in patients who underwent mastectomy as a primary treatment compared to those who went untreated, though the authors admit that it is difficult to obtain more recent data from untreated patients[13]. This phenomenon has also been reported in colorectal cancer in which surgery is the preferred method of treatment. In this context, it has been shown to accelerate growth of existing metastases or trigger the establishment and growth of micro metastases present at distant sites in the body but not yet visible at the time of surgery[14]. As such, the perioperative period is described as a largely understudied therapeutic window of opportunity to target the mechanisms driving surgery-induced metastasis[14]. This topic has been thoroughly reviewed and there are several proposed reasons for its occurrence, all of which highlight an array of physiological changes that take place as a result of surgical stress[14–18].

1.1.2 The physiological effects of surgery on the body

Circulating tumour cells (CTCs) can become released and disseminate during surgical resection of the primary tumour[19]. These CTCs should theoretically be very inefficient at establishing metastatic foci, however the surgically-stressed environment is optimal for metastasis to take place[20]. In addition to the release of CTCs upon resection of the primary tumour, patients can have existing, clinically undetectable micro metastases present within the body at distant sites from the primary tumour before surgery[21,22]. These micro metastases remain dormant largely due to the secretion of antiangiogenetic factors by the primary tumour, such as angiostatin[21]. Upon surgical resection, the concomitant resistance imparted by the primary tumour is lifted, creating the right conditions for outgrowth of these micro metastases[23].

There are many ways in which surgery promotes the development of a protumourigenic environment, both locally and systemically[24]. First, the surgical insult induces a hypercoagulable state in which pro-inflammatory cytokines increase the production of fibrinogen[25]. Anticoagulant drugs such as warfarin and heparin have antimetastatic effects which have been shown to be largely driven by natural killer (NK) cell activity[26]. Despite their importance in wound healing, platelets can contribute to postoperative metastasis[27]. Platelets and fibrin can form aggregates around tumour cell emboli (TCE), thereby blocking anti-tumour immune mechanisms[8,27]. Their activity can also promote adhesion to endothelial cells and angiogenesis[27]. Prevention of platelet activation has been shown to decrease CTCs in colorectal cancer patients[28]. Platelets also secrete transforming growth factor beta (TGF-β) upon activation, which is a pleiotropic cytokine that signals canonically through serine/threonine kinases and Smad proteins[29–33]. It has a

range of different effects on the body including apoptosis, wound healing, angiogenesis, and prevention of autoimmunity[29,34]. TGF-β has been previously recognized as a potent inhibitor of cell-mediated immunity, particularly by affecting NK cell activating receptor expression[30] and function[35], resulting in the inhibition of their proliferation, cytotoxicity and cytokine production[35–37].

Activation of the sympathetic nervous system is another hallmark systemic response to surgical stress[38]. The release of catecholamines, such as adrenaline, has been associated with metastasis and advanced disease[39]. This leads to activation of β-adrenoceptors which can have direct effects on tumour cells and induce tissue remodeling that promotes tumour progression[40]. Some of these changes include increasing tumour cell invasiveness[41] and affecting the immune system[42]. Activation of the sympathetic nervous system is accompanied by the production of vascular endothelial growth factor (VEGF), interleukin 6 (IL-6) and other pro-inflammatory cytokines which can promote remodeling of vasculature/angiogenesis and tumour cell infiltration[43,44]. Surgical stress is also characterized by neuroendocrine activation, specifically activation of the hypothalamic-pituitary-adrenal (HPA) axis which regulates the level of circulating glucocorticoids, such as cortisol[45]. Under steady-state conditions, levels of glucocorticoids are tightly controlled by the HPA axis and are important for maintaining homeostasis in response to both cognitive[46] and physical stress[47]. In short, the hypothalamus releases corticotropin-releasing hormone, which then stimulates the release of adrenocorticotropic hormone (ACTH) from the pituitary gland[48]. ACTH stimulates the production and release of cortisol from the adrenal cortex[48]. Circulating levels of cortisol provide negative feedback on this pathway[48]. During acute trauma or major surgery, plasma cortisol levels increase[47,49] and remain persistently elevated for days

postoperatively[50]. The degree of the cortisol spike is higher in invasive open surgeries compared to minor surgeries[47]. It is believed that the initial increase in cortisol is mediated by activation of the HPA axis, which largely occurs due to pro-inflammatory cytokine production, while the maintenance of elevated plasma cortisol may occur through alternative mechanisms likely driven by the effect of inflammatory mediators directly on the adrenal glands[51]. The presence of cortisol has been shown to contribute to compensatory suppression of inflammation following high circulating IL-6 levels induced by surgical stress[49]. Both glucocorticoids and catecholamines have been shown to exert suppressive effects on the immune system *in vitro*, particularly in NK cells, however it has been shown that catecholamines may be more central to the suppressive effects of sympathetic nervous system activation on NK cell function[42].

1.1.3 Sterile inflammation and the "ebb and flow" of surgical stress

Surgical tissue trauma releases danger signals known as damage-associated molecular patterns (DAMPs), leading to sterile inflammation, which is a process characterized by activation of immune cells in the absence of infectious agents[52]. Some examples of DAMPs include mitochondrial DNA, high mobility group box 1 (HMGB1) protein, heat-shock proteins, and adenosine triphosphate (ATP)[53]. DAMPs are recognized by receptors on innate immune cells called pattern recognition receptors (PRRs)[54]. Neutrophils are the first responders to the site of tissue damage, followed by monocytes, macrophages, and innate lymphoid cells[54,55]. Activation of the innate immune system leads to the secretion of pro-inflammatory cytokines such as tumour necrosis factor alpha (TNFα) and IL-6[56], whose serum levels peak between 4 and 24 hours after surgery[57]. Additional factors secreted by

immune cells include VEGF and matrix metalloproteinase 9, which can promote tumour progression[58]. IL-6 is a pleiotropic cytokine which has both pro[56,59] and anti-inflammatory activity[60]. Another inflammatory mediator produced in response to surgical stress is prostaglandin E2 (PGE2) generated by the enzyme cyclooxygenase 2 (COX2)[61]. IL-6 has been shown to induce PGE2 production. It can promote tumour growth both directly, and indirectly through having immunosuppressive effects[61]. PGE2 has been shown to increase the T_{reg} population while decreasing the CD8+ effector T cell population[62]. It can also negatively affect the *in vitro* cytotoxicity of human NK cells in response to co-culture with K562 targets as well as the production of interferon gamma (IFN-γ) following IL-15 stimulation[63]. This initial burst of inflammation is followed by a compensatory release of anti-inflammatory mediators such as IL-10[64] and TGFβ[65]. This is largely triggered by a process called emergency myelopoiesis, which is a rapid burst of myeloid cell production in the bone marrow following surgical stress[66], releasing a heterogeneous, immature population of myeloid cells that are recruited to the site of tissue damage[67]. These myeloid cells, collectively referred to as surgery-induced myeloid-derived suppressor cells (sxMDSCs), expand in both mice and humans following acute periods of inflammation, including bacterial infection, trauma, and surgery[68–72] and exert suppressive effects on immune cells through a variety of different mechanisms[5]. Tai et al. showed a roughly 2.5-fold increase in the proportion of MDSCs in the spleens of mice subjected to surgical stress compared to naïve mice that did not receive surgery[73]. In humans, these heterogenous, immature myeloid cells are identified as $CD33^+$ or $CD11b^+$ and lineage negative ($CD3^-CD19^-CD56^-$) and are characterized by their ability to suppress T and NK cell effector functions[68,74]. MDSCs can be divided into three main subtypes based on their surface expression of specific phenotypic

markers. $CD14^{+}CD15^{-}$ cells are monocytic, $CD14^{-}CD15^{+}$ are polymorphonuclear (PMN) and $CD14^{-}CD15^{-}HLA\text{-}DR^{-}$ are early/immature MDSCs[75,76]. We have found that in mice, PMN-MDSCs are the dominant subtype which expand after surgery and induce suppression of effector immune cells[4], while monocytic (M-MDSCs) prevail in human colorectal cancer surgery patients[2]. There have been many studies, including our own, analyzing the various ways in which MDSCs affect cell-mediated immunity. These studies have pointed towards several mechanisms including arginine depletion through high expression of arginase-1 (ARG1) and inducible nitric oxide synthase (iNOS), overproduction of nitric oxide (NO) and reactive oxygen species (ROS)[68,77].

The pro and subsequent anti-inflammatory events induced by surgical stress are accompanied by a metabolic "ebb and flow"[78]. Following acute trauma, the local and systemic inflammatory response triggers a hypermetabolic state which is accompanied by increased catabolism that can last for days to weeks[79]. This is thought to be driven by the stress hormones cortisol, glucagon and adrenaline, and the pro-inflammatory cytokines IL-6 and TNFα[80]. As such, the inflammatory and the metabolic ebb and flow of surgical stress are intertwined[81]. These stress-induced mediators result in increased catabolism within the body, and this in combination with insulin resistance results in a period of hyperglycemia and elevated circulating fatty acids and amino acids[80]. Despite the increased nutrient demand and apparent surplus of available glucose, the body is unable to utilize these nutrients during this time. As such, one of the hallmarks of this hypermetabolic state is the loss of muscle mass which can have a significant impact on recovery and rehabilitation[79].

In all, surgery results in an acute pro-inflammatory phase followed by a prolonged compensatory anti-inflammatory phase[9]. This creates a strongly immunosuppressive state

that significantly impacts cell-mediated immunity[65]. The impairment of cell-mediated immunity creates an opportunity for residual disease to spread and form distant metastatic foci elsewhere in the body. The severity and duration of this immunosuppression is directly proportional to the duration and invasiveness of surgery[9]. Though this period of immunosuppression is transient, its impact can have lasting consequences that may not be apparent until years later, highlighting the need to intervene during this uniquely vulnerable time.

1.2 Natural killer cells are dysfunctional postoperatively

1.2.1 NK cells as key players in cell-mediated immunity

NK cells, which originate from the common lymphoid progenitor, are cytotoxic lymphocytes of the innate immune system[1]. They make up 5-15% of peripheral blood mononuclear cells (PBMCs)[82]. NK cells are poised to kill their targets immediately upon encounter through pre-formed cytolytic granules containing perforin and granzymes which induce apoptosis in the target cell[83]. In humans, NK cells are characterized by their expression of the cell surface marker CD56 and the medium-low affinity Fc gamma receptor (FcγRIII; CD16)[84]. $CD56^{bright}CD16^{-}$ cells make up approximately 10% of peripheral blood NK cells and are predominantly cytokine-producing, while $CD56^{dim}CD16^{+}$ NK cells make up about 90% and are predominantly cytotoxic[84,85]. NK cells are known for their role in monitoring the health of autologous cells[86] through binding of a limited number of germline-encoded receptors[87]. Stressed cells, such as those that are virally infected or cancerous, will express stress-induced ligands[88] or lack constitutively expressed self-molecules, such as major histocompatibility complex (MHC) class I molecules[85,89]. The activation of NK cells is governed by a complex integration of activating and inhibitory receptors present on the cell

surface which become ligated by these stress-induced ligands or MHC molecules, respectively[88]. The activation and inhibitory receptors present on NK cells fall into different categories[90]. Many of these receptors are expressed on other effector immune cells, particularly T cells[91]. The natural cytotoxicity receptors (NCRs) are NK cell-specific activating receptors comprised of NKp30, NKp44, and NKp46[92,93]. Simultaneous engagement of multiple NCRs enhances the cytotoxic response, indicating that cancer cells likely express several ligands for these receptors[90]. These receptors are coupled to immunoreceptor tyrosine-based activation motifs (ITAMs) containing polypeptides which propagate signal through multiple pathways involving protein tyrosine kinases[94], ultimately resulting in the mobilization and release of pre-formed cytolytic granules[95]. The natural killer group 2, member D (NKG2D) is a type II lectin-like transmembrane activating receptor that is critical to regulating NK cell function[96,97]. The ligands for NKG2D are classified into two main subtypes: MHC class I chain related proteins A and B (MICA/B)[96] and six cytomegaloviral unique long 16-binding proteins (ULBP1-6)[98,99]. Unlike the NCRs, signaling downstream of NKG2D is not directly mediated by ITAMs associated with the receptor iteself[100]. The intracytoplasmic tail does not propagate signal directly, but rather it interacts with the adaptor protein DNAX-activating protein (DAP10) which activates the phosphoinositide 3-kinase (PI3K)/Akt pathway and Ca^{2+} influx essential for cell-mediated cytotoxicity[100]. To counteract the activating signals and protect healthy cells, NK cells express a series of inhibitory receptors on their surface[95]. In humans, these receptors are called the killer cell Ig-like receptors (KIRs) which are specific for MHC class I molecules that are expressed on healthy cells[101,102]. The intracytoplasmic domains of KIRs contain immunoreceptor tyrosine-based inhibition motifs (ITIMs) which become phosphorylated upon receptor ligation and recruit tyrosine phosphatases SHP-1 and SHP-2[101,102]. CD94-

NKG2A, which binds to non-classical MHC molecule HLA-E, is also an ITIM-containing inhibitory receptor expressed on the surface of NK cells[102]. The various activating and inhibitory signals ligated on NK cells determine their fate through multiple competing signals[91,92,95,103].

NK cells can also recognize antibody-opsonized targets through binding of FcγRIII (CD16)[104]. In addition to NK cells, there are many different immune cells that express Fcγ receptors and can perform antibody-dependent cell-mediated cytotoxicity (ADCC) including monocytes, neutrophils and eosinophils[104]. There are different types of Fcγ receptors, some of which can have an activating or an inhibitory effect on the associated immune cell[104]. One unique feature of NK cells is that they are the only immune cell which express solely the activating forms of the Fcγ receptors[104,105]. As such, NK-mediated ADCC is a major determinant of the efficacy of monoclonal antibody-based immunotherapy[106–108]. Briefly, antibodies targeting surface tumour-associated antigens (TAAs) will bind to and coat the surface of tumour cells. For instance, the monoclonal antibody cetuximab targets the epidermal growth factor receptor (EGFR), while trastuzumab targets the human epidermal growth factor receptor 2 (HER2)[106]. Engagement of the FcγRIII on NK cells by the Fc fragment of the antibody coating the target cell triggers release of lytic granules and pro-inflammatory cytokines and chemokines[109].

Following activation, NK cells exhibit several key effector functions. NK cell cytotoxicity is characterized by the release of perforin and granzymes, which perforate the membrane of target cells and induce apoptosis[110]. The interaction of an NK cell with its target is mediated through adhesion molecules expressed on the surface of NK cells, such as lymphocyte function-associated antigen (LFA-1), which allow for the formation of the

immunological synapse[111,112]. The synapse is arranged such that adhesion molecules cluster at the periphery, forming a tight connection between the NK cell and its target[111,113], while activation receptors cluster towards the centre of the immunological synapse[113]. Cytoskeleton rearrangement is a crucial factor in the proper exocytosis of lytic granules[113]. Signaling downstream of LFA-1 triggers initial activation events[112] and actin polymerization. Following this, the microtubule organizing centre (MTOC) translocates and carries lytic granules to the site of the immunological synapse using motor proteins[113]. Finally, the secretory lysosomes carrying lytic granules fuse with the plasma membrane[114] through a process mediated by the activity of SNARE proteins, resulting in degranulation[115]. This event can be detected through the accumulation of CD107a (LAMP1) on the surface of the NK cells[114].

In addition to cytolytic granule-mediated killing, NK cells also express death ligands including tumour necrosis factor-related apoptosis-inducing ligand (TRAIL)[116,117] and Fas ligand (FasL) which engage death receptors or Fas/CD95, respectively, on target cells, triggering extrinsic apoptosis in these cells[118]. Engagement of death receptors triggers a signaling cascade that leads to assembly of the death-inducing signaling complex (DISC) which activates caspases 8 and 10 and induces apoptosis[118]. TRAIL expression on NK cells can be stimulated by cytokines[119] or through interaction with a tumour cell, the latter resulting in TRAIL expression concentrated at the immune synapse[120]. TRAIL can also be shed from the NK cell membrane and become soluble, retaining the ability to induce apoptosis in neighbouring cells expressing the appropriate death receptors[121].

NK cells can also become activated through different combinations of cytokines including IL-2, 12, 15, 18[122] and type I interferons[123,124]. The signaling that occurs downstream of these cytokines is distinct from the signal transduction which triggers NK-

mediated cytotoxicity, and is responsible for NK cell development, maturation, proliferation, and effector molecule production[125]. Cytokines predominantly activate Janus kinase (JAK)/signal transducer and activator of transcription (STAT) signaling. Downstream of the JAK/STAT pathway is the initiation of expression of pro-inflammatory cytokines, namely IFN-γ[1]. Binding of a cytokine to its associated receptor leads to JAK recruitment to the intracellular portion of the receptor and subsequent phosphorylation. These phosphorylation events create docking sites for STAT proteins which also become phosphorylated. The STAT proteins then dimerize and enter the nucleus where they bind to enhancer or promoter regions and upregulate transcription of effector molecules[126]. There are many different JAK and STAT proteins downstream of various cytokines. The combination of IL-2 and IL-12 is a strong trigger for IFN-γ production and granzyme B and perforin expression[127]. This occurs downstream of activation of JAK2 and STAT4[127]. The IL-2 receptor is composed of three subunits: alpha, beta and gamma[128]. In addition to triggering signaling downstream of IL-2 through JAK2/STAT4, the IL-2Rβ subunit potentiates signaling downstream of IL-15 through JAK1/3 and STAT5, which is critical to NK cell development[129]. The IL-2Rγ subunit is also shared with IL-15[130]. Wang et al found that NK cells primed with IL-2 showed upregulation in expression of the IL-12Rβ1 and IL-12Rβ2, as well as upregulation of expression of STAT4. This increased the responsiveness of NK cells to IL-12[127]. As discussed, production of IFN-γ is a major functional readout following cytokine stimulation. IFN-γ is a type II interferon produced primarily by NK and T cells that plays an important role in protecting against tumour development[131]. This cytokine has pro-apoptotic, antiproliferative and anti-angiogenic effects[131]. It also plays a role in influencing the function of other immune cells such as macrophages, dendritic cells, T cells and B cells[131].

1.2.2 NK cells are dysfunctional following surgical stress, and this dysfunction is directly responsible for postoperative tumour growth

As discussed, NK cells are key players in cell-mediated immunity and therefore critical for recognizing and clearing residual cancer cells[132].Our lab and others have shown that NK cell effector functions are significantly impaired postoperatively[9,10,68]. Blood samples were collected from 42 colorectal cancer surgery patients at several postoperative timepoints and from 27 healthy donors (HDs) not receiving surgery. NK cell IFN-γ secretion and cytotoxicity were assessed following whole blood cytokine stimulation and by means of a ^{51}Chromium-release assay[1], respectively. The reduction in IFN-γ secretion was most pronounced 24 hours after surgery on postoperative day 1 (POD1) and persisted for over a month[1]. Cytotoxicity was significantly reduced by 24.6% on POD1[1]. The absolute number of circulating NK cells was not significantly different postoperatively compared to baseline (preoperative; BL) levels[1]. In animal models, postoperative NK cell suppression correlates with increased metastases in both spontaneous and implanted tumours[133]. Surgically stressed NK cells were adoptively transferred into NK-deficient mice. Upon tumour challenge, mice treated with surgically stressed NK cells exhibited a higher number of lung nodules compared to those that received naïve NK cells[133]. Surgery markedly reduced total NK cell numbers in the spleen and affected NK cell migration[133]. *Ex vivo* and *in vivo* tumor cell killing by NK cells was significantly reduced in surgically stressed mice[133]. NK cell dysfunction is suspected to play an important role in postoperative cancer recurrence and metastasis[68]. Further characterizing the nature of this dysfunction will enable the development of immunotherapeutics that can reverse this suppressed state and ultimately prevent metastasis following surgery[68].

1.3 NK cell metabolic activity sustains their effector function

1.3.1 The major bioenergetic pathways at work within NK cells

Cellular metabolism is a key regulator of immune cell function[134–136]. Glucose serves as the primary carbon fuel source for NK cells that supports the production of ATP[135]. Partial oxidation of glucose occurs when glucose is taken up into the cell through glucose transporters and enters glycolysis[82]. In humans, there are 14 different membrane-spanning glucose transporters referred to as GLUTs, where GLUT1 is the most abundantly expressed on the surface of NK cells and mediates the upregulation of glucose uptake in response to stimulation[82]. When glucose enters the cytosol, it gets phosphorylated by hexokinase, the first rate-limiting enzyme in glycolysis, into glucose-6-phosphate (G6P)[137]. G6P can either continue to be metabolized through glycolysis or enter the pentose phosphate pathway for the synthesis of nucleotides. Pyruvate is generated through glycolysis, along with nicotinamide adenine dinucleotide (NADH), which enters the mitochondria to be further oxidized into acetyl coenzyme A (acetyl-CoA). Next, acetyl-CoA enters the tricarboxylic acid (TCA) cycle to generate more NADH reducing equivalents that fuel oxidative phosphorylation (OxPhos) by driving production of a proton gradient between the mitochondrial intermembrane space and matrix[138]. The proton motive force generated by the electron transport chain (ETC) drives ATP synthase to produce ATP. Without molecular oxygen present as the final electron acceptor, pyruvate is converted into lactate instead of acetyl-CoA through anaerobic glycolysis[139]. Certain cell types undergo aerobic glycolysis, which is the production of ATP primarily through glycolysis despite the presence of oxygen, a phenomenon referred to as Warburg metabolism[140,141].This is a quicker but less efficient means of ATP production, generating a net of only 2 molecules of ATP per molecule of glucose[141,142]. It is preferred by

highly proliferative and metabolically active cancer cells[143]. On the other hand, production of ATP through glycolysis-driven OxPhos more efficiently produces approximately 30 molecules of ATP per molecule of glucose depending on oxygen availability[141,144]. In all, glycolysis and OxPhos are two distinct, yet closely intertwined pathways used for ATP generation.

NK cells exhibit a unique metabolic signature that distinguishes them from other immune cells. Assmann et al found that the upregulation of glucose metabolism that occurs following stimulation by the cytokines IL-2 and IL-12 is mediated by the activity of Srebp transcription factors[145]. In addition to the canonical control of lipid biosynthesis, Srebp activity mediates upregulation of glycolysis and OxPhos in response to IL-2/12 stimulation in murine NK cells[145]. Metabolic tracing using uniformly labelled $^{13}C_6$-glucose revealed that Srebp-mediated glucose metabolism passed through the citrate-malate shuttle instead of the TCA cycle to generate NADH and fuel the ETC and OxPhos[145]. Additionally, Loftus et al found that murine NK cells rely on the consistent uptake of amino acids through solute carrier (SLC)7A5 in response to IL-2/12 stimulation to sustain the constant synthesis and degradation of c-Myc, an important transcription factor promoting the expression of glycolytic enzymes and proteins involved in biosynthesis. Loss of c-myc has been shown to be correlated with impaired NK cell function[146,147].

1.3.2 NK cell metabolic preferences are dependent on their activation state

Under basal conditions, NK cells rely on OxPhos to produce ATP for maintaining basal cellular energy demands. Without a source of stimulation, the metabolic activity of NK cells is overall very low[148]. Following acute stimulation, NK cell effector functions rely predominantly on glycolysis to support the increased energy demand[149]. However, when

stimulated for longer periods of time (24 hours or more), NK cells shift towards a reliance on both glycolysis and OxPhos to meet the energy requirements for 1) producing biosynthetic precursors for proliferation and 2) carrying out their effector functions[149]. This increase in energy production has been shown to occur in response to both cytokine stimulation and activation receptor ligation[148]. When energy production by OxPhos is inhibited by oligomycin, an ATP synthase inhibitor, intracellular IFN-γ levels in response to cytokine stimulation decrease[150]. The same effect occurs when glycolysis is impaired by galactose, an alternative carbon source which cannot support an elevated rate of glycolysis[150]. In contrast to these reports, others have shown that NK cells can adapt to glucose restriction, suggesting a certain degree of metabolic flexibility. Picard et al demonstrated that blocking the glucose transporters GLUT1, 2, and 3 in NK cells, which effectively blocks glycolysis, inhibits proliferation and IFN-γ production but has little effect on cytotoxicity and serial killing[82].

1.3.3 Metabolic deficiency accompanies NK cell dysfunction across several disease states

TGF-β and mTORC1:

Given the close relationship between metabolism and function, metabolic deficits have been reported in several disease states in which NK cells are dysfunctional. An inability to undergo metabolic reprogramming and sustain elevated rates of glycolysis and OxPhos in response to stimulation results in functional impairment[150,151]. Slattery *et al* reported that reduced rates of glycolysis and OxPhos were accompanied by decreased IFN-γ production and cytotoxicity in peripheral blood NK cells from metastatic breast cancer patients compared to age and sex-matched healthy controls[152]. Both function and metabolism were

improved by blocking the activity of TGF-β through use of an anti- TGF-β monoclonal antibody[152]. Furthermore, Viel *et al* showed that TGF-β inhibits the mechanistic target of rapamycin complex 1 (mTORC1) through a non-canonical signaling pathway, suppressing NK cell metabolic activity[30,153]. mTORC1 is an important regulator of cell growth and metabolism[153,154]. Through association with different proteins, mTOR can form two complexes referred to as mTORC1 and mTORC2 that signal through unique pathways[155]. mTORC1 controls translation through phosphorylation of eukaryotic translation initiation factor 4E-binding protein 1 (4EBP1) and the S6 ribosomal kinase, which phosphorylates the ribosomal protein S6[156]. mTORC1 plays a role in controlling glycolysis, nutrient transport receptor expression, and lipid synthesis, mainly by controlling the expression of key proteins and transcription factors involved in these processes[156]. Donnelly *et al* showed that mTORC1 activity is necessary for activated NK cells to increase rates of glycolysis and produce IFN-γ and granzyme B[151]. Inhibition of mTORC1 by rapamycin resulted in decreased production of effector molecules. We have shown that mTORC1 signaling in response to IL-2/12 stimulation is reduced in NK cells on POD1[3]. This phenotype was replicated in healthy NK cells co-cultured with POD1 plasma and was reversed when TGF-β signaling was blocked through either pharmacological inhibition or by using a monoclonal antibody[3].

Aberrant lipid accumulation:

NK cell lipid accumulation has been linked to dysfunction[7,157,158]. In B cell lymphoma, NK cells are exposed to an abundance of fatty acids which have been shown to impair their function in both humans and lymphoma-bearing mice. This phenomenon has been linked to a metabolic switch to lipid metabolism as an adaptation to their environment

which is mediated by the activity of the transcription factor peroxisome activator receptor gamma (PPARγ)[157]. In obesity, lipid accumulation in NK cells results in metabolic and functional paralysis driven by the inhibition of mTOR-mediated glycolysis[158]. More specifically, there is reduced trafficking of cytolytic granules to the immune synapse. Given the role of NK cell activity in immunosurveillance, this is an important consideration since obesity has been directly linked to cancer[158]. Like in the case of B cell lymphoma, this aberrant lipid accumulation in NK cells due to obesity has been linked to the activity of PPARγ[157,158]. In high-grade serous ovarian cancer, malignant ascites fluid had a strongly immunosuppressive effect on NK cells which was found to be caused by increased uptake of polar lipids. This led to dysregulated lipid storage and impaired cytotoxicity[159]. Finally, both murine and human surgically stressed NK cells have increased lipid content after surgery which has been directly linked to impaired cytotoxicity and reduced cytolytic granule content[7]. The authors referred to these as "lipid-laden" NK cells which failed to have a protective effect in a lung tumour mouse model. This was associated with high expression of lipid scavenger receptors MSR1, CD36 and CD68[7].

Cancer:

There are many aspects of the tumour microenvironment (TME) which can affect the metabolism of NK cells. First, cancer cells are highly glycolytic, depleting the surrounding environment of critical nutrients which tumour-infiltrating NK cells require, such as glucose and glutamine[160]. The presence of highly metabolically active cancer cells results in the accumulation of lactate and subsequent acidification of the extracellular space, creating a harsh and suboptimal environment for NK cells[160–162]. MDSCs are also highly metabolically active cells and can deplete the TME of crucial nutrients, such as arginine, that fuel effector

immune cells. Arginine metabolism is important for regulating immune responses[163,164], and decreased circulating arginine levels have been shown to be a predictor of mortality in critical trauma patients[164]. We have shown that depletion of arginine by the activity of ARG1 in sxMDSCs is a major source of their suppressive activity on NK cells[4]. Another hallmark of the TME is hypoxia which results in increased expression of the transcription factor hypoxia inducible factor 1-alpha (HIF1α). While it acts as a metabolic regulator in CD8+ T cells that supports glycolysis through inducing the expression of glycolytic enzymes[165], HIF1α has been shown to negatively regulate cytotoxicity and inhibit IFN-γ production in NK cells[166]. However, the reports on the activity of HIF1α are context dependent. Lim et al showed that the metabolic reprogramming driving a shift from OxPhos to glycolysis caused by HIF1α helped NK cells to overcome hypoxia-induced functional impairment[167]. Hypoxia can also induce cancer cells to release adenine nucleotides[168]. The hydrolysis of these adenine nucleotides by ectonucleotidases CD39 and CD73 expressed on the surface of cancer cells and certain immune cell populations, including MDSCs, results in the production of adenosine in the extracellular space[169]. Adenosine signals in NK cells through binding to one of four adenosine receptors (mainly A_{2A}) and has been shown to have pleiotropic effects on NK cells. While adenosine has an overall downregulating effect on cellular metabolism, causing inhibition of both glycolysis and OxPhos, priming the NK cells with IL-12 and IL-15 resulted in enhanced production of effector molecules when exposed to adenosine[170]. The metabolic profile of NK cells exposed to the immunosuppressive ovarian cancer TME is characterized by decreased levels of OxPhos and glycolysis[171]. It is also associated with reduced expression of nutrient transporters such as the transferrin receptor (CD71), the large neutral-amino acid transporter (CD98), and GLUT1. Finally, tumour-

associated NK cells are characterized as having an overall low mitochondrial mass with a fragmented morphology, which all contribute to impaired function[171].

While there are several studies profiling the metabolic activity of NK cells under different disease states/immunosuppressive environments, to our knowledge the bioenergetic activity of dysfunctional postoperative NK cells has not been thoroughly explored. We have previously established a link between TGF-β signaling and reduced mTORC1 signaling in dysfunctional human NK cells on POD1[3]. Along with this data, we reported a downregulation of gene sets related to cellular respiration and OxPhos in NK cells within a cohort of six BL and POD1 colorectal cancer surgery patients[3]. Given the relationship between TGFβ, mTORC1 signaling, and metabolism, this data provided the groundwork to explore postoperative NK cell metabolism.

1.3.4 Methods of metabolic characterization of immune cells

Seahorse^{TM} extracellular flux analysis

There are several ways in which the metabolism of immune cells can be explored. A gold standard approach in the field of cellular metabolism is Seahorse^{TM} extracellular flux analysis, which measures the rates of oxygen consumption (OCR; pmol/min) and extracellular acidification (ECAR; mpH/min) in live cells[172]. OxPhos results in the reduction of O_2 as the final electron acceptor and subsequent production of water during ATP synthesis in the mitochondria[173]. As such, measurement of OCR is a readout of OxPhos in the cell[144]. Glycolysis results in the conversion of glucose to pyruvate and eventually to lactate in the cytoplasm. This is accompanied by the extrusion of protons and subsequent acidification of the extracellular medium, detected as ECAR[144]. This type of analysis can provide information on the metabolic activity and fitness of live cells which is done through injection

of different compounds which place metabolic stress on the cells[174]. The acute response to sequential addition of these compounds is detected in real-time and the corresponding ECAR and OCR values can be used to extrapolate parameters related to the metabolic fitness of the cells[174]. The parameters associated with OxPhos include their basal respiration, maximal respiration, spare respiratory capacity (SRC), and ATP-linked respiration[175]. Basal respiration indicates the cells' metabolic activity under steady-state conditions. The maximal respiration and SRC are indicators of the maximal rate of respiration that a cell can achieve as well as their ability to respond to a strong energetic demand[176]. ATP-linked respiration describes the proportion of respiration used to drive ATP synthesis, considering proton leak, which can signal mitochondrial damage[175]. The parameters associated with glycolytic activity include basal glycolysis, glycolytic capacity and glycolytic reserve[142].

Metabolomics

Two complementary methods of assessing the metabolism of immune cells are metabolomics and stable isotope tracing[177]. Metabolomics uses mass spectrometry to detect concentration levels of metabolites in either a targeted[178] or untargeted[179] manner. One important consideration is that the absolute concentration of a particular metabolite or series of metabolites alone can provide an indication of the metabolic state of the cell but do not provide the full picture of metabolic flux[177]. More specifically, metabolomics provides a static snapshot of the overall metabolite concentrations in a cell at the time of extraction. The concentration of a metabolite can be influenced by multiple factors including the rate of uptake, the level of *de novo* synthesis, and the rate of metabolism through a particular pathway[180]. For this reason, metabolomics data only depicts part of the metabolic landscape of a cell and is meant to accompany other metabolic readouts. One such readout is stable

isotope tracing. This technique uses radiolabeled metabolite tracers, such as glucose, to be able to track metabolic flux through different pathways based on the destination of carbon atoms[177,181].

Metabolic assessment with single cell resolution

The most accurate depiction of the metabolic activity of a cell is through the direct measurement of metabolic flux[144]. Despite this, there are several other methods used to assess metabolic activity which, when considered altogether, can generate a comprehensive picture of the metabolic signature of a cell. One approach is to measure mRNA expression of metabolic enzymes[182]. An important consideration is the discordance between mRNA abundance and protein levels of these enzymes[183], making it difficult to make metabolic conclusions from transcriptomic data alone[184]. Another way is to assess expression of nutrient transporters on the cell surface including CD71[150,151,171], CD98[150,151,171], GLUT1[82,150,151,171], and the lipid scavenger CD36[7]. NK cells are known to upregulate expression of these receptors in response to stimulation. Surface expression of these receptors is commonly measured when evaluating the metabolic state of immune cells, including NK cells.

A major limitation of many of the aforementioned metabolic techniques, particularly those detecting flux, is that they are bulk assays. Contrarily, assessing immune cell phenotype and function often requires single cell resolution. Novel immunometabolism techniques involve multiplexing metabolic and functional readouts at the single cell level. For example, “Met-Flow” is a technique used to measure expression of metabolic enzymes and transporters spanning diverse pathways including glycolysis, OxPhos, antioxidant defense, the pentose phosphate pathway, the TCA cycle, and fatty acid oxidation, within a

heterogenous cell population using spectral flow cytometry[185]. Another example is single cell energetic metabolism by profiling translation inhibition (SCENITH). This is a technique developed by Arguello et al which uses translation, an energetically demanding process, as a proxy readout of metabolism[186]. This technique relies on the metabolic inhibitors oligomycin, which blocks the activity of ATP synthase in the ETC[187], and 2-deoxyglucose (2-DG), which is a glucose analog that cannot be metabolized through glycolysis beyond phosphorylation by hexokinase[137,188]. SCENITH uses detection of *de novo* protein synthesis through puromycin incorporation as a metabolic readout by relying on the assumption that translation is a highly ATP consuming process, and that metabolic inhibition causes an immediate and proportional decrease in translation. The translational response to metabolic inhibition is then used to estimate dependence on OxPhos, glycolysis and/or alternative bioenergetic pathways[186]. Puromycin can either be detected using a fluorochrome-conjugated anti-puromycin antibody or by means of click chemistry. The click chemistry reaction uses O-propargylpuromycin (OPP), an alkyne conjugated form of puromycin that undergoes a "click" reaction with a fluorochrome-conjugated azide, allowing for the detection of puromycin incorporation[189]. This technique is advantageous because it can be conducted directly in whole blood, allowing for the measurement of metabolism within a mixed cell population with minimal manipulation.

Mitochondrial health

Finally, another way of determining the metabolic fitness of a cell is by measuring parameters related to mitochondrial health. Mitochondrial parameters can be assessed using tetramethylrhodamine (TMRM) dye, which is an indicator of mitochondrial membrane potential (MMP) and accumulates in healthy active mitochondria[190]. Mitochondrial mass can

be assessed using MitoTracker™ dyes. Dysfunctional NK cells have been reported as having less active mitochondria with an overall reduced mitochondrial mass, measured by decreased accumulation of TMRM and lower MitoTracker™ signal[191]. Dysfunctional mitochondria have been reported in NK cells in patients with different cancer types including ovarian[171], colorectal cancer metastasized to liver[161] and metastatic breast cancer[152]. These dysfunctional mitochondria can accumulate and lead to an overproduction of mitochondrial reactive oxygen species (mitoROS) which can induce oxidative stress in the NK cells, damaging DNA and even causing cell death[192]. There are enzymes that affect mitochondrial morphology and function, whose expression level and phosphorylation status can be indicators of mitochondrial health within the cell. This includes the mitochondrial fission protein dynamin-related protein 1 (DRP1) which can be phosphorylated and activated at the Ser616 site or phosphorylated and inhibited at the Ser637 site[193]. This also includes mitochondrial fusion proteins optic atrophy 1 (OPA-1) and mitofusins 1 and 2[193]. Analysis of each of these parameters related to mitochondrial health can give an indication of mitochondrial dynamics within the NK cell. Studying the mitochondrial health of NK cells is highly relevant to the study of postoperative NK cell metabolism in relation to postoperative dysfunction given the clear link between mitochondria and function. In addition, dysfunctional mitochondria in immune cells has been well documented in other disease states like cancer[194].

1.4 Fueling metabolism to power effector function

1.4.1 Metabolic modulation of NK cells

The purpose of studying postoperative NK cell metabolism can be viewed through two main objectives: 1) to identify potential targets to reverse or prevent dysfunction from

occurring or 2) to tailor allogeneic adoptive cell therapy for use in the perioperative period. Below we highlight some approaches to metabolically modulate NK cells.

Nutrient supplementation:

The metabolism of NK cells can be modulated by targeting the synthesis or uptake of immune suppressive metabolites and/or supplementing with additional nutrients. For instance, our group has studied the effects of perioperative arginine in murine models of surgical stress and showed that it accelerated the recovery of postoperative NK cell function[4]. Unfortunately, when evaluated in colorectal cancer patients undergoing surgery, oral arginine supplementation showed only modest benefits to NK cell cytotoxicity and did not prevent postoperative arginine depletion[2].

Mitochondrial activity:

Many of the strategies to metabolically modulate immune cells involve promoting OxPhos/sustaining mitochondrial function. One way that this can be done is through use of the compound sodium dichloroacetate (DCA). DCA inhibits the activity of pyruvate dehydrogenase kinase (PDHK), which is a kinase that phosphorylates and blocks the activity of pyruvate dehydrogenase (PDH). PDH is responsible for converting pyruvate into acetyl-CoA[195,196]. In all, DCA redirects glucose metabolism away from aerobic glycolysis and towards mitochondrial respiration, which has been shown to reverse the Warburg effect in cancer cells and slow their proliferation[147]. DCA is now being explored in the context of immune cell activity[197]. It is hypothesized to prevent or reverse exhaustion, including in NK cells[198], by redirecting glucose metabolism towards the mitochondria for more efficient energy production in response to stimulation. Following culture with DCA, NK92 cells were

shown to have improved function and higher rates of OxPhos when exposed to tumour supernatant from hepatocellular carcinoma[198]. Some other methods of mitochondrial modulation include modifying the quantity and structure of mitochondria for optimal activity. For instance, the transcription factor PPARγ coactivator 1α (PGC1α) is involved in promoting mitochondrial biogenesis, resulting in increased mitochondrial mass in response to cytokine stimulation in NK cells[199]. Blocking PGC1α prevented this increase in mitochondrial mass, impeding function[199]. Other strategies are targeted towards enzymes that govern mitochondrial architecture. For example, blocking the activity of mitochondrial fission protein DRP1 using the small molecule inhibitor mitochondrial division inhibitor 1 (mdivi-1) has been shown to both restore the function of TME NK cells in liver cancer, as well as maintain the *in vivo* efficacy of adoptively transferred NK cells in HepG2 tumour-bearing mice[191]. This positive effect on function was attributed to improved mitochondrial health and higher rates of OxPhos in mdivi-1 treated NK cells[191].

Ex vivo expansion:

NK cells can be expanded *ex vivo* over a period of three weeks with low dose IL-2 (100U/mL) and irradiated feeder cells engineered to express membrane-bound IL-21, referred to as artificial antigen presenting cells (APCs)[200–202]. The feeder cells most extensively reported are modified K562[203,204] or 721.221 cells[205]. *Ex vivo* expanded NK (exNK) cells are resistant to the immunosuppressive effects of the TME, and this has been shown to be largely mediated by their broad metabolic flexibility[171,204]. Tumour cells display characteristics of Warburg metabolism which include increased rates of glycolysis and anabolic metabolism coupled with a reduced reliance on OxPhos despite the presence of oxygen[140]. Signaling through STAT3 is important for Warburg metabolic reprogramming in

tumour cells, and IL-21 signaling through STAT3 is necessary to drive NK cell expansion[201]. Others have shown that exNK cells possess similar metabolic adaptions as tumour cells which allow them to thrive in the TME[171,204].

1.4.2 NK cells in the clinic

NK cells are an interesting option for adoptive cell therapy for the treatment of cancer due to their favourable safety profile, reduced risk of graft-versus-host disease, and cytotoxicity without the need for antigen priming, allowing for them to be used as an allogeneic "off-the-shelf" therapy[206,207]. They have been studied for use in leukemia and lymphoma[207]. Despite their potential, adoptively transferred NK cells are still subject to the metabolic stressors imposed by the TME and, for our interest, the surgically stressed environment. For this reason, strategies aimed at metabolically arming NK cells for adoptive cell therapy have been explored. Wang et al engineered NK92 cells to express a chimeric receptor which contained the extracellular and transmembrane domains of the TGFβRII with the intracellular domain of NKG2D. As a result, these engineered NK92 cells became activated instead of inhibited when encountering the immunosuppressive cytokine TGF-β, demonstrating improved functional capacity both *in vitro* and *in vivo*[208]. Zhu et al investigated the effect of knocking out cytokine-inducible SH2-containing protein (CIS), a member of the suppressor of cytokine signaling (SOCS) family, in human induced pluripotent stem cell-derived (iPSC) NK cells expanded *ex vivo*[202]. SOCS genes turn on in response to cytokine stimulation and enforce negative feedback by inhibiting cytokine signaling. Deletion of the *CISH* gene improved the *in vivo* efficacy and persistence of expanded iPSC NK cells, which was accompanied by augmented metabolic activity directly responsible for increased function[202].

In addition to engineering NK cells for improved metabolic fitness, NK cells can be treated during the *ex vivo* expansion process to modulate their activity and metabolism before *in vivo* delivery. For instance, Foltz et al introduced recombinant human TGF-β throughout the 14 days of K562 feeder cell-based *ex vivo* expansion of healthy primary human NK cells in a process referred to as "TGF-β imprinting". This resulted in increased secretion of both IFN-γ and TNFα in response to cytokine stimulation, as well as interaction with tumour targets[209]. This group later showed that the effects of TGF-β imprinting were mediated by an epigenetically induced metabolic change. More specifically, they noted increased OxPhos in TGF-β imprinted NK cells versus NK cells that underwent standard expansion, while glycolysis was not different between the two conditions. They found that this effect was caused by an epigenetic increase in CD38 expression on the surface of NK cells, which is involved in NAD+ synthesis[210]. Finally, NK cells can be treated *ex vivo* with a combination of cytokines, namely IL-12/15/18 prior to being adoptively transferred into patients. This endows them with memory-like properties, as they are referred to as cytokine-induced memory-like (CIML) NK cells[122,211]. These memory-like properties involve an enhanced IFN-γ response upon re-stimulation[122,212].

1.5 Rationale and Chapter Overview

While surgical resection of a primary or metastatic solid tumour offers patients the best chance of cure, it unfortunately creates an environment in the body that fosters tumour growth. We have previously shown that impaired NK cell function is central to this phenomenon in murine models of surgical stress. We have also shown that NK cell dysfunction is most pronounced on POD1 in colorectal cancer surgery patients. Given the importance of metabolic activity in sustaining effector function in immune cells, we sought to profile the metabolic signature of isolated POD1 NK cells, where dysfunction is at its peak. By correlating metabolic activity with impaired function, we have an opportunity to uncover the nature of postoperative NK cell dysfunction. These findings can inform the use of metabolic modulators to prevent NK cell dysfunction in surgical cancer patients or highlight potential avenues to metabolically arm adoptive NK cell-based therapies specifically for the perioperative period. A schematic representation of NK cell function and metabolism in the postoperative environment is depicted in Figure 1.1.

In **Chapter 3** we show that surgical stress impairs all major mechanisms of NK cell function in cancer patients. We highlight that this dysfunction persists upon isolation from whole blood. Based on the profound dysfunction that occurs in NK cells after surgery, and the compelling evidence linking effector function with metabolic capacity, we performed metabolic characterization of POD1 NK cells in **Chapter 4**. We found that POD1 NK cells have a profoundly impaired ability to perform OxPhos. Finally, in **Chapter 5** we attempted several approaches to metabolically modulate NK cells for better performance in the postoperative environment.

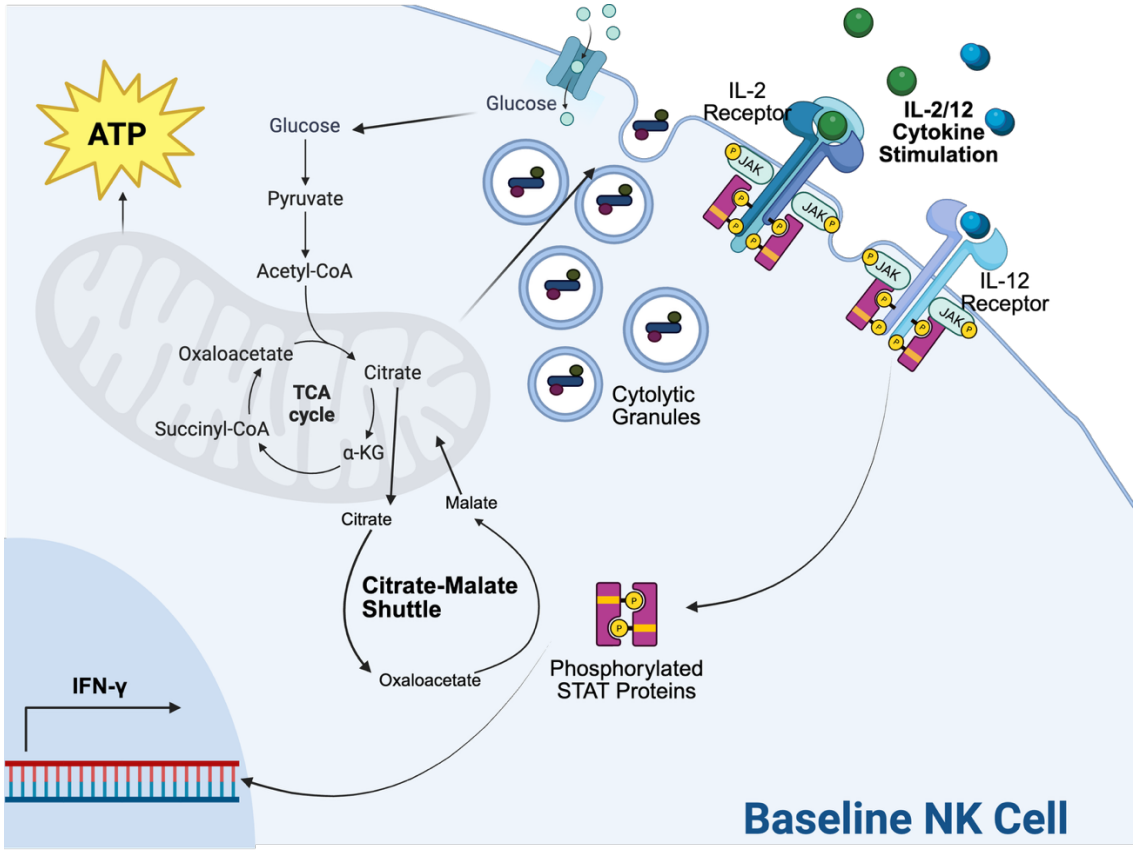
ATP
Glucose
Glucose
Pyruvate
Acetyl-CoA
Oxaloacetate
Citrate
TCA cycle
Succinyl-CoA
α-KG
Citrate
Malate
Citrate-Malate Shuttle
Oxaloacetate
IFN-γ
IL-2 Receptor
IL-2/12 Cytokine Stimulation
IL-12 Receptor
JAK
Cytolytic Granules
Phosphorylated STAT Proteins
Baseline NK Cell

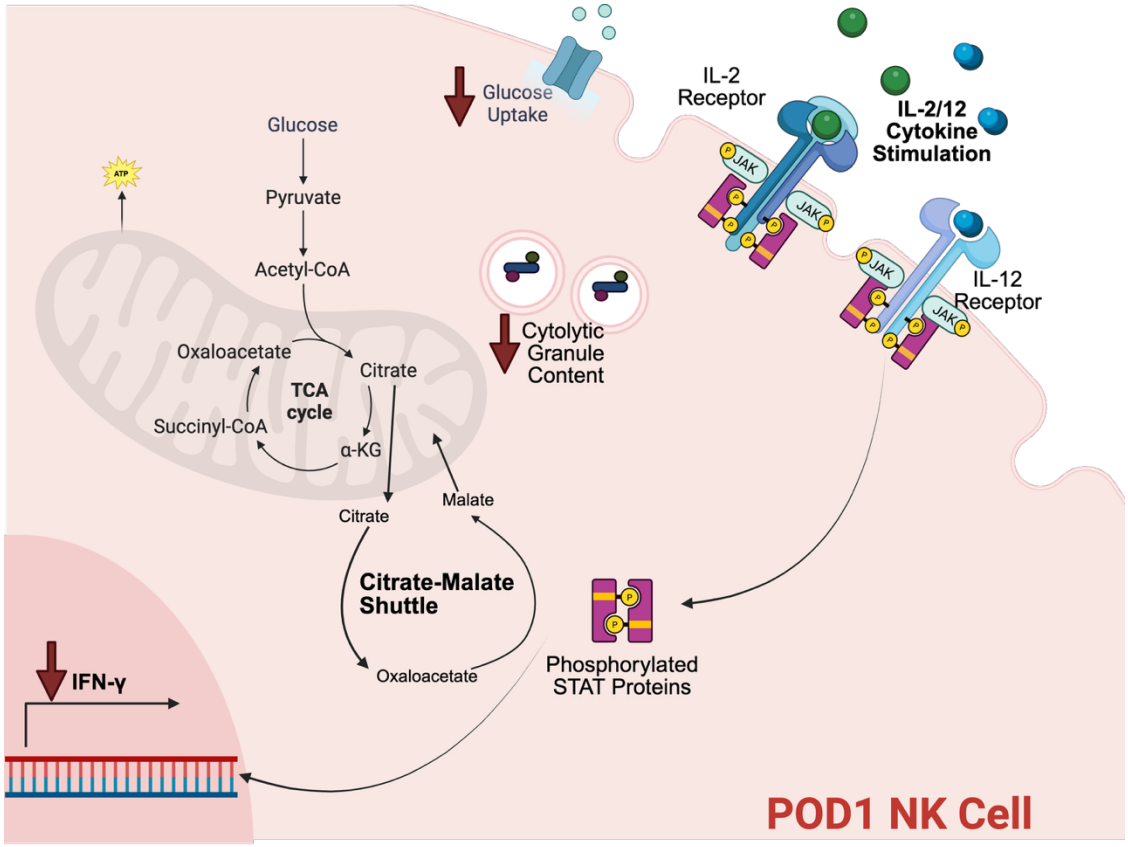
Glucose Uptake
Glucose
Pyruvate
Acetyl-CoA
Oxaloacetate
Citrate
TCA cycle
Succinyl-CoA
α-KG
Citrate
Malate
Citrate-Malate Shuttle
Oxaloacetate
IFN-γ
IL-2 Receptor
IL-2/12 Cytokine Stimulation
IL-12 Receptor
JAK
Cytolytic Granule Content
Phosphorylated STAT Proteins
POD1 NK Cell

Figure 1.1. Schematic representation of NK cell function and metabolism in response to IL-2/12 stimulation on BL and POD1. NK cell stimulation with IL-2/12 triggers JAK/STAT signaling events which initiate the expression of IFN-γ. Simultaneously, NK cells are poised to kill their target through pre-formed cytolytic granules containing perforin and granzymes. These granules are released upon encounter with a target cell. Stimulatory events are associated with an overall upregulation of metabolic activity to meet the energy demands for effector function. This corresponds to increased rates of glycolysis and OxPhos. All these parameters are decreased after surgery. Created in BioRender.

Chapter 2: Materials and Methods

2.1 WHOLE BLOOD COLLECTION AND NK CELL ISOLATION

2.1.1 Blood collection from cancer patients and healthy donors

Blood samples were collected from a total of 87 cancer surgery patients at the Ottawa Hospital under our Perioperative Human Blood and Tissue Specimen Collection Program (OHSN-REB #2011884-01H) lead by Dr. Rebecca Auer. Due to limitations in sample volume and NK cell yield, all 87 patients could not be included across all readouts presented in this study. The blood samples were collected immediately before surgery at baseline (BL) and within 24 hours after surgery on postoperative day 1 (POD1). The operating list was screened weekly and cancer patients undergoing surgical resection of a primary or metastatic tumour were contacted. Patients with pancreatic, bladder, prostate, gynecologic (endometrial, cervical, and ovarian), colorectal, liver, renal, thoracic, and soft tissue cancers were included in this study. The number of patients per cancer type was determined solely based on sample availability. Exclusion criteria included known autoimmune conditions, thyroid disease, HIV, or hepatitis infection. A summary of patient demographics is presented in Supplementary Table 1 (Appendix II) which includes median age, sex, surgery length and estimated blood loss for the 87 patients included throughout this study. None of the patients included in this study were reported to have received a blood transfusion during or after surgery. When possible, surgeries >3 hours were given priority. Healthy donors also satisfied the inclusion/exclusion criteria detailed above. Patient demographics for healthy donors is presented in Supplementary Table 2 (Appendix II). Healthy donors did not have a current or previous cancer diagnosis. All study participants were >18 years of age and were able to provide written informed consent independently or through a translator.

2.1.2 Human Blood Processing

Whole blood was diluted with an equal volume of sterile phosphate-buffered saline (PBS). The diluted blood was split in equal parts and overlayed onto 15mL of Ficoll-Paque (Cytiva) density gradient centrifugation medium. The blood was centrifuged at 400g for 30 minutes with low acceleration and deceleration to ensure adequate separation. The PBMC layer was collected, washed once with PBS, and counted for downstream applications. In some cases, a subset of PBMCs were cryopreserved in 90% heat-inactivated fetal bovine serum (FBS) and 10% dimethyl sulfoxide (DMSO; Fisher Bioreagents) for cryopreservation at -70°C for up to 18 months. The remaining PBMCs were used for NK cell isolation.

2.1.3 NK cell isolation from PBMCs

NK cells were isolated from PBMCs through magnetic sorting using the human NK cell isolation kit (Miltenyi Biotec). Briefly, PBMCs were resuspended in 40uL of sterile sorting buffer [PBS supplemented with 0.5% bovine serum albumin (BSA) and 2mM ethylenediaminetetraacetic acid (EDTA)] along with 10uL of NK cell Biotin Antibody Cocktail per 10^7 cells. The cells were incubated with the antibody for 5 minutes at 4ºC. After the incubation, 30uL of sorting buffer was added along with 20uL of NK cell Microbead Cocktail per 10^7 cells. The cells were incubated for 10 minutes, and untouched NK cells were isolated by depletion using an autoMACs Neo automatic magnetic cell sorter (Miltenyi Biotec; serial#196) at a 2mL/min flow rate. After the separation, the negative fraction containing the NK cells was centrifuged at 350g for 5 minutes. The cells were resuspended in 1-3mL of complete Roswell Park Memorial Institute (RPMI; Life Technologies) 1640

media (Gibco; complete media contains 10% heat-inactivated FBS), counted manually, and resuspended at a concentration of 1-2e^6 cell/mL in 90% heat-inactivated FBS and 10% DMSO for cryopreservation at -70°C for up to 18 months.

2.2. NK CELL FUNCTIONAL ANALYSIS

Isolated NK cells or PBMCs:

2.2.1 Extracellular staining for cell surface markers

Following the indicated stimulation/culture conditions outlined for each experiment, isolated NK cells were transferred to a 96-well V bottom plate and centrifuged at 500g for 3 minutes. The supernatant was removed and the cells were resuspended in fixable viability stain 510 (BD Bioscience) at a 1/500 dilution and incubated for 10 minutes at room temperature (RT) in the dark. The reaction was stopped by adding fluorescence-activated cell sorting (FACS) buffer (PBS supplemented with 0.5% BSA and 1mM EDTA). The cells were then centrifuged at 500g for 3 minutes, the supernatant removed, and the cells resuspended in human Fc block (BD Bioscience) and incubated for 5 minutes at 4ºC. The following antibodies were added in a 40uL staining volume for NK cell identification: CD3-FITC, CD56-BV421, CD16-BV650 and incubated for 20 minutes at 4ºC protected from light. When staining for extracellular nutrient transporters, the following antibodies were used: CD56-BUV563, GLUT1-Alexa Fluor 647, CD98-PE, CD71-R718, CD36-APC-Cy7. The cells were washed with FACS buffer and resuspended in 1% paraformaldehyde (PFA) for 15 minutes at 4ºC. The cells were resuspended in FACS buffer and stored at 4ºC for up to 72 hours prior to data acquisition by conventional flow cytometry on a BD LSR Fortessa or by spectral flow cytometry on a Cytek Aurora (for nutrient transporter measurements).

2.2.2 Intracellular staining for IFN-γ, granzyme B and perforin

Patient-matched BL and POD1 isolated NK cells or PBMCs were thawed and rested for 1 hour in complete RPMI media supplemented with 100U/mL IL-2 (Peprotech) at 37ºC in 5% CO_2. After the resting period, the NK cells were counted and stimulated with a combination of interleukins 2 and 12 (IL-2/12; Peprotech) at a concentration of 400U/mL and 20ng/mL, respectively. Brefeldin A (GolgiPlug™ Protein Transport Inhibitor; Fisher Scientific) was added at a dilution of 1/500 for the final 4 hours of the stimulation period. Staining for extracellular markers was completed as described in section 2.2.1. The cells were then fixed and permeabilized with BD Cytofix/Cytoperm solution for 20 minutes at 4ºC. The cells were washed twice with BD Perm/Wash buffer (contains saponin), diluted to 1X in milli-Q water, and incubated for 10 minutes at 4ºC. The cells were centrifuged at 500g for 3 minutes and resuspended in 100uL of 1X BD Perm/Wash buffer containing a combination of one or more of the following antibodies for intracellular markers: IFN-γ - APC, granzyme B – PerCP Cy5.5, and perforin-PE. The cells were incubated with the antibodies for 30 minutes at 4ºC in the dark, washed twice with BD Perm/Wash buffer, resuspended in FACS buffer and stored at 4ºC for up to 72 hours prior to data acquisition by conventional flow cytometry on a BD LSR Fortessa.

2.2.3 CD107a (degranulation)

Isolated patient-matched BL and POD1 NK cells were thawed and rested for 1 hour in complete RPMI supplemented with 100U/mL IL-2 at 37ºC in 5% CO_2. After the resting period, the NK cells were counted and co-cultured with K562 target cells at a 2:1 effector-to-target ratio in a 96-well V-bottom plate for 4 hours. Monensin (GolgiStop™; BD Bioscience) was added at dilution of 1/1000 along with an anti-CD107a-PE antibody at a 1/100 dilution for the full 4 hours of the co-culture. The cells were then stained for viability and NK cell markers as described in section 2.2.1. The cells were washed with FACS buffer and resuspended in 1% PFA for 15 minutes at 4ºC. The PFA was removed, cells were resuspended in FACS buffer and stored at 4ºC for up to 72 hours prior to data acquisition by conventional flow cytometry on a BD LSR Fortessa flow cytometer.

2.2.4. Cell lines and media

The K562 human leukemia cell line (ATCC) was maintained in RPMI 1640 media supplemented with 10% FBS, 100U/mL penicillin / 100ug/mL streptomycin (1% P/S; Gibco). The OVCAR8 high grade serous carcinoma cell line was a kind gift from Dr. Barbara Vanderhyden (OHRI) and maintained in Dulbecco's Modified Eagle Medium (DMEM) supplemented with 10% FBS, 2mM L-glutamine (Gibco), 10mM 4-(2-hydroxyethyl)-1-piperazineethanesulfonic acid (HEPES) buffer (Gibco), and 1% P/S. The SKOV3 ovarian serous cystadenocarcinoma (ATCC) and the HCT116 colon cancer cell lines (ATCC) were maintained in alpha Minimum Essential Medium (αMEM; Multicell) supplemented with 10% FBS, bacto-peptone (600ug/mL; Gibco), 10mM glucose (Agilent Technologies), and 1% P/S. Cells were cultured at 37ºC with 5% CO_2 and passaged every 2-3 days. Adherent cell lines were passaged using 0.05% trypsin 0.53mM EDTA (Corning).

2.2.5. In vitro cytotoxicity

Tumour targets (K562, OVCAR8, SKOV3, or HCT116 cells) were counted and resuspended to a final concentration of $2e^6$ cells/mL in PBS. The tumour targets were labelled with cell proliferation dye eFluor 450 (CP450; Life Technologies) at a 1/1000 dilution for 15 minutes in a 37ºC incubator with 5% CO_2. Isolated patient-matched BL and POD1 NK cells were thawed, rested for 1 hour in complete RPMI supplemented with 100U/mL IL-2, and counted. NK cells were serially diluted from $1e^5$ to $2.5e^4$ NK cells/well in a 96-well V-bottom plate, and 25000 tumour targets were plated with the NK cells. The effector-to-target ratios were 4:1, 2:1, and 1:1. A condition without NK cells was included to measure spontaneous lysis of the tumour targets. For measurement of ADCC, SKOV3 cells were resuspended in complete media at a concentration of $1e^6$ cells/mL and incubated with trastuzumab (Herceptin™, TOH Pharmacy) at 100ug/mL for 30 minutes at 37°C. Excess antibody was removed prior to co-culturing with NK cells. The NK cells were co-cultured with K562 cells for 4 hours, with SKOV3 or OVCAR8 cells for 5 hours, or HCT116 cells for 24 hours prior to staining for viability using fixable viability dye eFluor 780 (Ebioscience). Briefly, the cells were incubated for 15 minutes at RT with the viability dye at a dilution of 1/1000. A subset of target cells was heat killed for 10 minutes at 65ºC and stained for viability at the same time. The cells were fixed with 1% PFA for 15 minutes and data was acquired by conventional flow cytometry on a BD LSR Fortessa.

2.2.6 Culture of isolated NK cells with metabolic inhibitors

Isolated patient-matched BL and POD1 NK cells were stimulated with IL-2/12 for 24 hours as described in section 2.2.2 or co-cultured with K562s under the conditions described

in section 2.2.3. The metabolic inhibitors oligomycin (40nM) or 2-DG (10mM) were present for the duration of each respective culture period. Degranulation (measured by surface expression of CD107a) or intracellular IFN-γ were measured as functional readouts by conventional flow cytometry using a BD LSR Fortessa.

2.2.7 *Isolated NK cell treatment with sodium dichloroacetate*

Isolated patient-matched BL and POD1 NK cells were stimulated with IL-2/12 (400U/mL; 20ng/mL) for 24 hours along with 10mM sodium dichloroacetate (DCA; Tocris Bioscience). Intracellular IFN-γ was measured as the functional readout.

Whole blood:

2.2.8 Intracellular staining for IFN-γ, granzyme B and perforin

Whole blood was distributed into 300uL increments in 15mL conical tubes. The blood was either left untreated or stimulated with IL-2/12 (400U/mL;20ng/mL) for 24 hours. GolgiPlug protein transport inhibitor was added at a 1/200 dilution for the final 12-16 hours of the stimulation period. Red blood cells (RBCs) were lysed by mixing whole blood with 15 times the volume of BD Pharm/Lyse buffer diluted 1/10 with milli-Q water, vortexed for 10 seconds, and incubated for 10 minutes at RT in the dark. The cells were stained for viability followed by extracellular markers for NK cell identification. After this, BL cells were fixed with 1% PFA and stored at 4°C overnight until the POD1 co-culture was complete. At this point, intracellular staining on both BL and POD1 RBC-lysed cells was done at the same time by resuspending in 200uL of BD cytofix/cytoperm buffer for 20 minutes at 4°C. The cells were washed twice with BD perm/wash buffer diluted 1/4 with milli-Q water and

incubated for 10 minutes at 4°C. The cells were centrifuged and stained for intracellular IFN-γ, granzyme B, and perforin for 30 minutes at 4°C. Excess antibody was removed, the cells were resuspended in FACS buffer and stored for up to 72 hours at 4ºC prior to acquiring the data on a BD LSR Fortessa flow cytometer.

2.2.9 Whole blood treatment with sodium dichloroacetate

Whole blood was collected at BL and on POD1 as described above and treated with 10mM DCA for the duration of the 24-hour IL-2/12 (400U/mL; 20ng/mL) stimulation. Whole blood intracellular IFN-γ staining was performed as the functional readout.

2.3. NK CELL METABOLIC ANALYSIS

2.3.1 Seahorse extracellular flux analysis

NK cell preparation

Cryopreserved patient-matched BL and POD1 NK cells were thawed, rested for 1 hour in complete RPMI supplemented with 100U/mL IL-2 at 37ºC in 5% CO_2, counted and stimulated for 24 hours with IL-2/12 (400U/mL; 20ng/mL). Following stimulation, cells were washed and resuspended in serum-free Seahorse RPMI media (composition specific to the metabolic test being conducted). The cells were plated at 4-5e^5 cells per well (cell number normalized between perioperative timepoints for the same patient), with 2-3 technical replicates per condition in a Seahorse XFe 96 well plate. The wells were pre-coated with Cell Tak (22ug/mL) to allow for NK cell adhesion in a uniform monolayer. An unstimulated or “resting” condition was included to verify whether a metabolic response to the stimulation occurred. These cells were left in 100U/mL IL-2 for the full 24 hours.

Measurement of extracellular flux

Both ECAR and OCR were measured using a Seahorse XFe96 extracellular flux analyzer (Agilent Technologies). To assess glycolysis by means of a Glycolytic Stress Test, Seahorse XF RPMI media was supplemented with 2mM L-glutamine only. NK cells were subjected to sequential addition of glucose (11.1mM), oligomycin (2uM) and 2-DG (50mM). Data was exported using GraphPad Prism software (version 10.2.1). Changes in ECAR were used to calculate glycolysis, glycolytic capacity and glycolytic reserve. Similarly, OxPhos was assessed by a Mitochondrial Stress Test in which changes in OCR in response to sequential addition of oligomycin (2uM), carbonyl cyanide-4 (trifluoromethoxy) phenylhydrazone **(**FCCP; 2uM) and rotenone/antimycin A (0.5uM/1uM) were measured. For this assay, Seahorse XF RPMI media was supplemented with 11.1mM glucose, 1mM sodium pyruvate, and 2mM L-glutamine. Changes in OCR were used to calculate basal respiration, maximal respiration and spare respiratory capacity.

2.3.2. Metabolomic analysis

BL and POD1 NK cells were collected and cryopreserved as described in sections 2.1.2 and 2.1.3. Prior to the extraction, the cryopreserved BL and POD1 NK cells (n=3) were thawed, rested for 1-2 hours at 37°C and either stimulated for 24 hours with IL-2/12 (400U/mL; 20ng/mL) or rested in 100U/mL IL-2. After the stimulation period, extraction of aqueous metabolites was conducted for targeted metabolomic analysis of glycolytic intermediates, pentose phosphates, TCA cycle intermediates, short chain coenzyme A molecules, nucleotides and amino acids. The cells were centrifuged, resuspended in 2mL of ice cold 150mM ammonium formate buffer (pH 7.4), and transferred to pre-chilled 2mL

round bottom tubes (Eppendorf). The cells were resuspended in 380uL of a 50% methanol/50% water solution, pre-chilled to -20°C. At this point, 6 x1.4mm ceramic beads (Omni International, PN: 19-645-3), rinsed with milli-Q water, were added to the cells. Samples were vortexed for 10 seconds, 220uL of acetonitrile pre-chilled to -20°C was added, and the cells were vortexed for another 10 seconds. The cells were lysed for two rounds of 60 seconds each at 30 Hz using a bead beater, cooling the samples down on ice in between sets. Next, a 2:1 mixture of ice-cold dichloromethane and milli-Q water was added, samples were vortexed and left to partition on ice for 10 minutes. The samples were centrifuged at 4000rpm at 1°C and the aqueous upper polar layer was collected. The samples were dried using a speed-vac (chilled to 4°C) and resuspended in water. Samples were then run on an Agilent 6470A tandem quadruple mass spectrometer equipped with a 1290 Infinity II ultra-high-performance LC (Agilent Technologies) utilizing the Metabolomics Dynamic Multiple Reaction Monitoring Database and Method (Agilent), which uses an ion-pairing reverse phase chromatography[213]. Metabolites were quantified by integrating the area under the curve of each compound using external standard calibration curves with Mass Hunter Quant software (Version 10.2, Agilent Technologies)[214]. Based on our pilot study, we determined that a minimum of $5.95e^5$ cells were needed per condition for adequate metabolite detection. NK cell lysates were extracted from a different number of NK cells per condition depending on the number of cells recovered post-thaw. Metabolite concentrations are presented in nM/$1e^5$ cells to normalize for these differences in cell number. LC/MS grade solvents and milli-Q water were used for the extraction. All samples and reagents were kept cold on wet or dry ice for the duration of the extraction.

2.3.4. METAFlux

Our lab collected a single cell RNA sequencing dataset from six cryopreserved PBMCs from abdominal cancer surgery patients enrolled in the PERIOP-02 clinical trial (NCT02987296; OHSN-REB# 20160732–01)[2,215]. Three of these patients were instructed to take an arginine-rich oral supplement (Enhanced Medical Nutrition) and the other three were instructed to take a control supplement three times per day for five days before surgery and five days after. The initial collection and processing of the data is described by the analysis pipeline published by Angka et al, who confirmed no transcriptional differences attributable to the treatment[215]. As such, all six patients were combined for this analysis. As described by Angka et al, single cell RNA sequencing was performed using the 10x Genomics Chromium Single Cell 3' platform (StemCore Laboratories, OHRI)[215]. Gene expression libraries were prepared following the standard 10x Genomics protocol, sequenced to a depth of 20,000 reads/cell and processed using Seurat[215]. The results were normalized and integrated to combine data from each of the six patients at the two perioperative timepoints collected prior to performing clustering[215]. The NK cell cluster was defined based on expression of *NKG7* and *GNLY*.

The MetaFlux analysis pipeline was developed and published by Huang et al[182]. This approach uses previously proposed methods to infer metabolic reaction activity from gene expression data[216,217]. Metabolic reaction activity scores (MRAS) were determined based on the predefined relationships outlined in Human1 (current as of January 2026), a publicly available genome-scale metabolic model encoding approximately 13,000 reactions and 8000 metabolites[218]. Genes encoding different subunits of an enzyme or an enzyme complex were accounted for in this model. Flux constraints were set using the MRAS values, using the assumption that RNA expression levels correspond to the maximum protein products. The

nutrient availability profile was derived from a previously published plasma-like medium[219] which physiologically resembles what circulating immune cells are exposed to within human blood. The data is presented as the mean nutrient flux score ± standard error of the mean (SEM) of 100 bootstraps sampled from BL or POD1 data pooled from all six patient samples for each chosen nutrient/metabolite.

2.3.5. Glucose uptake

Isolated BL and POD1 NK cells were stimulated with IL-2/12 (400U/mL; 20ng/mL) for 4 hours prior to measuring glucose uptake. This was done to capture potential changes in glucose uptake occurring ahead of functional differences. Glucose uptake was measured using a luminescence-based assay according to the manufacturer's instructions (Glucose Uptake Glo™; Promega)[220]. This method relies on the uptake and phosphorylation of 2-DG to form 2-DG6P (2-deoxyglucose-6-phosphate) by hexokinase. 2-DG6P accumulates in the cell as it cannot be further metabolized through glycolysis. Following the 4-hour stimulation, the NK cells were incubated with 1mM 2-DG for 15 minutes at RT. The reaction was then stopped and neutralized to lyse the cells and eliminate endogenous nicotinamide adenine dinucleotide phosphate (NADPH). At this point, "2-DG6P detection reagent" which consists of NADP+, glucose-6-phosphate dehydrogenase, a reductase, proluciferin and Ultra-Glo™ luciferase enzyme, was added. Through a series of redox reactions, luminescence was detected using a microplate reader (Biotek) which was proportional to the amount of 2-DG6P present within the cells. To make comparisons between groups, 75000 cells were plated for each condition.

2.3.6. POD1 rescue with supplemental glucose, glutamine or arginine

Isolated BL and POD1 NK cells were stimulated with IL-2/12 (400U/mL; 20ng/mL). GolgiPlug protein transport inhibitor was added at a 1/500 dilution for the final 4 hours of the stimulation. The cells were cultured in control media (RPMI +10% FBS), or in media supplemented with additional glucose (25mM), glutamine (5mM) or arginine (2mM). These concentrations account for what is already present in RPMI base media. Following the 24-hour culture period, the cells were stained intracellularly for IFN-γ as described in section 2.2.2. The data was acquired by conventional flow cytometry on a BD LSR Fortessa.

2.3.7. SCENITH

Isolated BL and POD1 NK cells were stimulated with IL-2/12 (400U/mL; 20ng/mL) for 24 hours prior to conducting SCENITH. Metabolic inhibitors were prepared in serum-free RPMI media and added to the NK cells at the following final concentrations: oligomycin (1uM), 2-DG (100mM) or a combination of both at the same respective concentrations. Metabolic inhibition was done for 30 minutes prior to blocking translation for an additional 30 minutes with OPP (10uM), an alkyne analog of puromycin. Harringtonine was used as a positive control to confirm the detection of translational blockade. The cells were then stained for viability and NK cell extracellular markers as described in section 2.2.1. The NK cells were then fixed and permeabilized using BD Cytofix/Cytoperm solution and 1X BD Perm/Wash buffer solution. The NK cells were then incubated with "click buffer" which consists of copper (II) sulfate pentahydrate (1mM), sodium L-ascorbate (10mM), AzDye 647 azide plus (2uM) and tris-hydroxypropyltriazolylmethylamine (THPTA; 2mM) in PBS. This click chemistry reaction allowed for the detection of OPP incorporation into nascent proteins through a copper-catalyzed alkyne-azide conjugation with the AzDye 647 and the alkyne

group in OPP. Signal was detected by conventional flow cytometry using a BD LSR Fortessa.

2.3.8 Mitochondrial Staining

Isolated NK cells

Cryopreserved BL and POD1 NK cells were thawed and stimulated for 24 hours with IL-2/12 (400U/mL; 20ng/mL). Following the stimulation period, the cells were stained with fixable viability stain 510 at a 1/500 dilution followed by mitochondrial labelling. MitoTracker™ Deep Red (Invitrogen) was used at 400nM for measurement of mitochondrial mass. Tetramethylrhodamine methyl ester (Image-iT™ TMRM dye; Thermo Fisher) was used at 250nM to measure mitochondrial membrane potential. All incubations with mitochondrial dyes were done for 30 minutes at 37ºC in 5% CO_2 in PBS containing 0.1% BSA. Excess dye was removed and the cells were resuspended in pre-warmed FACS buffer. Data was acquired immediately using a BD LSR Fortessa flow cytometer.

Whole blood NK cells

Whole blood was collected on BL and POD1 and stimulated with IL-2/12 for 24 hours (400U/mL; 20ng/mL). Following the stimulation period, whole blood was incubated with 15 times the volume of BD Pharm/Lyse solution (diluted 1/10 in milli-Q water) for 10 minutes at RT, protected from light. After the red blood cell lysis, the cells were stained with fixable viability stain 510 followed by mitochondrial staining. The cells were incubated with 400nM MitoTracker™ Deep Red and/or 250nM Image-iT™ TMRM dye for 30 minutes at 37ºC. The cells were then stained for extracellular markers for NK cell identification. Data was acquired immediately using a BD LSR Fortessa flow cytometer.

2.4. EX VIVO EXPANSION

2.4.1. Generation of exNK cells

The feeder cells used for *ex vivo* expansion were 721.221 human B-lymphoblastoid cells engineered to express membrane-bound IL-21 as described in Yang et al[205]. The engineered feeder cells were a kind gift from Dr. Seung-Hwan Lee at the University of Ottawa. Feeder cells were cultured in complete RPMI media supplemented with 1% P/S until 70% confluent. The feeder cells were counted and irradiated at 100 gray using x-ray radiation. Following irradiation, the cells were resuspended in fresh media immediately. Freshly isolated healthy NK cells were co-cultured with irradiated 721.221 feeder cells at a 2:1 feeder-to-NK cell ratio, with a final total cell concentration of $2.5e^5$ cells/mL in complete RPMI media supplemented with 100U/mL IL-2. To start the expansion (day 0), $5e^5$ NK cells were co-cultured with $1e^6$ irradiated feeder cells in a T25 cell culture flask. On day 3 of the expansion, 50% of the media was replenished and fresh IL-2 was added. On day 5, a full media change was done in which all the cells were removed from the flask and resuspended in fresh media with 100U/mL IL-2. On day 7, the majority of the exNK cells were cryopreserved in 90% FBS + 10% DMSO and stored at -70° for downstream assays. A subset of $2e^6$ NK cells were left to continue expanding and were co-cultured with freshly irradiated 721.221 feeder cells at a 1:1 ratio. Over the total expansion period, the culture was sampled every 3 days to verify the purity of the NK cells, the efficiency of expansion, and the elimination of feeder cells.

2.4.2. Whole blood co-culture

The whole blood co-culture model was developed by PhD candidate Henna Mistry (Auer Lab) using healthy human NK cells (Mistry et al. 2026, manuscript under review). This assay has been adapted to measure the functional resistance of the exNK cells to surgical stress. Whole blood was collected at the BL timepoint and distributed in 300uL increments in 15mL conical tubes for each treatment or stimulation condition. Cryopreserved exNK cells were thawed and rested in complete RPMI supplemented with 100U/mL IL-2 overnight at 37°C. The exNK cells were counted, resuspended in complete RPMI and mixed at a 1:1 ratio with 2X carboxyfluorescein succinimidyl ester (CFSE; BD Bioscience) fluorescent dye diluted in PBS. The cells were labelled with CFSE for 15 minutes at 37°C and excess dye was washed out. Cells were resuspended in complete RPMI with 100U/mL IL-2 and $6e^4$ CFSE-labelled exNK cells were added to the whole blood. A condition without exNK cells was included to determine the endogenous function of the BL NK cells without interference from the exNK cells. The cells were either stimulated with IL-2/12 (400U/mL; 20ng/mL, respectively) or left unstimulated for 24 hours total in a 37°C incubator with 5% CO_2. GolgiPlug protein transport inhibitor was added for the final 12-16 hours of culture. Following the 24-hour stimulation period, the cells were stained for viability and NK cell identification and fixed with 1% PFA. Fixed samples were stored at 4°C overnight until the POD1 co-culture was complete. The entire procedure was repeated with fresh patient-matched POD1 whole blood. Intracellular staining for IFN-γ was done on both the BL and POD1 co-culture samples at the same time as described in section 2.2.8.

2.5. IN VIVO EXPERIMENTS

2.5.1. Mice and injections

All murine experiments were conducted using female NCG (NOD-Prkdc^{em26Cd52}Il2rg^{em26Cd22}/NjuCrl) mice housed at the University of Ottawa Animal Care and Veterinary Services facility. NCG mice are severely immune deficient lacking functional T, B and NK cells, and are specialized for housing human immune components[221]. OVCAR8 human ovarian carcinoma cells expressing luciferase (OVCAR8-Luc) were generated by Dr. Ali Ashkar's lab (McMaster University). Cryopreserved isolated BL and POD1 NK cells were thawed, rested for 1-2 hours at 37°C and washed twice with sterile PBS + 0.1% BSA. NK cells from each condition were pooled prior to being counted and resuspended to 4e^5 cells per injection (100uL injection volume) in PBS. Each injection volume contained a dose of 10,000U of carrier-free IL-2 (R&D Systems) to support the human NK cells *in vivo*. OVCAR8 cells were lifted with trypsin-EDTA and washed twice with sterile PBS + 0.1% BSA. All injections were intraperitoneal (ip). Two variations of an engraftment prevention model were performed. In the first version, both OVCAR8-Luc and NK cells were injected at the same time. In the second version, the OVCAR8-Luc cells were injected 2 days prior to injection of NK cells. Tumour burden was quantified by IVIS imaging at several timepoints. For experiments implicating surgical stress, mice received OVCAR8-Luc cells ip 2 days prior to undergoing a laparotomy with left nephrectomy. After closing, the mice received an ip injection of NK cells with IL-2. To determine the *in vivo* persistence of the human NK cells, a peritoneal wash with PBS + 3%FBS and 1mM EDTA was done on day 7 post NK cell injection. Cells within the peritoneal wash were stained with antibodies against the human NK cell markers CD56 and CD45.

2.5.2. IVIS Imaging

To monitor tumour burden, the mice were injected with XenoLight D-Luciferin potassium salt (Revvity) freshly reconstituted in sterile PBS at a dose of 150mg/kg, assuming a weight of 25g. The optimal time to quantify tumour burden post-luciferin injection was found to be 20 minutes based on a luciferin kinetic curve test done with this model. The mice were anesthetized by isoflurane and tumour burden was quantified by bioluminescence using an IVIS™ Spectrum machine (Perkin Elmer), with average radiance measurements quantified by Living Image Software within a defined region of interest (ROI), consistent across all mice from each experimental group. For the final *in vivo* experiment presented in Chapter 5, the IVIS™ Spectrum (Perkin Elmer) was replaced by the Vilber Newton 7.0.

2.6. DATA AND STATISTICAL ANALYSIS

Flow cytometry data was analyzed using FlowJo software version 10.10. All data visualization and statistical analyses were performed using GraphPad Prism 10. The Shapiro-Wilk and Kolmogorov-Smirnov tests were done to verify normal distribution prior to conducting two-tailed paired or unpaired t-tests between two groups. In cases where the sample size was sufficient, the Anderson-Darling and D'Agostino-Pearson tests were also done to confirm normal distribution. When comparing two paired groups (BL versus POD1) under multiple treatment conditions, paired t-tests were performed using the Holm- Šídák correction for multiple comparisons. Two-way ANOVA with Šídák correction for multiple comparisons was performed to determine statistical differences in cytotoxicity between BL and POD1 NK cells across each effector-to-target ratio. The cytotoxicity data is normalized to each respective BL condition at the 4:1 ratio, presented as the mean ± standard deviation.

The alpha was set to 0.05 for all analyses to determine statistical significance. Each data point represents an individual patient sample collected at either BL or POD1, which we define as a biological replicate. When specific values are highlighted in the text, these are the mean $\pm$ standard deviation.

Table 1. List of reagents

Reagent	Company	Catalogue#
Human NK cell isolation kit (contains NK cell Biotin Antibody Cocktail and NK cell Microbead Cocktail)	Miltenyi Biotec	130-092-657
Ficoll-Paque Plus	Cytiva – GE Healthcare	17-1440-03
RPMI	Life Technologies	11875176
Seahorse XF RPMI	Agilent Technologies	103576-100
GolgiPlug Protein Transport Inhibitor (containing Brefeldin A)	BD Bioscience	BDB555029
GolgiStop Protein Transport Inhibitor (containing monensin)	BD Bioscience	554724
0.5M EDTA, pH 8	Invitrogen	15575-038
Bovine serum albumin	BioShop	ALB001.100
Oligomycin A	Sigma-Aldrich	75351-5MG
FCCP	Tocris	0453/10
Rotenone	Agilent Technologies (Mito Stress Kit)	103010100
Antimycin A	Agilent Technologies (Mito Stress Kit)	103010100
2-Deoxy-D-glucose (2-DG)	Sigma-Aldrich	D8375-5G
Seahorse XF Glucose Solution, 1.0M	Agilent Technologies	103577-100
Sodium pyruvate (100mM)	Thermo Scientific	11360070
Cell Tak	Fisher Scientific	C354240
L-glutamine	Fisher Scientific	25030081
BD Pharm Lyse™ Lysing Buffer 10X	BD Bioscience	555899
BD Cytofix/cytoperm Fixation and Permeabilization Solution	BD Bioscience	554722
BD Perm/Wash Buffer, 10X	BD Bioscience	554723
Fixable Viability Stain 510	BD Bioscience	564406
Ebioscience™ Fixable Viability Dye eFluor™ 780	Thermo Scientific	65-0865-14
Human IL-2 Recombinant Protein	Peprotech	200-02-50UG
Human IL-12 p70 Recombinant Protein	Peprotech	200-12H-10UG
Human IL-2 (carrier-free)	R&D Systems	202-IL-050/CF
BD Horizon CFSE	BD Bioscience	565082
Cell Proliferation Dye eFluor® 450	Life Technologies	65-0842-90
Molecular Probes OPP (O propargyl puromycin)	Thermo Scientific	C10459

Harringtonine Ready for Reconstitution (Solid + Solvent)	MedChem Express	HY-N0862
Copper (II) sulfate pentahydrate	Sigma-Aldrich	C8027-500G
THPTA	Vector Laboratories	CCT-1010-100
Sodium L-ascorbate crystal	Sigma-Aldrich	A7631-25G
AzDye azide 647	Vector Laboratories	CCT-1482-1
Glucose Uptake-Glo Assay ™	Promega	J1342
Molecular Probes MitoTracker Deep Red FM	Thermo Fisher Scientific	M22426
Image-iT™ TMRM Reagent (mitochondrial membrane potential indicator)	Thermo Fisher Scientific	I34361
XenoLight D-Luciferin	Revvity	122799(PE)

Table 2. List of antibodies

Marker	**Fluorophore**	**Clone**	**Host Species/Isotype**	**Company**	**Cat#**
CD3	FITC	HIT3a	Mouse IgG2a, kappa	ThermoFisher Scientific	11-0039-42
CD3	Pe-Cy7	OKT3	Mouse IgG2a, kappa	BioLegend	317334
CD56	BV421	NCAM-16.2	Mouse IgG2b, kappa	BD Bioscience	562751
IFN-γ	APC	4S.B3	Mouse IgG1, kappa	eBioscience	17-7319-82
CD16	BV650	3G8	Mouse IgG1, kappa	BD Bioscience	563692
CD14	APC-Cy7	MOP9	Mouse IgG2b, kappa	BD Bioscience	557831
CD107a	PE	H4A3	Mouse	BD	555801
Glut1	AF647	202915	Mouse IgG2b, kappa	BD Bioscience	566580
CD71	R718	M-A712	Mouse	BD Bioscience	567496
CD98	BV750	UM7F8	Mouse	BD Bioscience	747390
CD36	APC-Cy7	CB38	Mouse IgG2a, kappa	BioLegend	
Granzyme B	PerCP-Cy5.5	QA16A02	Mouse IgG1, kappa	BioLegend	372212
Perforin	PE	B-D48	Mouse IgG1	BioLegend	353304

Chapter 3: Human NK cells are intrinsically dysfunctional on POD1

Rationale

The extracellular environment has a tremendous influence on the metabolic activity of immune cells. NK cells require an external stimulus, such as exogenous cytokine stimulation, activating receptor ligation, or culture with cancer cells to be able to assess their function *ex vivo*. To begin our study of the metabolic activity of dysfunctional POD1 NK cells, we first aimed to analyze the various mechanisms of NK cell function and demonstrate that dysfunction persists even after removal from whole blood. The primary objective of this chapter is to highlight that NK cells are broadly dysfunctional across a wide array of effector readouts and that this dysfunction is present within isolated NK cells. The secondary objective is to determine the type and duration of stimulation which results in the most pronounced POD1 dysfunction to be used for downstream metabolic readouts.

3.1 The frequency of peripheral blood NK cells does not change from BL to POD1

One consideration in the study of postoperative NK cell function is determining whether the observed differences are attributable to a change in circulating NK cell frequencies after surgery or whether the differences are occurring on a cell-per-cell basis. This is particularly important when assessing the function of NK cells within PBMCs or directly in whole blood, where NK cell numbers are not normalized between perioperative timepoints. To address this, we quantified NK cell abundance on BL and POD1. PBMCs were isolated from whole blood samples by density gradient centrifugation, followed by magnetic enrichment of NK cells. NK cell counts were expressed both as absolute numbers

per millilitre of whole blood and per 10^6 PBMCs (Fig. 3.1 A-B). Across a cohort of 15 surgical cancer patients, there was no significant difference in the number of circulating NK cells from BL to POD1. These findings indicate that postoperative changes in NK cell function are unlikely to be driven by differences in cell frequency, supporting a cell intrinsic basis of dysfunction.

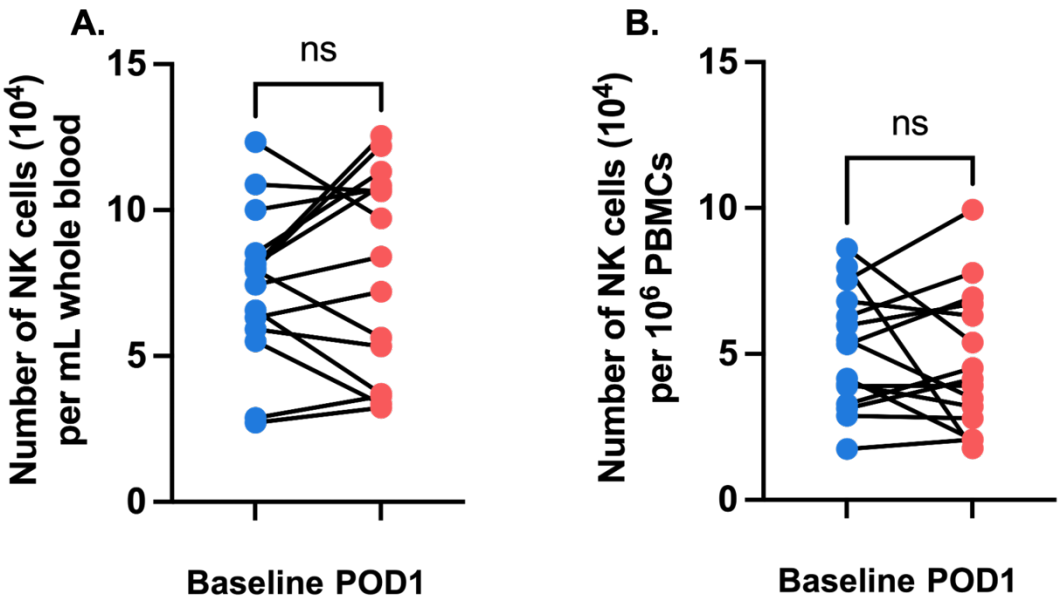

Figure 3.1. Absolute numbers of NK cells per mL of whole blood and per 10^6 PBMCs do not change after surgery. Whole blood was collected immediately before surgery (baseline) and then the day after surgery on POD1 from cancer patients. PBMCs were isolated through density gradient centrifugation and NK cells were further isolated by magnetic sorting using an autoMACS™ Neo magnetic cell separator. The total NK cell yield was used to calculate **(A)** the absolute NK cell number per mL of whole blood collected and **(B)** the absolute NK cell number per 10^6 PBMCs isolated from each corresponding blood sample (n=15). Paired two-tailed t-tests were performed to determine statistical significance. Normality was confirmed using the Anderson-Darling, D'Agostino-Pearson, Shapiro-Wilk, and Kolmogorov-Smirnov tests. ns: not significant.

Human circulating NK cells can be subdivided based on CD56 and CD16 surface expression most commonly into $CD56^{dim}CD16^{bright}$ and $CD56^{bright}CD16^{dim}$, though more subsets have been reported[222]. In our analyses, three predominant NK cell subsets were identified: $CD56^{bright}$, $CD56^{dim}$ and $CD16^{-}$ (Fig. 3.2). Consistent with previous reports[222], the $CD16^{-}$ subset increased following cytokine stimulation (Fig. 3.2A-B), and is associated with a corresponding decrease in the $CD56^{dim}$ frequency. Across all samples, the $CD56^{dim}$ subset made up most of the bulk NK cell population (average frequency of 56.67 $\pm$12.18% at BL), while the $CD56^{bright}$ made up the least (average frequency of 6.76 $\pm$3.242% at BL) (Fig. 3.3). The $CD16^{-}$ population comprised an intermediate proportion with an average frequency of 26.07 $\pm$9.271% at BL (Fig. 3.3). Importantly, there were no significant differences in the frequencies of each subset from BL to POD1. These data indicate that postoperative changes in NK cell function are not attributable to shifts in subset composition, further supporting a cell intrinsic mechanism of dysfunction.

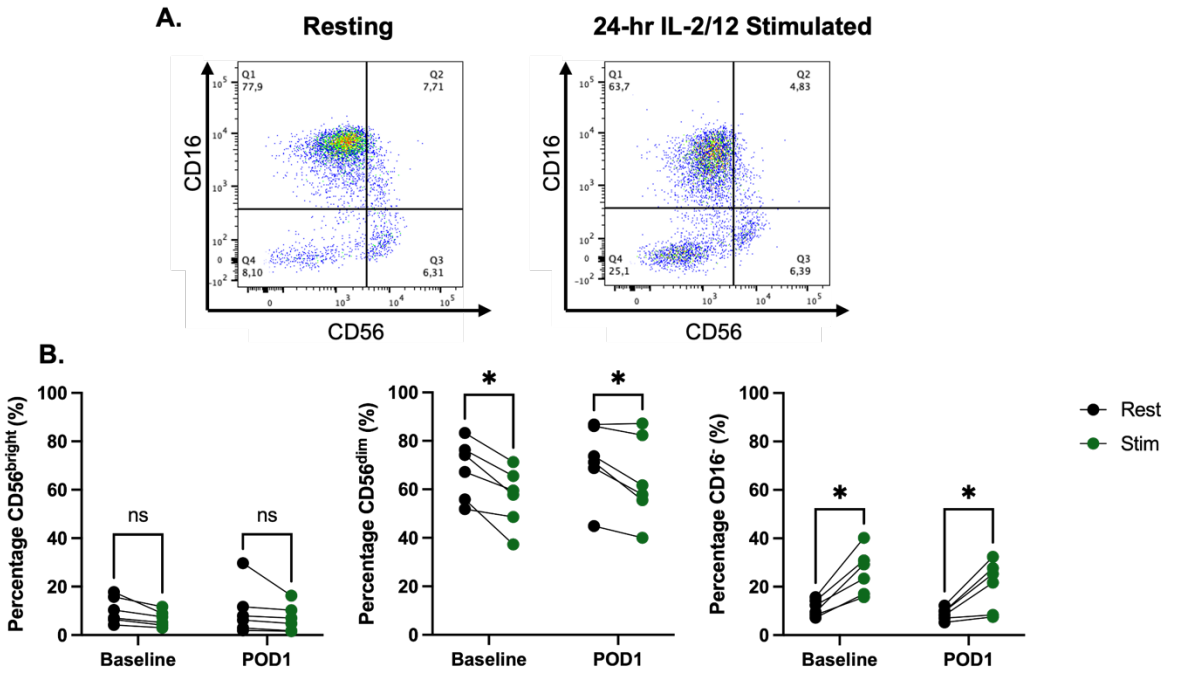

Figure 3.2. Isolated BL and POD1 NK cells can be divided into three distinct subsets based on their surface expression of CD56 and CD16, which shift upon cytokine stimulation. Cryopreserved patient-matched BL and POD1 NK cells were thawed and rested for 1 hour with 100U/mL rhIL-2 at 37°C in 5% CO_2. The NK cells were then either stimulated for 24 hours with IL-2/12 (400U/mL; 20ng/mL) or cultured in 100U/mL IL-2 for the full 24 hours, referred to as the "resting" condition. The cells were then stained for the extracellular NK cell surface markers CD56 and CD16. The data was acquired on a BD LSR Fortessa flow cytometer. **A)** Representative flow cytometry plots. **B)** NK cell subset frequency shifts in n=6 BL and POD1 NK cells with IL-2/12 stimulation. Paired two-tailed t-tests were performed to determine statistical significance with Holm-Šídák correction for multiple comparisons. Normality was confirmed using the Shapiro-Wilk, and Kolmogorov-Smirnov tests. ns: not significant, *$p<0.05$

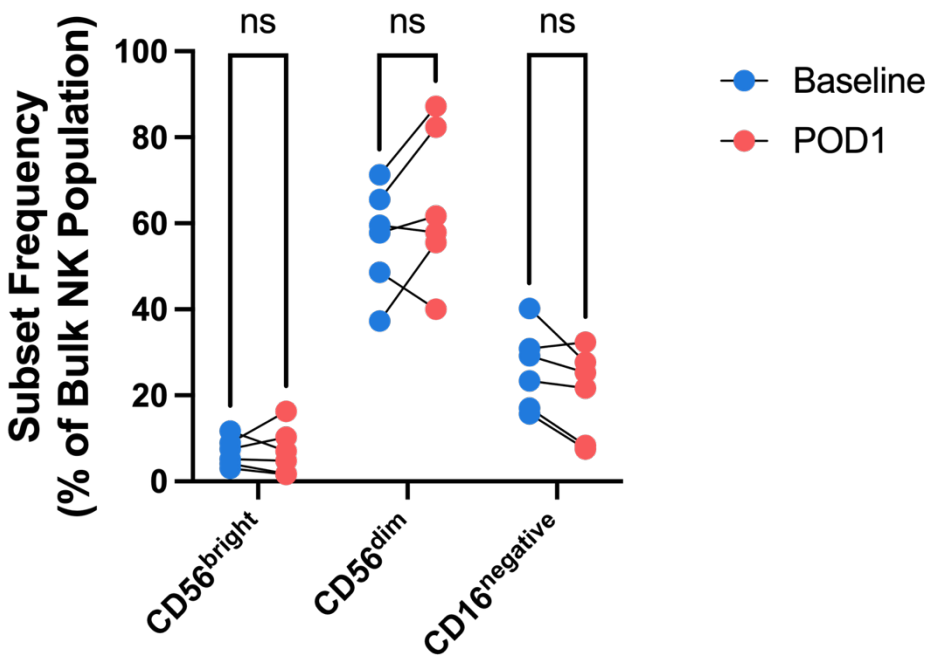

Figure 3.3. The frequencies of CD56^{dim}, CD56^{bright}, and CD16^{-} peripheral blood NK cell subsets do not change from BL to POD1. The frequency of each subset in baseline and POD1 NK cells was measured following 24 hours of IL-2/12 stimulation in isolated NK cells (n=5). The data was acquired on a BD LSR Fortessa flow cytometer. Paired two-tailed t-tests were performed to determine statistical significance with Holm-Šídák correction for multiple comparisons. Normality was confirmed using the Shapiro-Wilk, and Kolmogorov-Smirnov tests. ns: not significant.

3.2 POD1 NK cells are functionally impaired within whole blood and PBMCs

To assess NK cell function in a physiologically relevant context, fresh whole blood was stimulated for 24 hours with IL-2/12 (400U/mL; 20ng/mL) at BL and on POD1. Production of IFN-γ, as well as granzyme B and perforin content were measured within the NK cell population identified by the gating strategy depicted in Figure 3.4A. Following stimulation, POD1 NK cells exhibited a marked reduction in functional responsiveness compared to BL. Specifically, IFN-γ production was significantly decreased (mean 23.01$\pm$11.78% responsive NK cells on BL and only 11.46 $\pm$8.211% responsive on POD1; p=0.0008) as well as their granzyme B content [mean BL median fluorescence intensity (MFI) of 3940 $\pm$1640 and mean POD1 MFI of 2562 $\pm$996.7; p=0.0472] (Fig. 3.4B and C). This reduction in granzyme B was observed in both the resting and IL-2/12 stimulated conditions. In comparison, perforin 1 levels were not significantly different in the stimulated condition (mean BL MFI of 4406 $\pm$1498 and mean POD1 MFI 4558 $\pm$1014; p=0.69) (Fig. 3.4D). Interestingly, perforin levels were modestly increased on POD1 (p=0.0355) compared to BL in the resting condition.

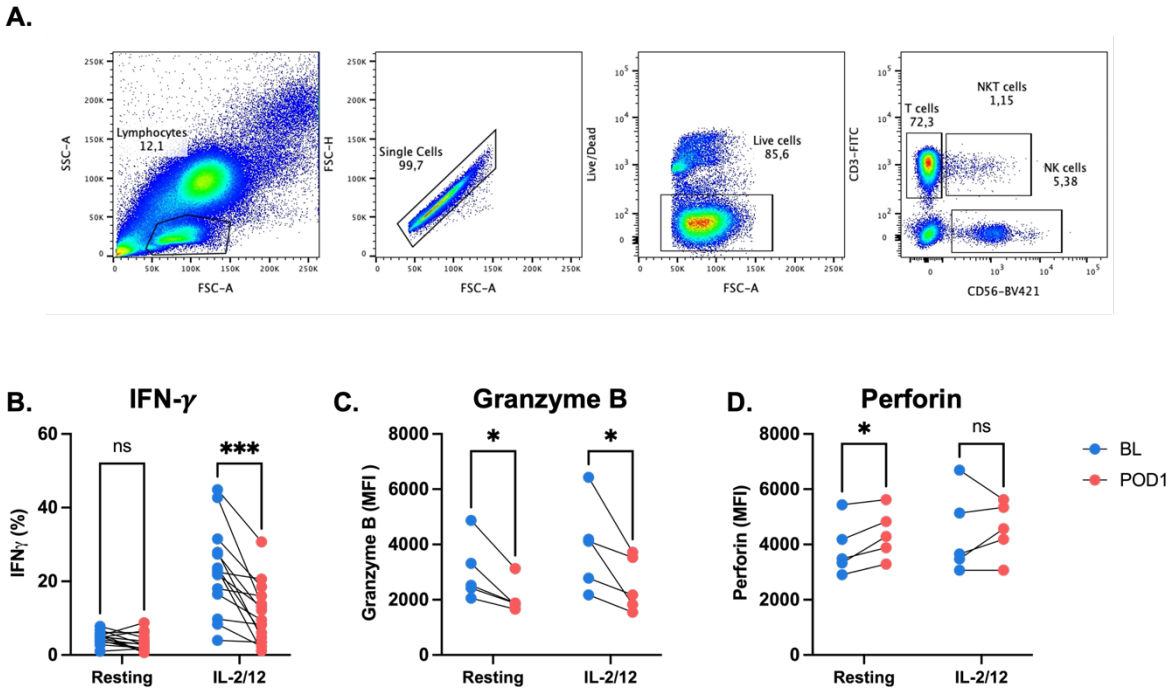

Figure 3.4. Whole blood POD1 NK cells have a dysfunctional response to IL-2/12 stimulation, measured through production of IFN-γ, granzyme B, and perforin. Fresh patient-matched baseline (BL) and POD1 whole blood was collected and stimulated for 24 hours with IL-2/12 (400U/mL; 20ng/mL) or left unstimulated for an equivalent length of time at 37°C in 5% CO_2. Protein transport was blocked for the final 12-16 hours of stimulation. The red blood cells were lysed, and the remaining cells were stained for viability and the extracellular markers CD3 and CD56. The cells were then fixed, permeabilized, and stained for intracellular markers. The data was acquired on a BD LSR Fortessa flow cytometer. **A)** Representative gating strategy depicting the identification of NK cells within whole blood. The response to IL-2/12 at BL and on POD1 was determined by **(B)** the percentage (%) of NK cells containing intracellular IFN-γ (n=14) as well as the median fluorescence intensity (MFI) of the intracellular cytolytic mediators granzyme B (n=5) **(C)** and perforin (n=5) **(D)**. Paired two-tailed t-tests were performed to determine statistical significance with Holm-Šídák correction for multiple comparisons. Normality was confirmed using the Anderson-Darling, D'Agostino-Pearson, Shapiro-Wilk, and Kolmogorov-Smirnov tests. ns: not significant; *p<0.05; **p<0.01; ***p<0.001.

Following these observations in whole blood, NK cell function was next assessed following isolation of PBMCs to determine whether functional impairments persisted outside of the postoperative systemic environment. A subset of $1e^6$ PBMCs per timepoint were either stimulated for 24 hours with IL-2/12 (400U/mL; 20ng/mL) or rested in a maintenance dose of IL-2 (100U/mL) for the same length of time. As was done in whole blood, the production of IFN-γ, as well as granzyme B and perforin content were measured. On BL, a mean of 32.58 $\pm$19.77% of NK cells were responsive to stimulation, while only 16.56 $\pm$4.702% were responsive on POD1, indicating a trend (p=0.07) in reduced production of IFN-γ on POD1 (Fig. 3.5A). In terms of cytolytic granule content, granzyme B was significantly (p=0.0059) down with a mean MFI of 3714 $\pm$373.9 on BL and only 2968 $\pm$387.6 on POD1. The levels of perforin did not change from BL to POD1 (p=0.67) (Fig 3.5 B-C). In all, we have demonstrated that postoperative NK cell dysfunction is detectable within whole blood where all suppressive factors are present and persists upon PBMC isolation in which soluble factors are removed.

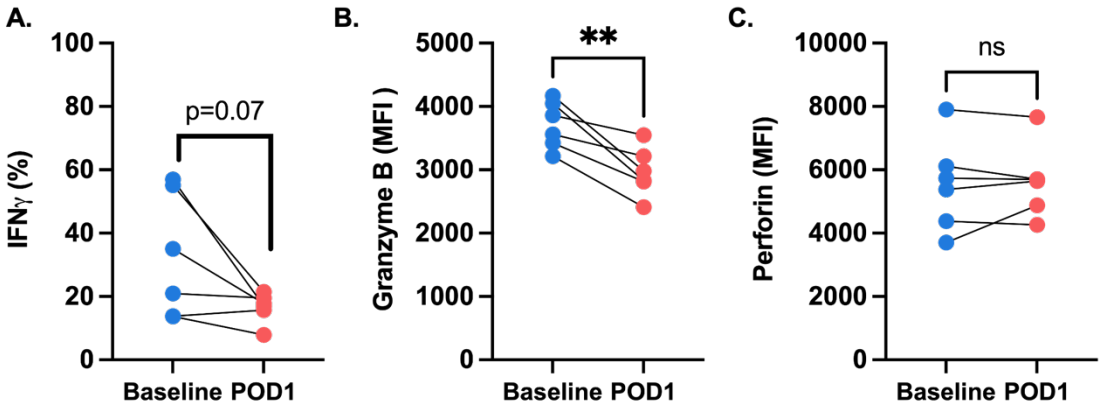

Figure 3.5. NK cells within PBMCs are dysfunctional in response to IL-2/12 stimulation on POD1. Cryopreserved patient-matched BL and POD1 PBMCs were thawed, rested for 1 hour in 100U/mL IL-2, and stimulated for 24 hours with IL-2/12 (400U/mL; 20ng/mL) at 37°C in 5% CO_2. Protein transport was blocked for the final 4 hours of stimulation. At the end of the stimulation period, the cells were stained for viability and extracellular markers (CD3 and CD56). The cells were then fixed, permeabilized, and stained for intracellular markers. The data was acquired on a BD LSR Fortessa flow cytometer. The response to IL-2/12 at BL and on POD1 was determined by **(A)** the percentage (%) of NK cells containing intracellular IFN-γ as well as the median fluorescence intensity (MFI) of the intracellular cytolytic mediators granzyme B **(B)** and perforin (n=6) **(C)**. N=6 for all. Paired two-tailed t-tests were performed to determine statistical significance. Normality was confirmed using the Shapiro-Wilk, and Kolmogorov-Smirnov tests. ns: not significant; *p<0.05; **p<0.01. Reproduced from Scaffidi, M and Mistry, H. et al. (in press). Surgical stress triggers widespread impairment of NK cell cytotoxicity and cytokine release. Cancer Immunology, Immunotherapy. DOI: 10.1007/s00262-026-04438-4, under a Creative Commons Attribution 4.0 International licence.

3.3 Postoperative NK cell dysfunction persists in isolated NK cells

To further determine whether postoperative NK cell dysfunction is cell-intrinsic, NK cells were isolated from BL and POD1 whole blood samples, cryopreserved, and later used in functional assays. To assess the IFN-γ response to cytokine stimulation, patient-matched isolated NK cells from both perioperative timepoints were thawed and stimulated for 24 hours with IL-2/12 (400U/mL; 20ng/mL). Figure 3.6A shows representative plots of the BL and POD1 response in bulk NK cells. The responses of the three NK cell subsets are shown in Figure 3.6B. Of the three subsets, the $CD56^{bright}$ NK cells were the most responsive with a mean of 77.01% responding at BL. The $CD56^{dim}$ subset had the lowest response with a mean of 33.2% of NK cells responding at BL, and the $CD16^{-}$ subset had an intermediate response with a BL mean of 53.66%. All three subsets produced significantly less IFN-γ on POD1 compared to BL. Altogether, bulk POD1 NK cells were functioning at an average of 55.5% of their BL capacity.

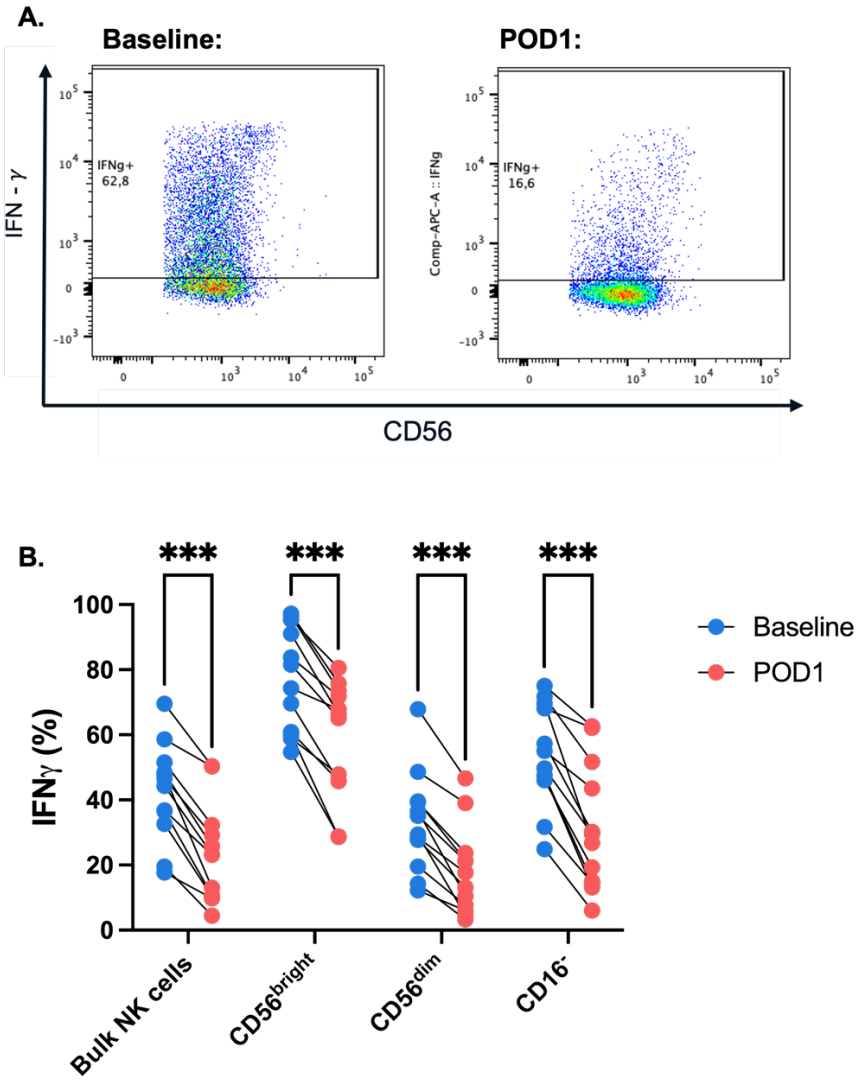

Figure 3.6. Isolated POD1 NK cells have significantly impaired IFN-γ production in response to IL-2/12 stimulation, which spans across the CD56^{bright}, CD56^{dim}, and CD16^{-} subsets. Cryopreserved patient-matched BL and POD1 isolated NK cells were thawed, rested for 1 hour in 100U/mL IL-2, and stimulated for 24 hours with IL-2/12 (400U/mL; 20ng/mL) at 37°C in 5% CO_2. Protein transport was blocked for the final 4 hours of stimulation. At the end of the stimulation period, the cells were stained for viability and the extracellular markers CD16 and CD56 to stratify the NK cell subsets. The cells were then fixed, permeabilized, and stained for intracellular IFN-γ. The data was acquired on a BD LSR Fortessa flow cytometer. **A)** Representative flow cytometry plots showing the bulk percentage of responsive NK cells (IFN-γ+) at baseline and on POD1 from one surgical cancer patient. **B)** The percentage of IFN-γ-producing NK cells within the bulk NK cell population as well as the response stratified between the CD56^{bright}, CD56^{dim} and CD16^{-} subsets (n=12). Paired two-tailed t-tests were performed to determine statistical significance with Holm-Šídák correction for multiple comparisons. Normality was confirmed using the Anderson-Darling, D'Agostino-Pearson, Shapiro-Wilk, and Kolmogorov-Smirnov tests. ***p<0.001.

To indirectly measure cytotoxic function, isolated BL and POD1 NK cells were co-cultured at a 2:1 ratio with K562 target cells for 4 hours, and degranulation was measured by CD107a surface expression. Figure 3.7A shows representative plots of the BL and POD1 degranulation response in bulk NK cells. An average of 59.3% of the $CD56^{bright}$ NK cells, 41.1% of the $CD56^{dim}$, and 61.13% of the $CD16^{-}$ were degranulating at BL (Fig. 3.7B). All subsets showed a decrease in CD107a levels on POD1 compared to BL, with the $CD56^{bright}$, $CD56^{dim}$, and total bulk NK cells being significant. Overall, bulk POD1 NK cells retained approximately 76% of their baseline degranulation capacity.

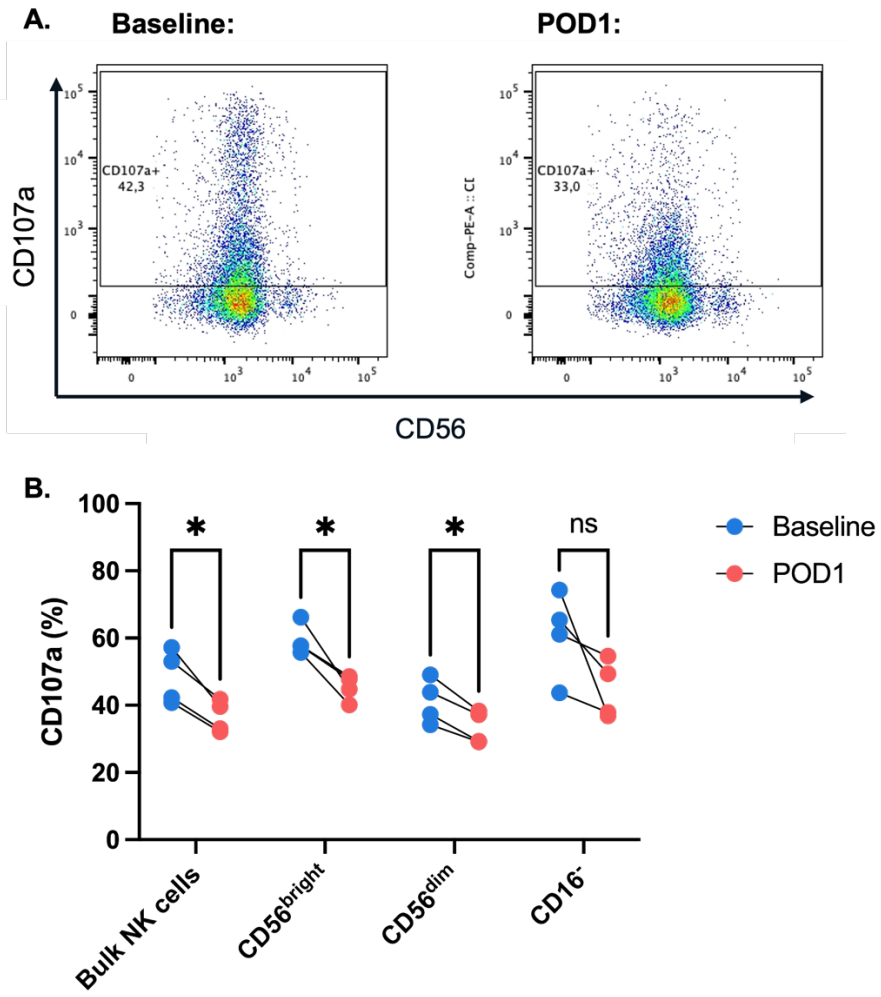

Figure 3.7. Isolated POD1 NK cells have a significantly impaired ability to degranulate in response to co-culture with K562 target cells, which spans across the CD56^{bright}, CD56^{dim}, and CD16^{-} subsets. Cryopreserved patient-matched BL and POD1 NK cells were thawed, rested for 1 hr with 100U/mL IL-2, and co-cultured for 4 hours with K562 tumour targets along with monensin (GolgiStop) and an anti-CD107a antibody at 37°C in 5% CO_2. Following the co-culture period, the cells were stained for viability and NK cell identification markers (CD16 and CD56). The data was acquired on a BD LSR Fortessa flow cytometer. **A)** Representative flow cytometry plots showing the percentage (%) of responsive NK cells (CD107a+) at baseline and on POD1 from one surgical cancer patient. **B)** Degranulation measured across the peripheral NK cell subsets at baseline and on POD1 (n=4). Paired two-tailed t-tests were performed to determine statistical significance with Holm-Šídák correction for multiple comparisons. Normality was confirmed using the Shapiro-Wilk test. ns: not significant; *p<0.05.

To directly investigate NK cell cytotoxic function across distinct activation pathways, we co-cultured BL and POD1 NK cells with three different cancer cell lines each representing a different mechanism of killing. K562 cells express the NKG2D ligands MICA and MICB[223] while OVCAR8 cells express low levels of MHC class I[224]. SKOV3 cells express HER2 which is recognized by the monoclonal antibody trastuzumab (Herceptin™), thereby enabling measurement of ADCC[225]. The SKOV3 cells were pre-treated with trastuzumab or the corresponding isotype control antibody for 30min prior to co-culture with the NK cells. The cytotoxicity data presented in Figure 3.8 are shown as the killing normalized to each respective BL 4:1 ratio. NK cell-mediated killing was the most significantly reduced towards K562 cells on POD1 across all effector-to-target ratios (Fig. 3.8A), functioning at approximately 70% of their BL capacity at the 4:1 ratio. We observed a significant reduction in the killing of POD1 NK cells against OVCAR8 targets with the average killing at the 4:1 ratio also being approximately 70% ($p=0.0057$) of the BL capacity (Fig. 3.8B). We did not observe a significant reduction in ADCC with the POD1 NK cells functioning at about 82% of their BL killing capacity ($p=0.27$) against SKOV3 cells at a 4:1 ratio (Fig. 3.8C). SKOV3 killing in the isotype-treated group was very low for both BL and POD1 NK cells, highlighting ADCC as the major mechanism of killing. Despite the activation signals being distinct among these cell lines, in each instance killing was mediated through cytolytic granules. To assess whether TRAIL-mediated killing was impaired on POD1, we co-cultured BL and POD1 NK cells with the colorectal cancer cell line HCT116. These cells are known to be highly sensitive to TRAIL-mediated killing[226]. We observed a trend towards reduction in TRAIL-mediated killing in POD1 NK cells which were functioning at an average of about 79% ($p=0.051$) of their BL capacity at the 4:1 effector-to-target ratio.

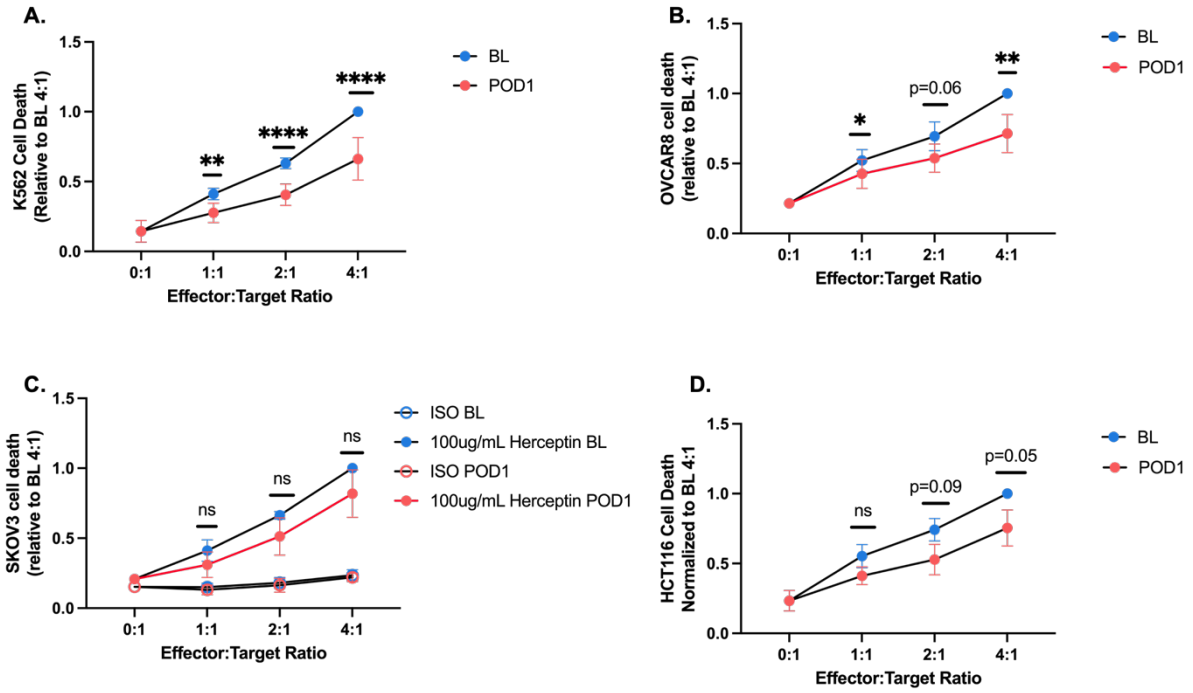

Figure 3.8. NK cell cytotoxicity against K562, OVCAR8, SKOV3, and HCT116 tumour targets is impaired on POD1. Cryopreserved patient-matched isolated BL and POD1 NK cells were thawed, rested for 1 hour in 100U/mL IL-2 and then co-cultured with several tumour targets at 37°C in 5% CO_2. The tumour targets were first labelled with Cell Proliferation Dye eFluor 450 before co-culture with the NK cells at 4:1, 2:1 or 1:1 effector-to-target ratios. Viability of the target cells was assessed by staining the cells with fixable viability stain eFluor780. Adherent cells were dissociated with trypsin-EDTA for 3min prior to staining for viability. The data was acquired on a BD LSR Fortessa flow cytometer. **A)** NK cells co-cultured with K562 cells for 4 hours (n=6). **B)** NK cells co-cultured with OVCAR8 cells for 5 hours (n=7). **C)** Antibody-dependent cell-mediated cytotoxicity: NK cells co-cultured with SKOV3 cells for 5 hours (n=5). SKOV3 cells were first opsonized with trastuzumab (Herceptin™, 100ug/mL) or respective isotype antibody for 30min at 37°C in 5% CO_2. Excess antibody was removed prior to co-culture with the NK cells. **D)** NK cells co-cultured with HCT116 cells (n=5). Data is presented as the mean of all biological replicates ± standard deviation, normalized to the death measured in the BL 4:1 ratio. Two-way ANOVA with Šídák correction for multiple comparisons was performed to determine statistical significance between BL and POD1 NK cell killing at each effector-to-target ratio (*p<0.05, **p<0.01, ***p<0.001, ****p<0.0001). Reproduced from Scaffidi, M and Mistry, H. et al. (in press). Surgical stress triggers widespread impairment of NK cell cytotoxicity and cytokine release. Cancer Immunology, Immunotherapy. DOI: 10.1007/s00262-026-04438-4, under a Creative Commons Attribution 4.0 International licence.

Chapter Summary:

We have shown that POD1 NK cell dysfunction persists after isolation and removal from the immunosuppressive whole blood environment, suggesting an intrinsic reprogramming that occurs because of surgical stress. This dysfunction spans the different aspects of NK cell effector function and is present to varying degrees depending on the readout. In all, cytotoxicity-related readouts including degranulation, granzyme B levels, and direct killing consistently showed POD1 NK cells functioning between 70-80% of their measured BL capacity. Contrarily, production of IFN-γ in response to IL-2/12 stimulation showed that POD1 NK cells functioned at a mere 55% of their BL capacity. In the following chapters, metabolic readouts will be measured in response to IL-2/12 stimulation, when dysfunction is at its peak.

Chapter 4: Dysfunctional NK cells have reduced metabolic activity on POD1

Rationale

There is a well-defined connection between upregulation of metabolic activity in response to stimulation and subsequent effector function in NK cells[135,145,148,150,151]. There have been numerous studies characterizing the metabolic profile of dysfunctional NK cells across different disease states[152,158,159,171]. Previous work from our lab has formed a connection between blocking TGF-β signaling and preventing both dysfunction and reduced mTORC1 signaling in healthy NK cells within a POD1 plasma co-culture model[3]. Furthermore, we reported an overall decrease in the expression of gene sets involved in cellular respiration and OxPhos in POD1 NK cells within a single-cell RNA sequencing dataset generated from BL and POD1 PBMC samples[3]. Given the broad and profound functional suppression we observed in isolated POD1 NK cells from surgical cancer patients in Chapter 3, we sought to characterize their metabolic profile in-depth to determine whether a measurable metabolic deficiency accompanies their functional impairment in response to IL-2/12 stimulation.

4.1 OxPhos is significantly downregulated in response to cytokine stimulation in POD1 NK cells

Seahorse™ Extracellular Flux Analysis:

The most significant transcriptional differences in metabolism-associated genes were related to OxPhos and cellular respiration[3]. Due to the dynamic and interconnected nature of metabolic flux within a cell and the well-known discordance between the gene expression of

metabolic enzymes and their activity[184], we sought to measure real-time metabolic activity rates in primary human NK cells. To do this, we conducted Seahorse™ extracellular flux analysis on cytokine-stimulated isolated BL and POD1 NK cells. Briefly, cryopreserved BL and POD1 NK cells were thawed and stimulated for 24 hours with IL-2/12 (400U/mL; 20ng/mL). Since Seahorse™ assays require a substantial number of pure NK cells which are difficult to obtain from patient samples, most of the cells were used for the stimulated condition. The number of NK cells plated per technical replicate was optimized to be 4-5e^5, with the number of cells matched between BL and POD1 for each patient. The viability of the NK cells was measured at 4 and 24 hours post-stimulation to ensure that no notable loss in viability was occurring over the course of the stimulation period (Supp. Fig. 1). When extra cells remained, the patient-matched BL and POD1 NK cells were combined for the resting condition in which the cells were treated with maintenance IL-2 (100U/mL) for 24 hours as a confirmation of a metabolic response to stimulation. We completed both the glycolytic and mitochondrial stress tests designed by Agilent[187,188] to assess parameters related to the NK cells' glycolytic capacity and oxidative metabolism. Table 3 outlines the injection strategies for both the mitochondrial and glycolytic stress tests. Figure 4.1A depicts a representative ECAR (mpH/min) plot showing BL (blue) and POD1 (red) IL-2/12 stimulated NK cells and the combined resting (black) condition for one patient for a glycolytic stress test, along with the corresponding OCR response to the injection compounds in Figure 4.1B. The ECAR values generated from the glycolytic stress test were used to calculate glycolysis, glycolytic capacity and glycolytic reserve as previously described[188] for our sample size of seven cancer surgery patients (Fig. 4.2). None of these glycolytic parameters were found to be significantly different between BL and POD1 cytokine-stimulated isolated NK cells in our patient cohort. The basal glycolysis of IL-2/12-

stimulated BL NK cells was an average of 10.87 ±5.565mpH/min and 7.83 ±3.928mpH/min on POD1, which is the only glycolytic parameter that approached statistical significance (p=0.05).

Table 3. Injection compounds for the Seahorse Glycolytic and Mitochondrial Stress Tests

Compound Name	**Seahorse Test**	**Target/Mechanism of Action**
Oligomycin	Mito and Glycolytic Stress Tests	Blocks ATP synthase (Complex V of the ETC)
Glucose	Glycolytic Stress Test	Fuels glycolysis
2-deoxyglucose	Glycolytic Stress Test	Glucose analog which inhibits glycolysis
FCCP	Mito Stress Test	Stimulates the ETC to function at maximum capacity
Rotenone/Antimycin A	Mito Stress Test	Blocks Complex I and III of the ETC, respectively
Monensin	Mito Stress Test	Na+/K+ ionophore

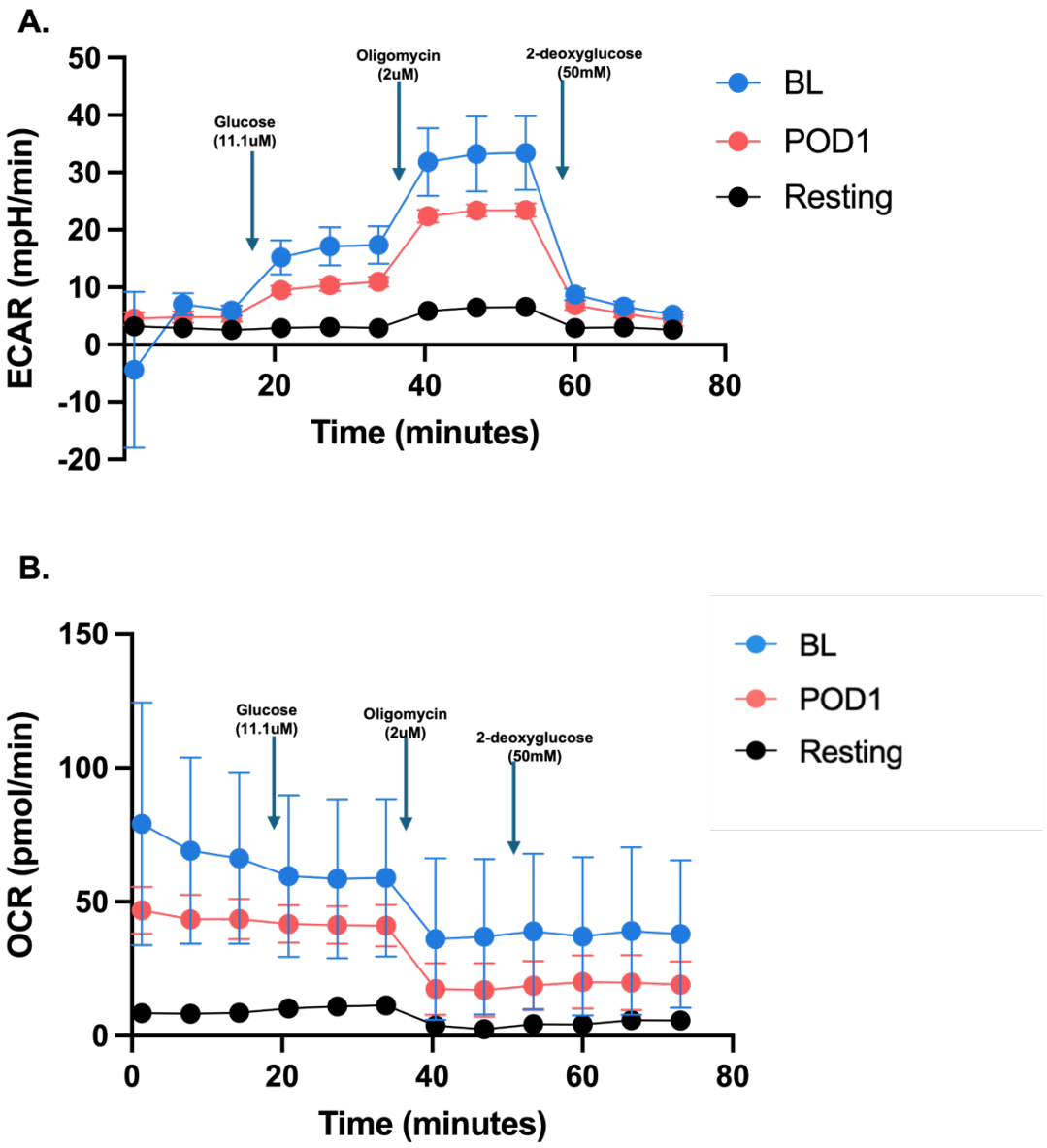

Figure 4.1. Representative ECAR and corresponding OCR plots from a glycolytic stress test depicting the metabolic profiles of baseline, POD1, and associated resting NK cells from one patient. Cryopreserved, patient-matched baseline (BL) and POD1 NK cells were thawed, rested for 1 hour in 100U/mL IL-2, and stimulated for 24 hours with IL- 2/12 (400U/mL; 20ng/mL) at 37°C in 5% CO2. The cells were washed in RPMI media (serum-free with no buffering capacity) and supplemented with 2mM glutamine, pH 7.4 +/-0.03. After washing, 4-5e^5 cells were seeded per technical replicate, with 2-3 technical replicates per condition onto a Seahorse XFe96-well plate coated with Cell Tak (22.4ug/mL). A Seahorse^{TM} Glycolytic Stress Test was performed using a Seahorse^{TM} XFe96 Extracellular Flux Analyzer. The data is normalized to cell number. Injection strategy for the Seahorse^{TM} XF Glycolytic Stress Test: glucose (11.1mM), oligomycin (2uM), and 2-deoxyglucose (2-DG) (50mM). **A)** Representative ECAR plot and (**B)** Corresponding OCR plot.

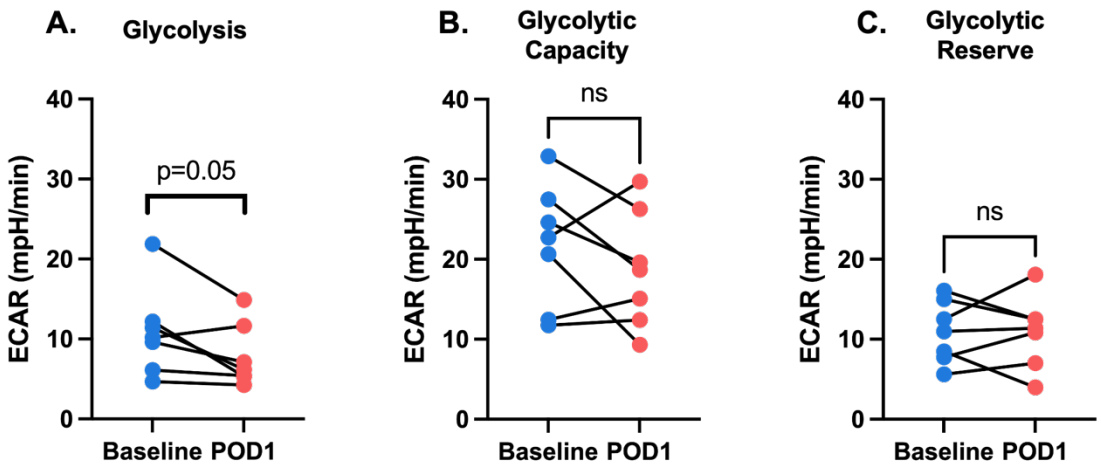

Figure 4.2. Glycolysis measured in response to 24 hours of IL-2/12 stimulation is not significantly reduced in POD1 NK cells. A) Glycolysis, **(B)** glycolytic capacity and **(C)** glycolytic reserve are all parameters related to the glycolytic activity of NK cells that are calculated using the ECAR measurements generated in response to the Seahorse™ Glycolytic Stress Test injection strategy: glucose (11.1mM), oligomycin (2uM), and 2-deoxyglucose (2-DG) (50mM). N=7. Paired two-tailed t-tests were performed to determine statistical significance. ns: not significant; *p<0.05. Normality was confirmed using the Shapiro-Wilk and Kolmogorov-Smirnov tests.

Conducting a mitochondrial stress test to assess OxPhos in the NK cells follows the same workflow. However, the injection strategy differs, with oligomycin used for both glycolytic and mitochondrial stress tests (Table 3). Figure 4.3A depicts a representative OCR (pmol/min) plot, and Figure 4.3B shows the corresponding ECAR response to the injection compounds. These plots clearly demonstrate that when OxPhos is inhibited by oligomycin, NK cells exhibited an immediate compensatory spike in glycolysis, indicated by the increase in ECAR. The OCR data generated from the mitochondrial stress test were used to calculate basal respiration, maximal respiration, SRC and ATP-linked respiration as previously described[187] for our sample size of six cancer surgery patients (Figure 4.4). The basal respiration of IL-2/12-stimulated NK cells decreased from an average of 42.59 ±10.03pmol/min on BL to 35.08 ±5.665pmol/min on POD1, however this was not significant (p=0.157) (Fig. 4.4A). Similarly, ATP-linked respiration dropped from an average of 39.97 ±10.46pmol/min at BL to 32.96 ±4.98pmol/min, which was also not significant (p=0.158) (Fig. 4.4C). The maximal respiration and SRC, which highlight the cells' ability to respond to a strong energetic demand, were both significantly reduced on POD1. The average maximal respiration exhibited a stark drop from 133.9 ±25.98pmol/min at BL to just 78.24 ±8.798pmol/min on POD1 (p=0.0036). Similarly, the SRC went from 91.29 ±18.95pmol/min at BL to 43.16 ±7.566pmol/min on POD1 (p=0.0010) (Fig. 4.4B and D). Overall, the average maximal respiration attained by POD1 NK cells was about 58% of the average BL capacity, and the SRC in POD1 NK cells was about 47% of the BL capacity within this patient cohort.

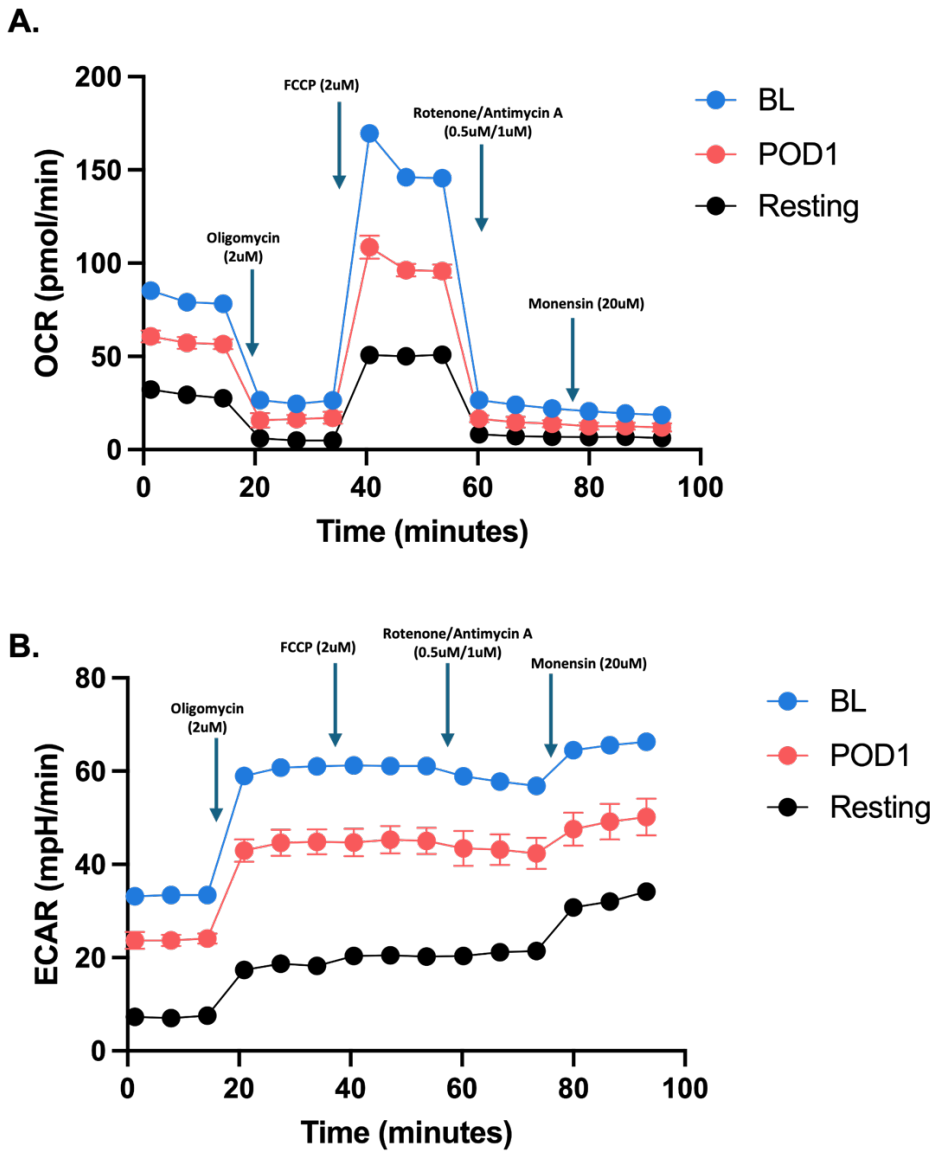

Figure 4.3. Representative OCR and corresponding ECAR plots from a mitochondrial stress test depicting the metabolic profiles of baseline, POD1, and associated resting NK cells from one patient. Cryopreserved, patient-matched baseline (BL) and POD1 NK cells were thawed, rested for 1 hour in 100U/mL IL-2, and stimulated for 24 hours with IL- 2/12 (400U/mL; 20ng/mL) at 37°C in 5% CO2. The cells were washed in media (no buffering capacity or phenol red) and supplemented with 11.1mM glucose, 1mM pyruvate and 2mM glutamine, pH 7.4 +/-0.03. After washing, 4-5e^5 cells were seeded per technical replicate (2-3 technical replicates per condition) onto a Seahorse XFe96-well plate coated with Cell Tak (22.4ug/mL). A Mitochondrial Stress Test was performed using a Seahorse^{TM} XFe96 Extracellular Flux Analyzer. The data is normalized to cell number. Injection strategy for the Seahorse^{TM} XF Mitochondrial Stress Test: oligomycin (2uM), FCCP (2uM), rotenone/antimycin A (0.5uM/1uM), and monensin (20uM). **A)** Representative OCR plot and (**B)** Corresponding ECAR plot.

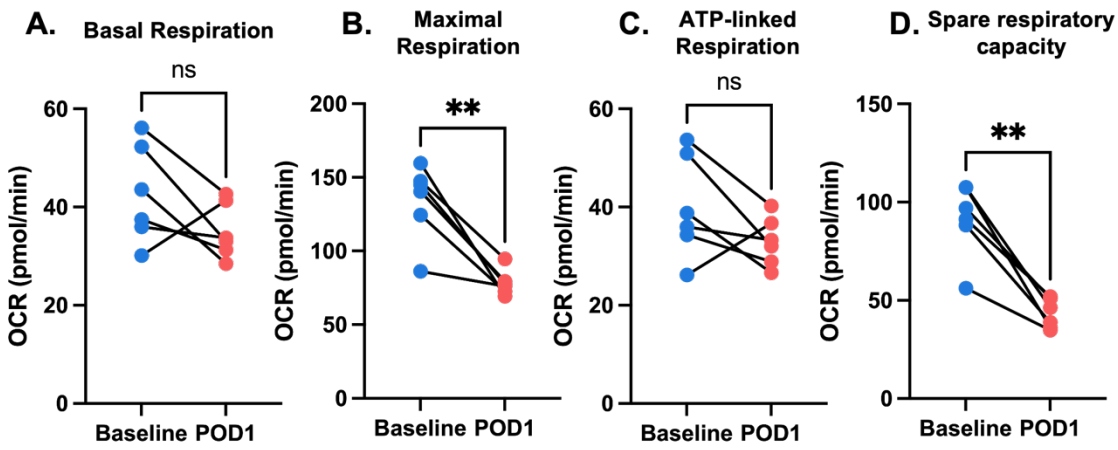

Figure 4.4. OxPhos is strongly reduced in POD1 NK cells. A) Basal respiration, **(B)** maximal respiration, **(C)** ATP-linked respiration and **(D)** spare respiratory capacity are all parameters related to the NK cells' ability to perform OxPhos that are calculated using the OCR measurements generated in response to the Seahorse™ Mitochondrial Stress Test injection strategy:oligomycin (2uM), FCCP (2uM), and rotenone/antimycin A (0.5uM/1uM). N=6. Paired two-tailed t-tests were performed to determine statistical significance. ns: not significant; *p<0.05; **p<0.01. Normality was confirmed using the Shapiro-Wilk and Kolmogorov-Smirnov tests.

Mitochondrial factors in BL and POD1 NK cells:

Based on the Seahorse™ results presented above, the most prominent differences were in OxPhos-related parameters. Given the importance of mitochondrial health in supporting OxPhos, we chose to measure fundamental parameters related to mitochondria within NK cells. These include measuring the overall mitochondrial mass using MitoTracker™ dye and mitochondrial membrane potential using tetramethylrhodamine (TMRM) dye. The MitoTracker Deep Red™ dye used here is a carbocyanine-based dye that accumulates within healthy active mitochondria and can indicate the total mitochondrial mass within the cells[227]. Similarly, the TMRM dye accumulates within cells with healthy mitochondria and intact membrane potentials[190]. Mitochondrial mass did not significantly change from BL to POD1 in either the resting or IL-2/12 stimulated conditions (Fig. 4.5A). Mitochondrial membrane potential decreased significantly from BL to POD1 in both the resting (mean MFI of 13308 ±6076 at BL and 10517 ±5934 on POD1) and IL-2/12-stimulated (mean MFI of 15690 ±6959 at BL and 12836 ±6967 on POD1) conditions (Fig. 4.5B). When assessing intracellular IFN-γ production within these NK cells, a trend towards reduction on POD1 was observed (mean of 52.03 ±10.92% responsive NK cells at BL and 35.25 ±14.71% responsive on POD1, p=0.075) (Fig. 4.5C). All parameters were assessed by flow cytometry, therefore detailed features of mitochondrial architecture (elongated, branched, or fragmented) were not captured. It has been previously shown that a strong positive linear correlation between mitochondrial mass and membrane potential is indicative of healthy and functional mitochondria[152]. The linear correlations between mitochondrial mass and membrane potential differed significantly from zero in both perioperative timepoints and in both the resting and IL-2/12-stimulated conditions, with the strongest

correlation being in the BL resting condition (r^2=0.9373, p=0.0015) (Fig. 4.5D). Interestingly, we did not observe any correlation between POD1 dysfunction in IFNγ production and either mitochondrial parameter (Supp. Fig. 2)

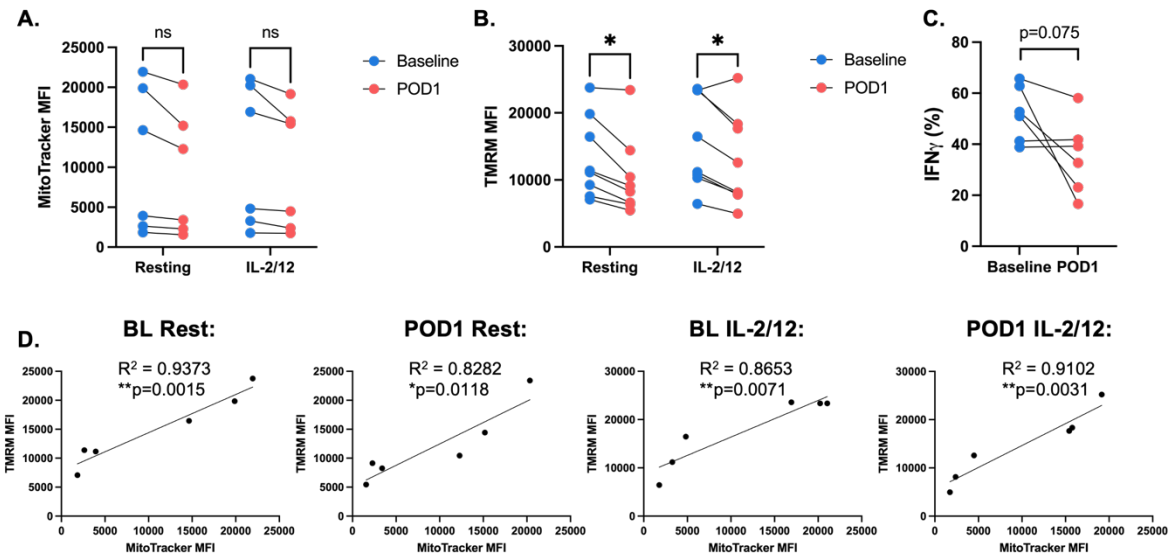

Figure 4.5. Mitochondrial membrane potential is reduced in dysfunctional POD1 NK cells. Cryopreserved patient-matched BL and POD1 NK cells were thawed, rested for 1 hr with 100U/mL IL-2, and stimulated for 24 hours with IL-2/12 (400U/mL; 20ng/mL) at 37°C in 5% CO_2. Following stimulation, cells were stained for viability followed by 400nM MitoTracker Deep Red (n=6) in **(A)** and 250nM tetramethylrhodamine (TMRM) (n=8) in **(B)**, for 30min at 37°C in 5% CO_2. The signal is presented as the median fluorescence intensity (MFI) within the bulk NK cell population, detected by flow cytometry. **C)** Associated intracellular IFN-γ production. Paired two-tailed t-tests were performed to determine statistical significance. ns: not significant; *p<0.05; **p<0.01. Normality was confirmed using the Shapiro-Wilk and Kolmogorov-Smirnov tests. **D)** Linear regression analysis between TMRM and MitoTracker signals in BL and POD1 NK cells in both the resting and IL-2/12-stimulated conditions.

4.2 Metabolic dysfunction in POD1 NK cells is associated with inefficient uptake and use of available nutrients

After establishing that the most pronounced metabolic differences in NK cells on POD1 were related to their ability to perform OxPhos, we conducted additional supporting metabolic assays to generate a more comprehensive landscape of the metabolic signature of POD1 NK cells. NK cells increase their rate of glucose uptake in response to external stimulation to meet the increased energy demand required to carry out their effector functions[150,151,228]. To assess whether surgery affects the rate of glucose uptake, we stimulated isolated BL and POD1 NK cells for 4 hours with IL-2/12 (400U/mL; 20ng/mL) or rested them in a maintenance dose of IL-2 (100U/mL) for the same duration. We measured glucose uptake at this point in the stimulation period to identify metabolic changes that may occur ahead of the functional differences observed after 24 hours. Using a bulk luminescence-based glucose uptake assay[220], we compared the response of BL versus POD1 NK cells to cytokine stimulation (Figure 4.6), with the results normalized to cell number. As expected, both BL and POD1 NK cells significantly upregulated their rate of glucose uptake 4 hours into the cytokine stimulation period (Figure 4.6A). The NK cells increased their rate of uptake with stimulation to a similar degree with an average of 46% increase (3.82 $\pm$1.335fmol/cell/min at rest to 5.572 $\pm$1.424fmol/cell/min with stimulation) in glucose uptake rate on BL, and an average of 42% increase (3.113 $\pm$1.510fmol/cell/min at rest to 4.408 $\pm$1.594fmol/cell/min with stimulation) on POD1 (Figure 4.6A). When directly comparing BL to POD1, resting BL NK cells had a significantly ($p=0.03$) higher rate of glucose uptake compared to POD1, while the difference between BL and POD1 was approaching significance ($p=0.05$) in the IL-2/12 stimulated condition (Figure 4.6B). These changes in glucose uptake rate were not accompanied by significant differences in either the

percentage of NK cells expressing the glucose transporter GLUT1 (Fig. 4.7A), nor the degree of expression (presented as the MFI; Fig. 4.7B) at the same stimulation time (4 hours). Interestingly, there was no change in expression of GLUT1 between the resting and IL-2/12 stimulated conditions at either perioperative timepoint, despite the clear increase in glucose uptake. Similar results were observed after 24 hours of IL-2/12 stimulation, where there was no significant difference in expression of GLUT1 as well as other nutrient transporters of interest including CD98, CD71 and CD36 between BL and POD1 (Fig. 4.8A-B).

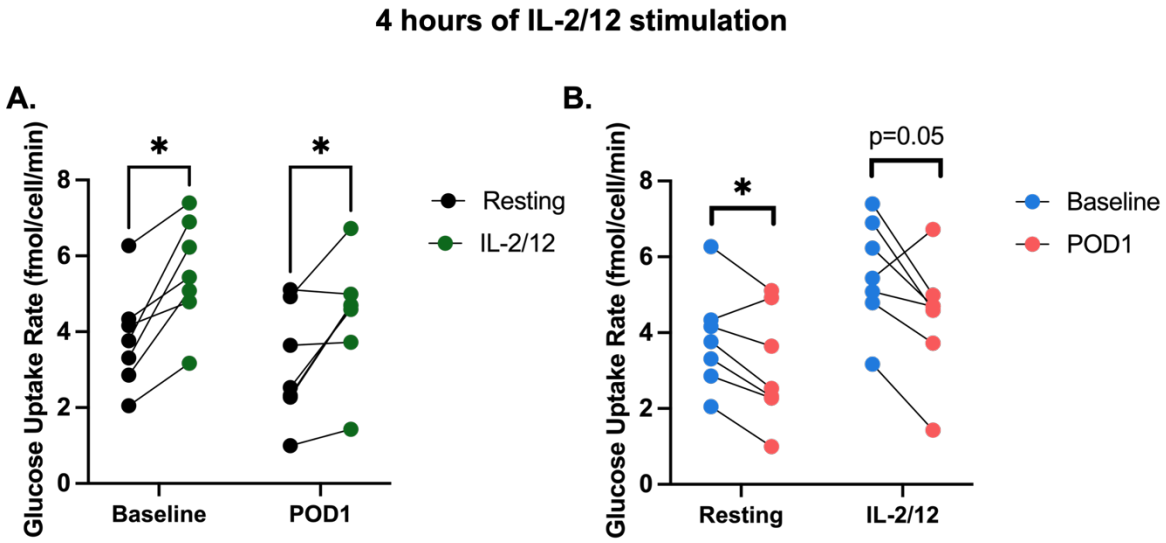

Figure 4.6. Dysfunctional POD1 NK cells have a reduced rate of glucose uptake compared to BL. BL and POD1 NK cells were stimulated for 4 hours with IL-2/12 (400U/mL; 20ng/mL) at 37°C in 5% CO_2. Assessment of glucose uptake was done using the Promega Glucose Uptake Glo™ assay kit which uses luminescence-based detection of 2DG6P to measure glucose uptake. The rate of glucose uptake was calculated using the following equation: Rate of glucose uptake = ([2DG6P] x (volume of sample)) / ((number of cells) x (time of uptake)). Shown is the rate of glucose uptake in resting (100U/mL IL-2) and 4-hour IL-2/12 (400U/mL; 20ng/mL) stimulated BL and POD1 NK cells comparing the resting and cytokine-stimulated conditions in **(A)** and comparing BL and POD1 in **(B)** within the same n=7 patient cohort. Paired two-tailed t-tests were performed to determine statistical significance with Holm-Šídák correction for multiple comparisons. *$p<0.05$. Normality was confirmed using the Shapiro-Wilk and Kolmogorov-Smirnov tests.

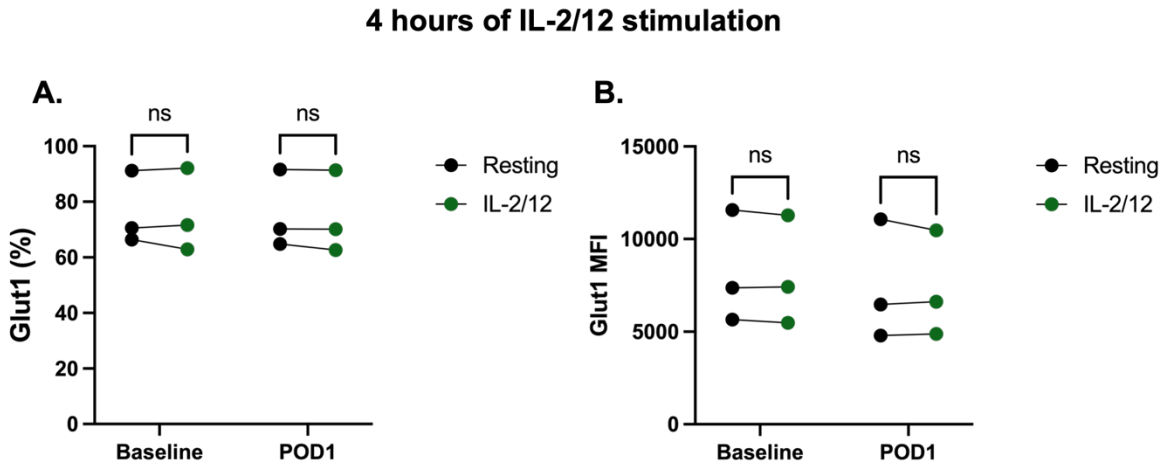

Figure 4.7. Decreased glucose uptake is not accompanied by a change in expression of GLUT1 on POD1. BL and POD1 NK cells were stimulated for 4 hours with IL-2/12 (400U/mL; 20ng/mL) at 37°C in 5% CO_2. Following stimulation, expression of GLUT1 on the NK cells was assessed by flow cytometry. Expression in resting and 4-hour IL-2/12 stimulated bulk NK cells presented as **(A)** percentage (%) of the NK cell population and **(B)** median fluorescence intensity (MFI) (n=3). Paired two-tailed t-tests were performed to determine statistical significance with Holm-Šídák correction for multiple comparisons. ns: not significant. Normality was confirmed using the Shapiro-Wilk test.

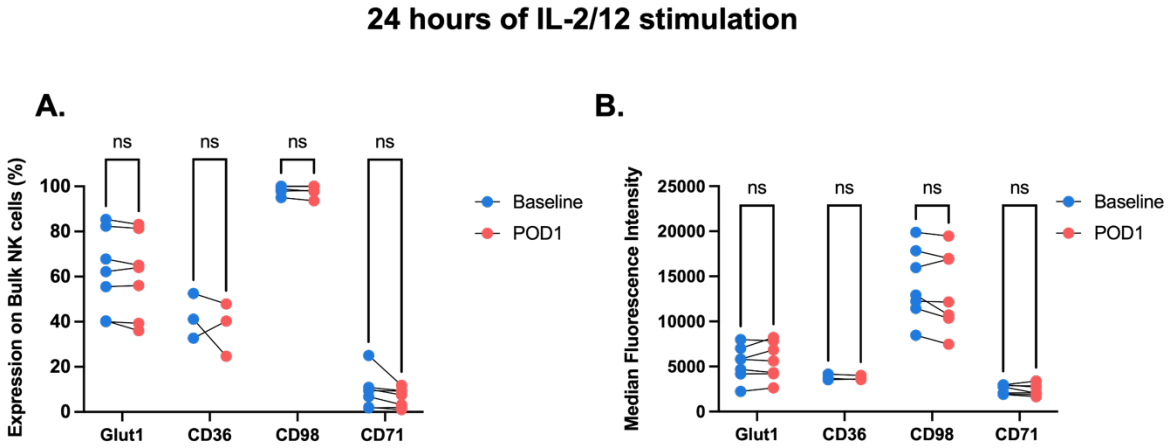

Figure 4.8. The expression of nutrient transporters does not change from BL to POD1 in 24-hour IL-2/12 stimulated NK cells. BL and POD1 NK cells were stimulated for 24 hours with IL-2/12 (400U/mL; 20ng/mL) at 37°C in 5% CO_2. Following stimulation, expression levels of GLUT1, CD36, CD98 and CD71 were assessed by flow cytometry. Expression in resting and 24-hour IL-2/12 stimulated bulk NK cells presented as **(A)** percentage (%) of the NK cell population and **(B)** median fluorescence intensity (MFI) (n=7). Paired two-tailed t-tests were performed to determine statistical significance with Holm-Šídák correction for multiple comparisons. ns: not significant. Normality was confirmed using the Shapiro-Wilk and Kolmogorov-Smirnov tests.

4.3 BL and POD1 NK cells have the same reliance on glycolysis and OxPhos to carry out their effector functions

To assess whether metabolic inhibition affects BL or POD1 NK cells differently, isolated BL and POD1 NK cells were cultured for 24 hours with oligomycin (40nM) or 2-DG (10mM), or the corresponding vehicle control, which was DMSO for oligomycin and complete media for 2-DG. The NK cells were stimulated with IL-2/12 (400U/mL; 20ng/mL) for the duration of the 24-hour culture, and production of IFN-γ was measured thereafter. As expected, the $CD56^{bright}$ subset produced the most IFN-γ overall, the $CD56^{dim}$ subset produced the least, and the $CD16^{-}$ was intermediate (Fig. 4.9A-B). All subsets had significantly reduced IFN-γ production at both the BL and POD1 timepoints when OxPhos was blocked with oligomycin except for the $CD16^{-}$ subset on POD1 which approached significance (p=0.05) (Fig. 4.9A). Bulk BL NK cells were functioning at an average of 52.6% capacity in the presence of oligomycin compared to the DMSO control, while the POD1 bulk NK cells were functioning at an average of 47.2% capacity with oligomycin (Fig. 4.9A). All subsets showed a trend in the reduction of IFN-γ production when glycolysis and glycolysis-driven OxPhos were blocked by 2-DG at both timepoints (Fig. 4.9B). When looking at bulk NK cells, the trend was approaching significance at both BL and POD1 (p=0.08 for both) (Fig. 4.9B). The BL bulk NK cells were functioning at an average of 31% capacity in the presence of 2-DG compared to the media control and the POD1 bulk NK cells were functioning at 28.6% capacity with 2-DG (Fig. 4.9B).

The effect of metabolic inhibition on NK cell degranulation was also assessed. Isolated BL and POD1 NK cells were cultured at a 2:1 ratio with K562 cells for 4 hours with either oligomycin (40nM) or 2-DG (10mM), or the corresponding vehicle control (Fig.

4.10A-B). Interestingly, under these culture conditions, blocking OxPhos with oligomycin did not affect degranulation, as indicated by surface CD107a expression, in any of the NK cell subsets at either perioperative timepoint (Fig. 4.10A). More specifically, both the bulk BL and POD1 NK cells were still degranulating at over 90% capacity in the presence of oligomycin compared to the DMSO control (Fig. 4.10A). When examining the effects of blocking glycolysis and glycolysis-driven OxPhos through 2-DG, only the $CD56^{dim}$ subset degranulated significantly less with 2-DG treatment (Fig. 4.10B). Bulk BL NK cells showed a clear trend of reduced degranulation ($p=0.06$), and bulk POD1 NK cells demonstrated a significant reduction in the presence of 2-DG compared to the media control. Both the bulk BL and POD1 NK cells were functioning at an average of around 60% capacity in the presence of 2-DG compared to the media control (Fig. 4.10B).

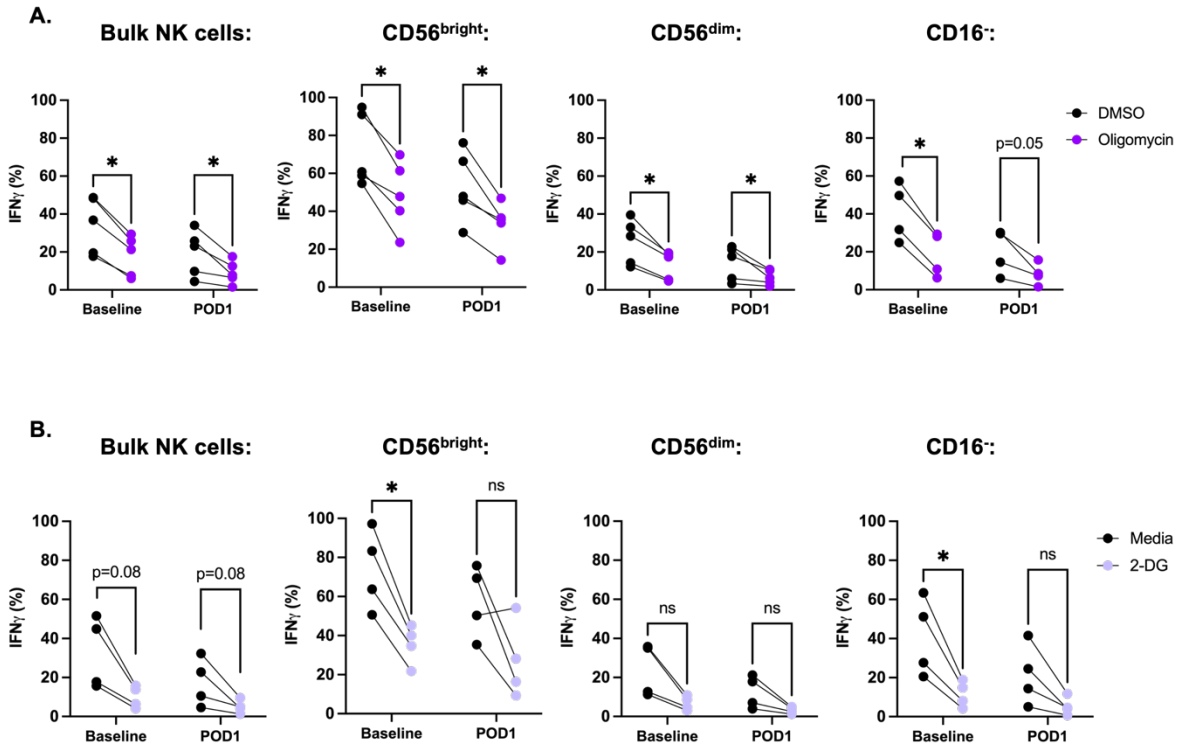

Figure 4.9. CD56^{bright}, CD56^{dim} and CD16^{-} NK cells have impaired ability to produce IFN-γ following 24-hour IL-2/12 stimulation with metabolic inhibition. Cryopreserved patient-matched BL and POD1 NK cells were thawed, rested for 1 hour, and stimulated for 24 hours with IL-2/12 (400U/mL; 20ng/mL)**.** BL and POD1 IFN-*γ* production across the peripheral NK cell subsets (n=5) ± 40nM oligomycin **(A)** or 10mM 2-DG **(B)**. Paired two-tailed t-tests were performed to determine statistical significance with Holm-Šídák correction for multiple comparisons. ns: not significant. *p<0.05. Normality was confirmed using the Shapiro-Wilk test.

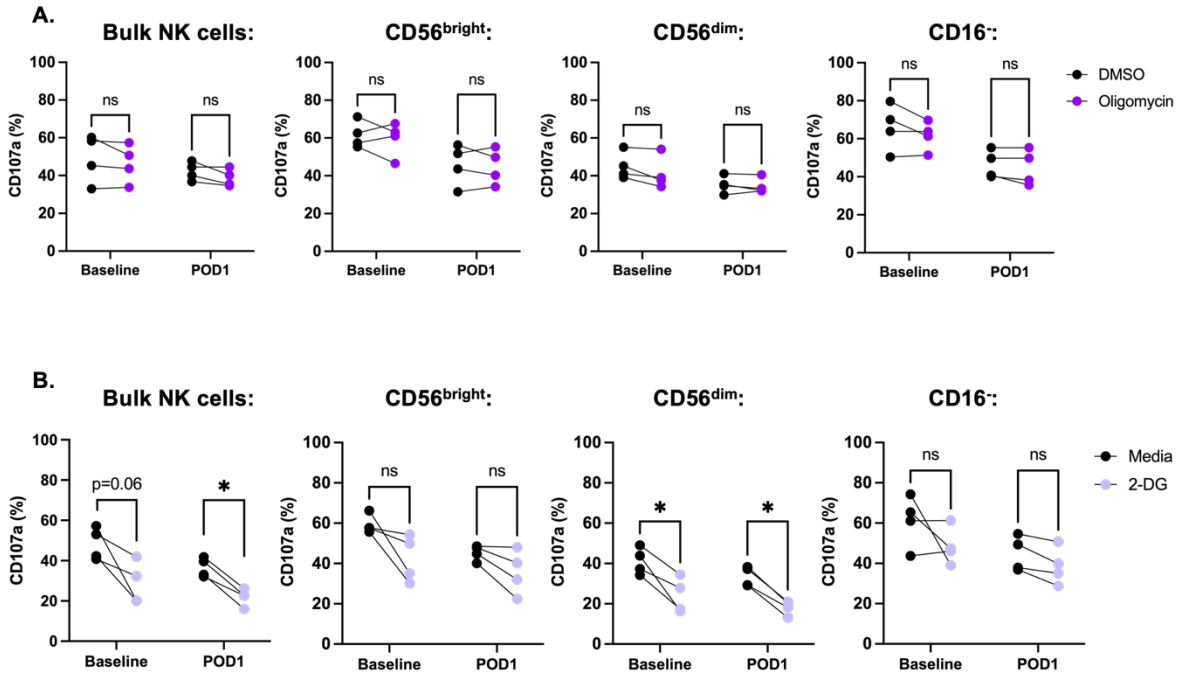

Figure 4.10. Blocking OxPhos with oligomycin had no impact on the ability of CD56^{bright}, CD56^{dim} or CD16^{-} NK cells to degranulate, while blocking glycolysis through 2-DG inhibited degranulation at both perioperative timepoints. Cryopreserved patient-matched BL and POD1 NK cells were thawed, rested for 1 hour, and stimulated for 4 hours with K562 tumour targets (2:1 effector-to-target ratio), monensin (GolgiStop) and an anti-CD107a antibody. BL and POD1 degranulation across the peripheral NK cell subsets (n=4) ± 40nM oligomycin **(A)** or 10mM 2-DG **(B)**. Paired two-tailed t-tests were performed to determine statistical significance with Holm-Šídák correction for multiple comparisons. ns: not significant. *p<0.05. Normality was confirmed using the Shapiro-Wilk test.

Thus far, we have demonstrated that while BL and POD1 NK cells rely on the same bioenergetic pathways for function, POD1 NK cells exhibit significantly reduced metabolic flux through OxPhos which coincides with their dysfunctional state. This reduction in real-time metabolic activity is accompanied by reduced glucose uptake despite no difference in glucose transporter expression after surgery. As a final series of experiments to complete our metabolic characterization of POD1 NK cells, we chose to assess metabolite abundance. This was both estimated based on transcriptional data through a computational framework called METAFlux and quantified by metabolomics.

4.4 METAFlux and metabolomics analysis highlight metabolic differences between BL and POD1 NK cells

METAFlux analysis was performed on the same single-cell RNA sequencing dataset previously collected and published by our lab which showed significant downregulation of gene sets related to cellular respiration and OxPhos[3]. Cryopreserved BL and POD1 PBMCs collected from six colorectal cancer surgery patients enrolled in the PERIOP-02 (NCT02987296) clinical trial were used for the RNA sequencing[2]. Three patients were in the control arm, and 3 patients received supplemental arginine immunonutrition. In this analysis, the two groups were not distinguished. The NK cell cluster was identified based on expression of *NKG7* and *GNLY.* The initial findings which suggest impairment of OxPhos/cellular respiration were obtained by gene set enrichment analysis (GSEA) which assesses the expression of metabolism-associated genes within a pre-defined pathway[229]. This approach does not consider the fact that metabolic networks are highly dynamic and interconnected. Although this served as an initial indicator of metabolic differences in NK cells after surgery, there is more information that can be inferred from the transcriptional data regarding metabolic flux. As such, we conducted METAFlux[182] on the same dataset. This is a published computational framework that uses Human1, a metabolic model which encodes the mechanistic relationships between genes, metabolites, and reactions in a human cell[218]. METAFlux considers the nutrient composition of the extracellular medium; for our dataset the reference used was *human blood*[182]. Huang et al composed this list of 64 metabolites representing human blood[182] based on the composition of a human plasma-like medium developed by Cantor et al[219].This framework requires that there be stoichiometric balance between the cells and their extracellular medium[182]. As a result, a nutrient flux score is calculated for the associated products of the metabolic reactions encoded in Human1.

Therefore, the only input is gene expression data, and the output data are nutrient flux scores. These arbitrary scores are meant to serve as a prediction of a cell population's uptake or release of a given nutrient[182]. A negative score indicates that the cell of interest is estimated to take up the nutrient in question (the more negative, the more uptake), and a positive score indicates release of the nutrient (the more positive the score, the greater the release). As these are strictly predictions, there are no conclusions that can be made directly from the results of METAFlux alone. These scores are meant to serve as additional supporting data to accompany the other more direct metabolic readouts that we have presented earlier. Shown in Figure 4.11 are the nutrient flux scores for O_2, H^+, and glucose. The data is presented as the mean nutrient flux score $\pm$ SEM of 100 bootstraps from BL or POD1 NK cells. The corresponding METAFlux scores estimate that BL NK cells take up significantly more glucose than POD1 NK cells, which aligns with our direct glucose uptake measurements presented in Figure 4.6. Furthermore, with positive nutrient uptake scores, both the BL and POD1 NK cells are estimated to be releasing H^+ to a similar degree (Fig. 4.11). This aligns with our Seahorse™ glycolytic stress test data in which minimal differences were observed in ECAR between BL and POD1 NK cells. Interestingly, while our Seahorse™ mitochondrial stress test data aligns very closely with our previously published GSEA suggesting that cellular respiration is decreased in POD1 NK cells, the METAFlux estimations gathered from this same dataset suggest the opposite. Unexpectedly, the POD1 NK cells have a nutrient flux score that predicts they would take up more O_2 from the extracellular environment than their BL counterparts.

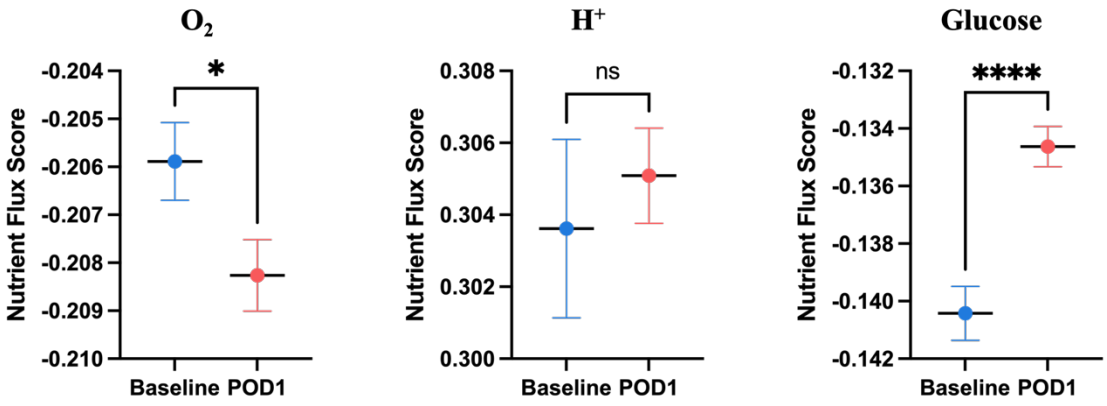

Figure 4.11. METAFlux analysis shows differences in nutrient flux scores for O_2, H^+ and glucose between BL and POD1 NK cells. METAFlux[182] analysis was conducted on single cell RNA sequencing data from BL and POD1 PBMCs collected from six colorectal cancer surgery patients part of the PERIOP-02 (NCT02987296)[2] clinical trial. The analysis was done specifically on the NK cell cluster identified by expression of *NKG7* and *GNLY.* Nutrient flux scores are shown for O_2, H^+, and glucose. A negative score indicates that the cell of interest is estimated to take up the nutrient, and a positive score indicates release of the nutrient. The data is presented as the mean nutrient flux score ± SEM of 100 bootstraps from BL or POD1 NK cells. Unpaired two-tailed t-tests were performed to determine statistical significance. ns: not significant, *p<0.05, ****p<0.0001. METAFlux analysis performed by Dr. Sarah Nersesian.

Finally, we generated a metabolomics dataset from three IL-2/12 stimulated BL and POD1 NK cell samples for targeted analysis of aqueous metabolites in collaboration with the uOttawa Metabolomics Core Facility (Fig. 4.12A). The initial processing of the raw mass spectrometry data was done by the core facility, which showed 105 out of approximately 200 possible hits. The raw data was converted to concentration (nM) normalized to cell number prior to running further analysis. Partial-least squares discriminant analysis (PLS-DA) showed relatively clear separation between the two experimental groups (Fig. 4.12B). Unfortunately, only one metabolite (inosine) approached statistical significance, showing higher levels in BL NK cells (Fig. 4.12C). Despite this, there are still notable trends that can be observed in the data. One metabolite of interest that showed up as being increased over two-fold on POD1 was cystine (Fig. 4.12C). Given the involvement of cystine in generating glutathione[230], this suggests a possible response to oxidative stress on POD1. Another notable finding was that many of the metabolites that had a two-fold increase or more on POD1 were amino acids (Fig. 4.12C). We then assessed the METAFlux predictions calculated from our single-cell RNA sequencing dataset for some of the metabolite hits that we reported from our metabolomics dataset (Fig. 4.13). The nutrient flux scores for hypoxanthine, pyridoxine, inosine and the amino acids valine, tryptophan, and leucine suggested the opposite trend compared to the actual metabolite concentrations determined by metabolomics. It should be noted that the single-cell RNA sequencing was conducted on resting cryopreserved PBMCs immediately post-thaw, while the metabolomics was conducted on cryopreserved BL and POD1 isolated NK cells following 24 hours of IL-2/12 stimulation. We emphasize that this analysis was exploratory and direct comparisons cannot be made.

In addition to looking at the relative abundance of the metabolite hits on BL versus POD1, we have also presented significant associations between metabolites through Pearson correlation analysis (Fig. 4.14). Briefly, the concentration of each metabolite for each individual replicate was compared against the mean concentration across the three biological replicates per timepoint. Pearson correlation coefficients were calculated between metabolites. This coefficient carries a value between -1 and +1, with a coefficient of 0 indicating no correlation between two metabolites. Positive correlations are depicted by the blue lines while negative correlations are shown in red. Shown in Fig. 4.14 are the most significant correlations ($p<0.003$). Overall, there are notably more significant correlations between metabolites on POD1 than on BL, with the majority being positive. Again, several of these metabolites with significant correlations on POD1 were amino acids.

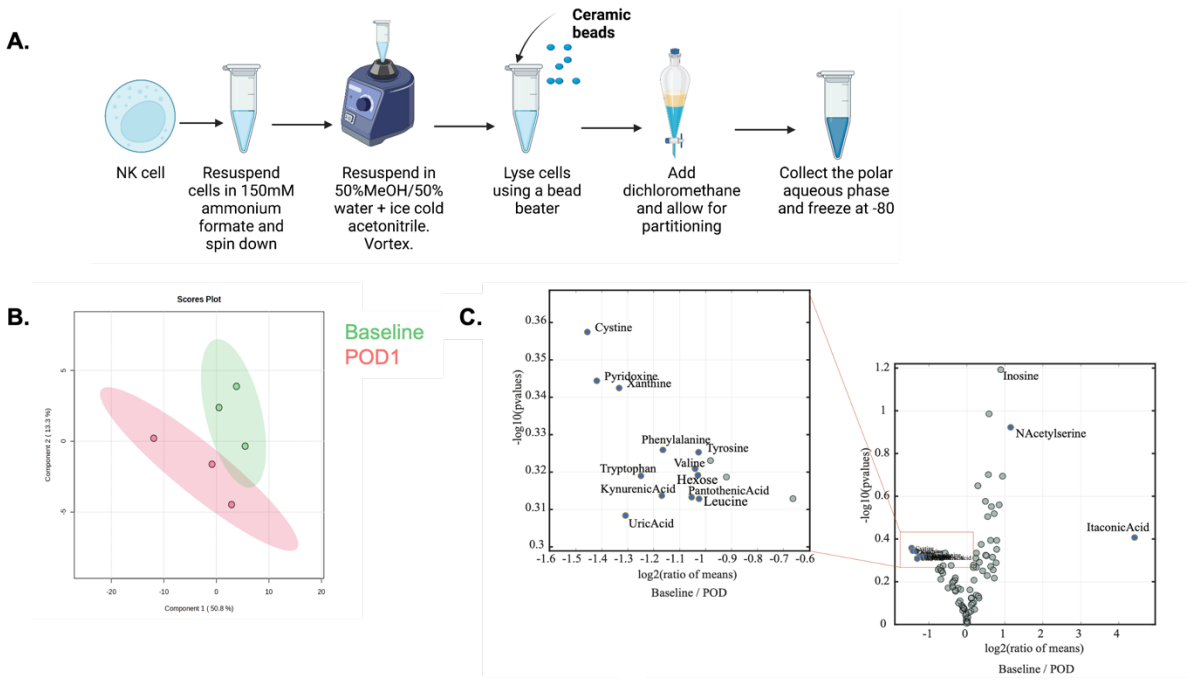

Figure 4.12. Targeted metabolomics analysis reveals differences in metabolite concentrations, particularly amino acids, in POD1 NK cells compared to BL. A. Schematic overview of the sample preparation. Briefly, frozen isolated NK cells were thawed, rested for 1 hour and then stimulated with IL-2/12 (400U/mL;20ng/mL) for 24 hours (n=3). Aqueous metabolites were extracted using mass spectrometry grade solvents, plasticware, and ceramic beads provided by the uOttawa Metabolomics Core Facility. The cells were washed with 150mM ammonium formate and resuspended in a 50% methanol:50% water solution along with ceramic beads. The cells were lysed using a bead beater, and acetonitrile was added. To separate the aqueous and organic layers, dichloromethane and water were added and the layers were left to partition on ice for 10 minutes. The samples were centrifuged, the upper aqueous layer was collected, dried, and stored at -80 degrees prior to LC-MS/MS data collection. **B.** Partial-least squares discriminant analysis (PLS-DA) plot comparing IL-2/12 stimulated BL and POD1 NK cells. **C.** Volcano plot depicting the $\log_2$ ratio of the baseline/POD1 mean concentration of metabolites against their respective $-\log_{10}$(p-values). Panel **C** was generated by Dr. Miroslava Cuperlovic-Culf (NRC). Schematic in panel A made with BioRender.

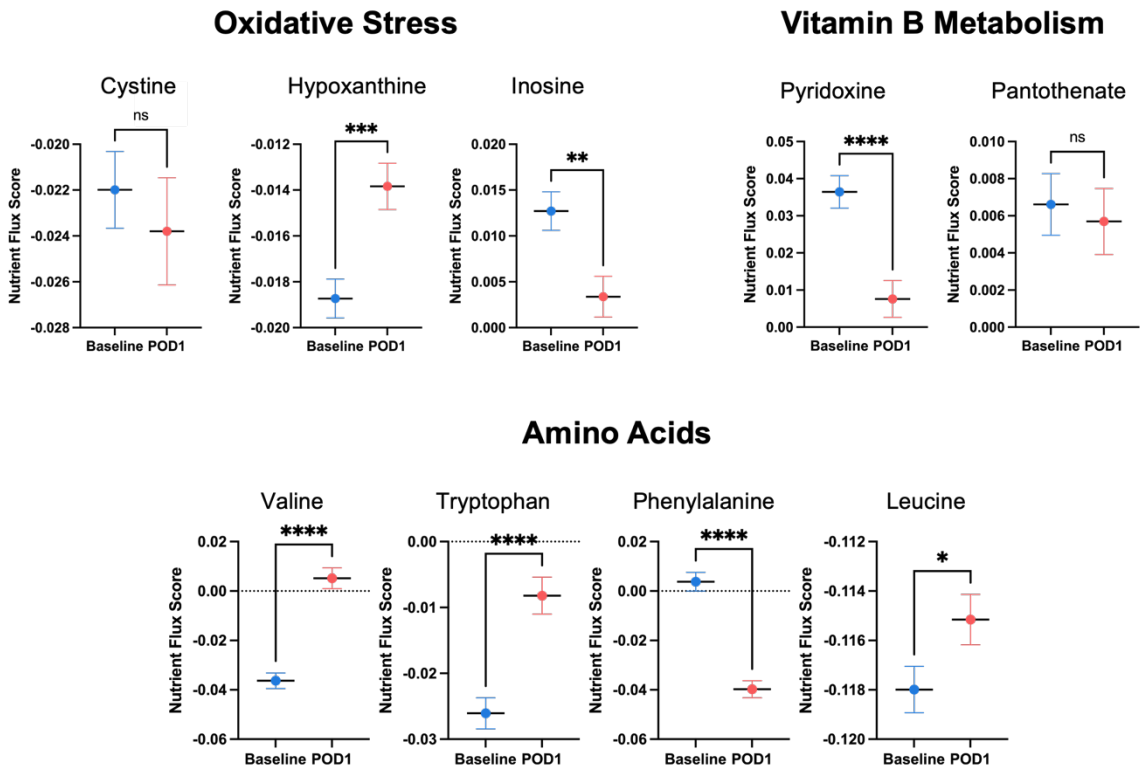

Figure 4.13. MetaFLUX predictions for specific metabolites identified as having a 2-fold increase or more by metabolomics analysis. METAFlux[182] analysis was conducted on single cell RNA sequencing data from BL and POD1 PBMCs collected from six colorectal cancer surgery patients part of the PERIOP-02 (NCT02987296)[2] clinical trial. The analysis was done specifically on the NK cell cluster identified by expression of *NKG7* and *GNLY.* Nutrient flux scores are shown for several metabolites related to the oxidative stress response, vitamin B metabolism, and amino acids which were identified as having a 2-fold increase or more on POD1 from our metabolomics dataset. A negative score indicates that the cell of interest is estimated to take up the nutrient, and a positive score indicates release of the nutrient. The data is presented as the mean nutrient flux score ± SEM of 100 bootstraps from BL NK cells or POD1 NK cells. Unpaired two-tailed t-tests were performed to determine statistical significance. ns: not significant, *p<0.05, **p<0.01, ***p<0.001, ****p<0.0001. METAFlux analysis performed by Dr. Sarah Nersesian.

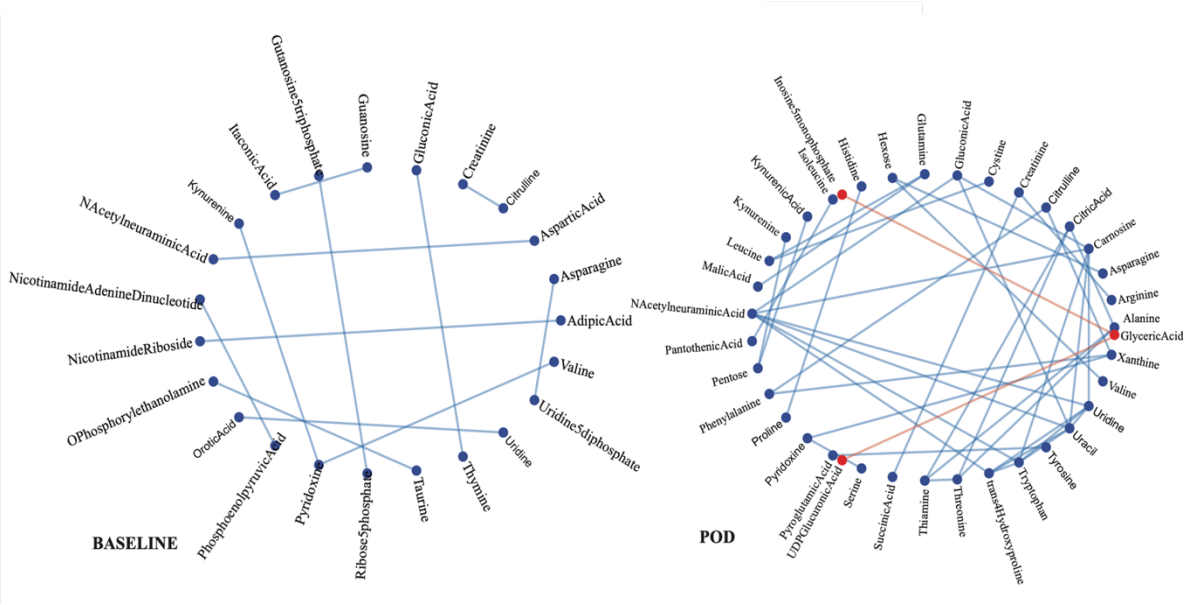

Figure 4.14. Pearson correlations between metabolites in baseline (left) and POD1 (right) NK cells. Only Pearson correlation coefficients with $p<0.003$ are shown. Blue lines indicate positive correlations, while red lines depict negative correlations. Generated by Dr. Miroslava Cuperlovic-Culf (NRC).

Chapter Summary:

Here we established the metabolic state of POD1 NK cells under the same conditions in which peak functional impairment was determined in Chapter 3. Our real-time extracellular flux data corroborate our findings at the transcriptional level indicating that POD1 NK cells are metabolically dysfunctional in their ability to carry out cellular respiration. This was accompanied by a minor decrease in their basal glycolysis. In addition to our Seahorse™ extracellular flux data, we performed several supplementary readouts to obtain a comprehensive overview of the metabolic profile of NK cells in response to IL-2/12 stimulation. POD1 NK cells demonstrated reduced mitochondrial membrane potential compared to BL, with no corresponding difference in overall mitochondrial mass. This suggests the presence of impaired mitochondrial function on POD1 which supports our hypothesis that OxPhos is the main source of metabolic dysfunction in POD1 NK cells. We also showed that NK cells have reduced glucose uptake on POD1 which was not caused by a change in expression of the facilitative glucose transporter GLUT1. Furthermore, we found that while metabolic inhibition negatively impacted function, there was no difference in the effect of oligomycin and 2-DG on POD1 NK cell function compared to BL, suggesting that surgery does not affect reliance on specific bioenergetic pathways. Finally, we conducted METAFlux analysis[182] on our published single-cell RNA sequencing dataset[3], as well as metabolomics analysis on isolated IL-2/12 stimulated BL and POD1 NK cells. In our final result's chapter, we explore metabolic modulation as an approach to rescue the function of POD1 NK cells and/or arm NK cell-based adoptive cell therapy for administration in the perioperative period.

Chapter 5: Metabolic modulation supports NK cell function under surgical stress

Rationale

To strengthen the relationship between the dysfunctional phenotype of POD1 NK cells and changes in their metabolic activity induced by surgical stress, we pursued metabolic modulation to rescue effector function. In Chapter 4, we characterized the metabolism of POD1 NK cells using a diverse set of readouts to provide a comprehensive overview of their metabolic signature. In this chapter, we attempt to rescue POD1 NK cell function both extrinsically through nutrient supplementation and intrinsically by modifying their metabolic activity. The latter was done through two main approaches: 1) pharmacological metabolic modulation and 2) *ex vivo* expansion.

5.1 Nutrient supplementation and metabolic modulation cannot rescue the function nor boost the metabolic activity of POD1 NK cells

First, we measured whether supplementing with additional nutrients could rescue the function of POD1 NK cells. If NK cells experience a change in nutrient availability after surgery which is contributing to their dysfunction, then providing them with a surplus of nutrients known to support proper immune cell function could potentially rescue them. This also addresses whether NK cell metabolic differences are intrinsic or environmental, though it should be noted that cell culture media is inherently more nutrient-rich than the environment NK cells experience in whole blood. Briefly, we cultured isolated NK cells with supplemental glucose (25mM), glutamine (5mM) and arginine (2mM) throughout the 24-

hour IL-2/12 stimulation. These are the final concentrations accounting for what is already present in RPMI base media[231]. In all, neither the $CD56^{bright}$, $CD56^{dim}$, or $CD16^{-}$ NK cells could have their function significantly increased by supplemental glucose (p=0.24, 0.24, and 0.23, respectively) (Fig. 5.1A), arginine (p=0.35, 0.4, and 0.4, respectively) (Fig. 5.1B), or glutamine (p=0.97, 0.93, and 0.93, respectively) (Fig. 5.1C). All the patients presented in Figure 5.1 exhibited POD1 NK cell IFN-γ dysfunction across the subsets. When examining responses at the individual patient level, it can be noted that nutrient supplementation partially rescued IFN-γ production in some POD1 NK cells, while others remained hyporesponsive. Taken together with our metabolic phenotyping data presented in Chapter 4, this suggests an intrinsic defect in the NK cells that impedes nutrient uptake, particularly glucose, independent of nutrient transporter expression levels. Notably, providing POD1 NK cells with additional nutrients known to be critical for NK cell responses does not rescue their function to BL capacity, suggesting that changes in nutrient availability are not responsible for their dysfunctional phenotype.

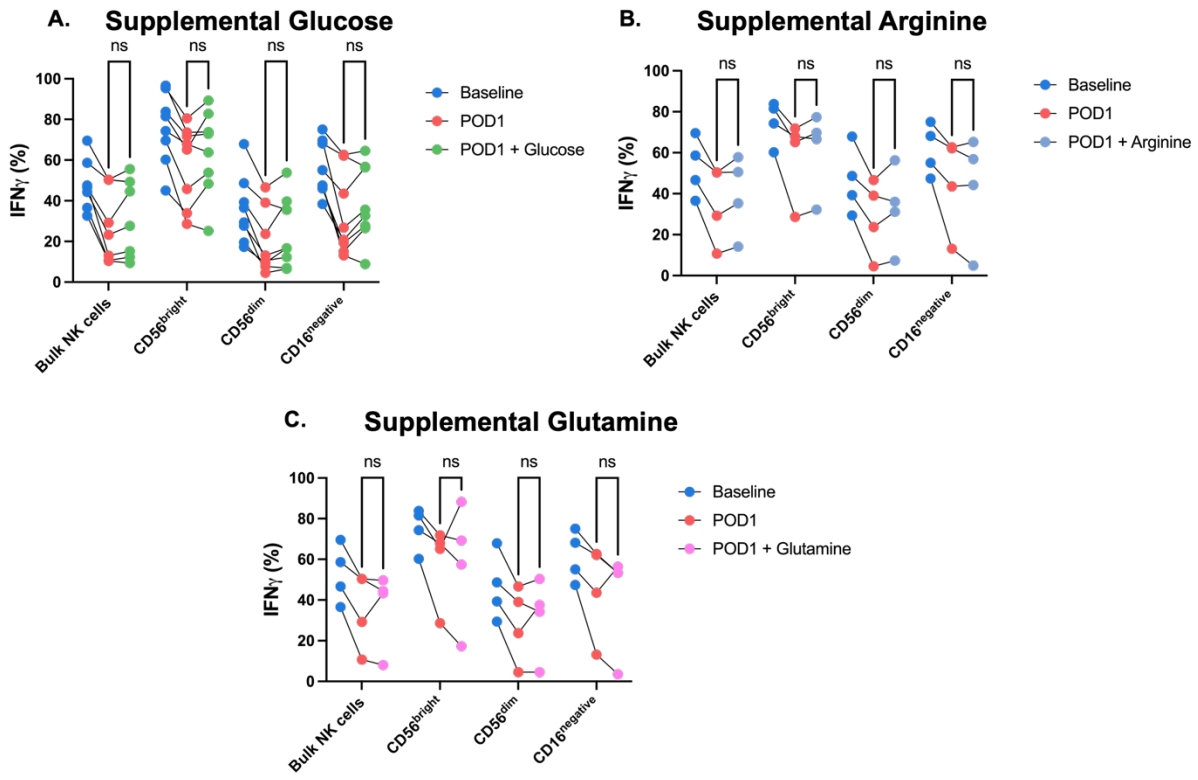

Figure 5.1. POD1 NK cell function cannot be rescued with supplemental glucose, arginine, or glutamine. Cryopreserved patient-matched BL and POD1 isolated NK cells were thawed, rested for 1 hour in 100U/mL IL-2, and stimulated for 24 hours with IL-2/12 (400U/mL; 20ng/mL) at 37°C in 5% CO_2. Supplemental glucose (**A**, 25mM), arginine (**B**, 2mM), or glutamine (**C**, 5mM) was added to the culture media for the duration of stimulation. Final nutrient concentrations account for what is already present in RPMI base media. Protein transport was blocked for the final 4 hours of stimulation. At the end of the stimulation period, the cells were stained for viability and the extracellular markers CD16 and CD56 to stratify the NK cell subsets. The cells were then fixed, permeabilized, and stained for intracellular IFN-γ. The data was acquired on a BD LSR Fortessa flow cytometer. The data is presented as BL and POD1 IFN-γ production (% responsive NK cells) across the peripheral NK cell subsets (**A**: n=8; **B and C**: n=4). Paired two-tailed t-tests were performed to determine statistical significance with Holm-Šídák correction for multiple comparisons. ns: not significant. Normality was confirmed using the Shapiro-Wilk and Kolmogorov-Smirnov tests.

We subsequently tested whether we could intrinsically modulate the NK cells' metabolic activity to improve their function. The compound sodium dichloroacetate (DCA) has been shown to divert glucose utilization away from glycolysis and towards mitochondrial respiration[232]. While this has been studied in the context of blocking cancer cell proliferation[232,233], it has more recently been studied as a means of supporting immune cell function over longer periods of stimulation[197]. As such, we treated whole blood at BL and on POD1 with 10mM DCA for the duration of the 24-hour IL-2/12 stimulation to determine whether this would affect the IFN-γ response. A schematic representation of the mechanism of action of DCA within the mitochondria, along with an overview of the experimental procedure is shown in Figure 5.2A-B, respectively. Treatment with DCA in whole blood did not significantly influence the IFN-γ response in either BL [p=0.55 (percentage); p=0.27 (MFI)] or POD1 [p=0.55 (percentage); p=0.15 (MFI)] NK cells compared to each respective vehicle control group (Fig. 5.2C). To assess whether DCA was having any effect on the metabolism of POD1 NK cells despite showing no improvement in function, we measured the mitochondrial mass and membrane potential within POD1 NK cells $\pm$ DCA treatment. Like the response to nutrient supplementation, the effect of DCA on mitochondrial mass and membrane potential varied between individual patients. Overall, we did not observe a significant change in mitochondrial mass in [p=0.65 (percentage); p=0.34 (MFI)] or membrane potential [p=0.23 (percentage); p=0.68 (MFI)] in POD1whole blood NK cells upon treatment with DCA (Fig. 5.2D-E). Finally, we tested the functional impact of DCA on isolated NK cells, thereby eliminating potential confounding variables introduced from the other cell types present in whole blood. Shown in Figure 5.3 is the functional response of isolated BL NK cells upon treatment with 10mM DCA throughout the duration of the IL-2/12 stimulation period. The presence of DCA at this concentration resulted in near complete

ablation of IFN-γ production (Fig. 5.3A) while having no impact on the viability of the cells (Fig. 5.3B). One challenge with the use of DCA is that the promotion of OxPhos results in excessive production of mitochondrial ROS which can negatively impact the cells[234]. Although further optimization of the culture conditions or the addition of an antioxidant may enhance outcomes, POD1 NK cell function was not rescued under the conditions tested herein. As a result, we proceeded with an alternative approach to better address the underlying mechanisms of dysfunction.

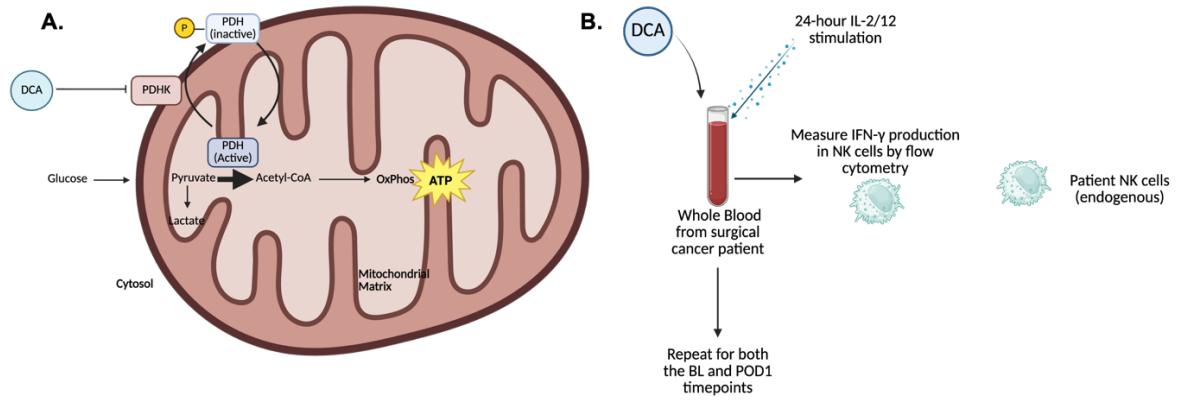
A.
P
PDH (inactive)
DCA
PDHK
PDH (Active)
Glucose
Pyruvate
Acetyl-CoA
OxPhos
ATP
Lactate
Cytosol
Mitochondrial Matrix
B.
DCA
24-hour IL-2/12 stimulation
Measure IFN-γ production in NK cells by flow cytometry
Patient NK cells (endogenous)
Whole Blood from surgical cancer patient
Repeat for both the BL and POD1 timepoints

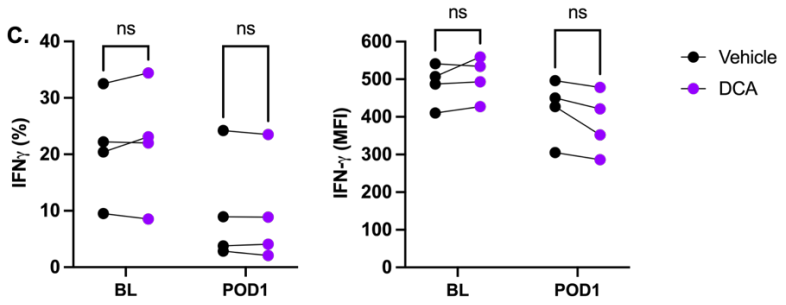
C.
ns
ns
IFNγ (%)
0
10
20
30
40
BL
POD1
ns
ns
IFN-γ (MFI)
0
100
200
300
400
500
600
BL
POD1
Vehicle
DCA

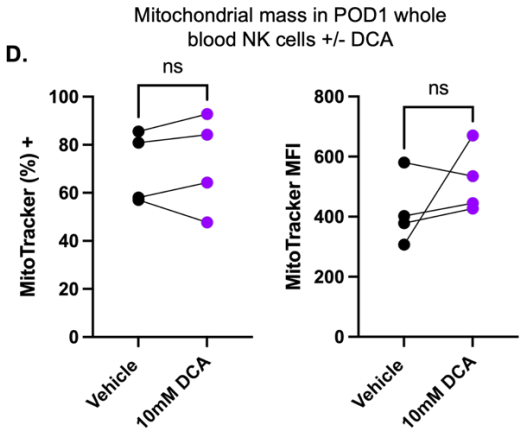
D.
Mitochondrial mass in POD1 whole blood NK cells +/- DCA
ns
MitoTracker (%) +
0
20
40
60
80
100
Vehicle
10mM DCA
ns
MitoTracker MFI
0
200
400
600
800
Vehicle
10mM DCA

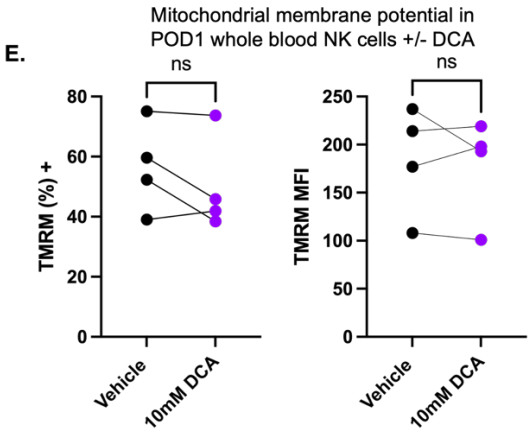
E.
Mitochondrial membrane potential in POD1 whole blood NK cells +/- DCA
ns
TMRM (%) +
0
20
40
60
80
Vehicle
10mM DCA
ns
TMRM MFI
0
50
100
150
200
250
Vehicle
10mM DCA

Figure 5.2. DCA cannot rescue IFN-γ production nor impact the metabolism of whole blood POD1 NK cells. A. Schematic depiction of the mechanism of action of DCA. **B.** Overview of whole blood treatment and subsequent IFN-γ functional readout. Patient-matched BL and POD1 whole blood was collected and stimulated for 24 hours with IL-2/12 (400U/mL; 20ng/mL) ± 10mM DCA or corresponding vehicle control at 37°C in 5% CO_2. **C.** Protein transport was blocked for the final 12-16 hours of stimulation. The red blood cells were lysed, and the remaining cells were stained for viability and the extracellular markers CD3 and CD56. The cells were then fixed, permeabilized, and stained for IFN-γ. The data was acquired on a BD LSR Fortessa flow cytometer. The IFN-γ response is presented as both the percentage (%) of NK cells containing intracellular IFN-γ as well as the median fluorescence intensity (MFI) (n=4)**.** To assess mitochondrial parameters, following red blood cell lysis and staining for viability and NK cell-identifying extracellular markers, the cells were stained with 400nM MitoTracker Deep Red in **D)** and 250nM tetramethylrhodamine (TMRM) in **E)**, for 30min at 37°C. The signal is presented as both the percentage of the NK cell population as well as the MFI. Protein transport was not inhibited when assessing mitochondrial parameters. Paired two-tailed t-tests were performed to determine statistical significance with Holm-Šídák correction for multiple comparisons. ns: not significant. Normality was confirmed using the Shapiro-Wilk test. Schematic in panel A made with BioRender.

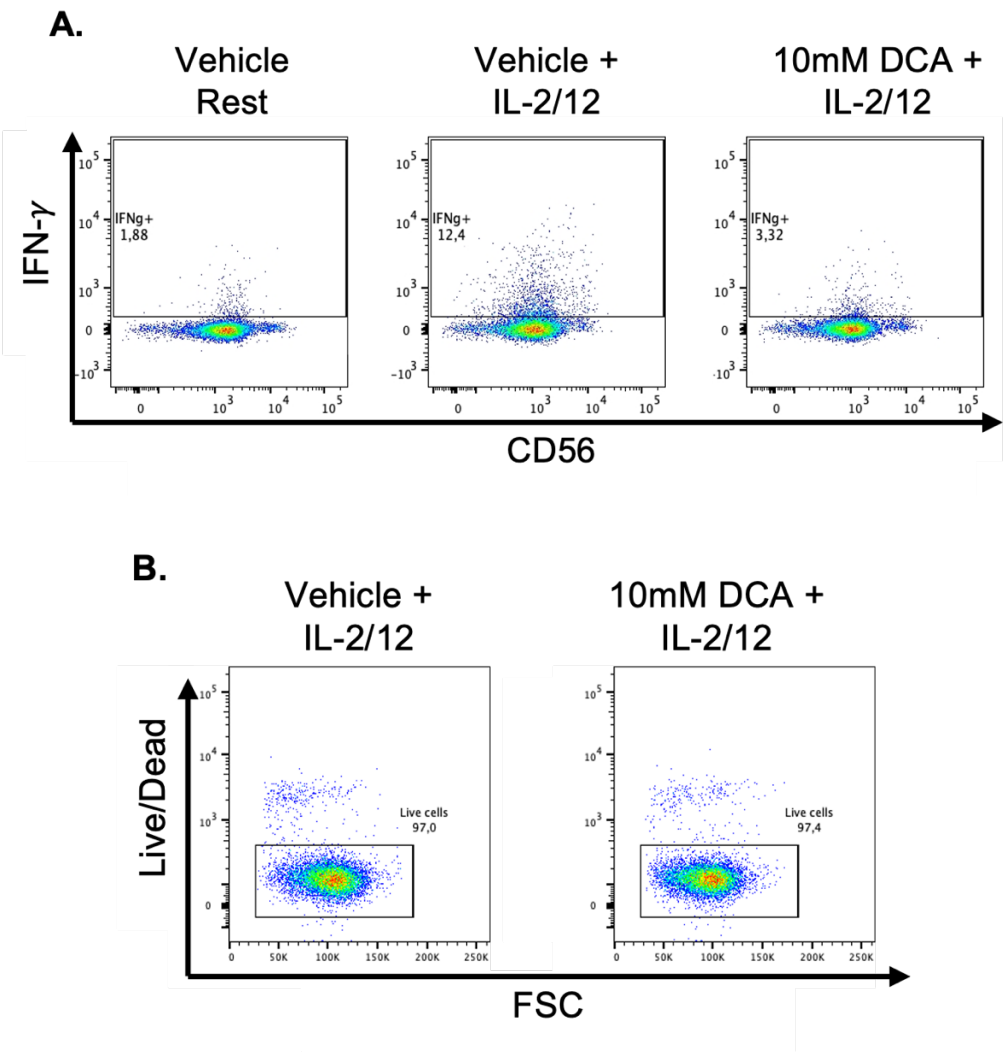

Figure 5.3. DCA impaired IFN-γ production in isolated NK cells while having no effect on cell viability. BL NK cells were stimulated for 24 hours with IL-2/12 (400U/mL; 20ng/mL) ± 10mM DCA or corresponding vehicle control at 37°C in 5% CO_2. At the end of the stimulation period, the cells were stained for viability and the extracellular marker CD56. The cells were then fixed, permeabilized, and stained for intracellular IFN-γ. The data was acquired on a BD LSR Fortessa flow cytometer. **A.** Representative flow cytometry plots depicting the percentage (%) of NK cells expressing IFN-γ in the vehicle treated groups (resting and IL-2/12 stimulated) and the 10mM DCA (IL-2/12 stimulated) group. **B.** NK cell viability with IL-2/12 stimulation ± 10mM DCA treatment.

5.2 Primary human NK cells can be expanded *ex vivo*

A well-reported method for modifying the metabolism of NK cells is *ex vivo* expansion[205,235]. This technique has been shown to change both the functional and metabolic profiles of NK cells, conferring a more robust phenotype[171,205]. Briefly, we generated exNK cells using fresh primary human NK cells from healthy donors with irradiated 721.221 feeder cells expressing membrane-bound IL-21 (221-mbIL-21) at a 2:1 ratio (feeder-to-NK cell). This was done in complete RPMI media containing 100U/mL IL-2 according to the diagram in Figure 5.4. Our procedure closely follows what was previously published by Yang et al[205]. The media was changed every 2-3 days based on cell growth. Freshly irradiated feeder cells were added after 7 days. A subset of the exNK cells was cryopreserved on day 7 of the expansion, and the remaining cells continued expanding until day 14. The 221-mbIL-21 feeder cells were a kind gift from Dr. Seung-Hwan Lee from the University of Ottawa. A sample of the culture was collected every few days to assess purity (Fig. 5.5). The expression of CD56 became brighter throughout the duration of the expansion, which aligns with Poznanski *et al* who found that *ex vivo* expansion resulted in NK cells with high CD56 expression ($CD56^{super\ bright}$ NK cells) which were highly cytotoxic against ovarian cancer cells[204]. The efficiency of the expansion was largely donor dependent.

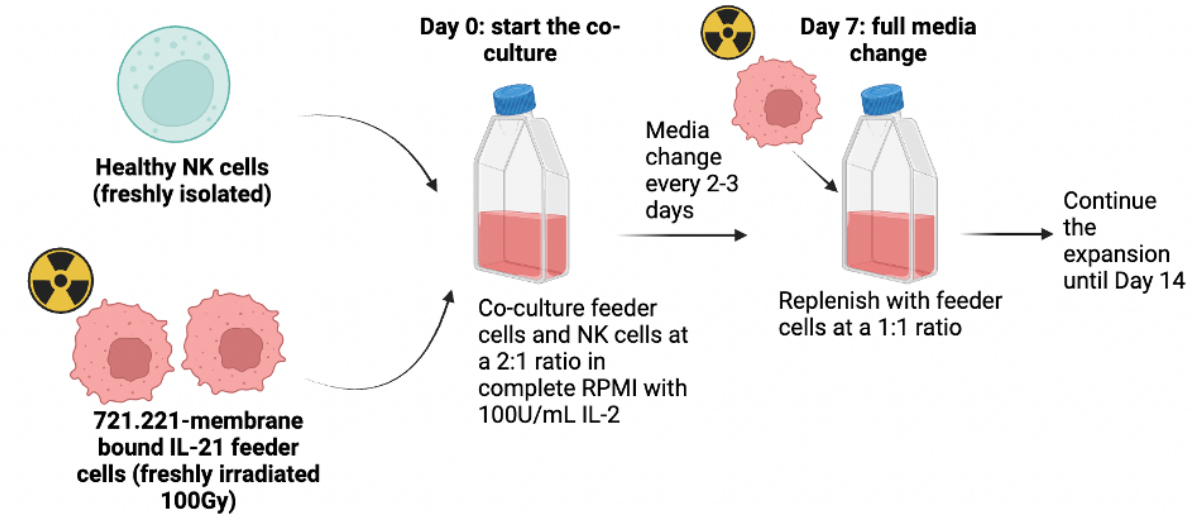

Figure 5.4. Outline of the *ex vivo* expansion procedure. Freshly isolated primary human NK cells collected from healthy donors were co-cultured with freshly irradiated (100 Gy) 221-mb-IL-21 feeder cells at a 2:1 ratio (feeder-to-NK cell) in complete RPMI media supplemented with 100U/mL recombinant human IL-2 at a total cell concentration of $2.5e^5$ cells/mL. The media was changed every 2-3 days depending on cell growth. Freshly irradiated feeder cells were added on day 7 of the expansion at a 1:1 ratio. Most of the day 7 exNK cells were cryopreserved for downstream functional assays, while a subset continued expanding until day 14. Schematic made with BioRender.

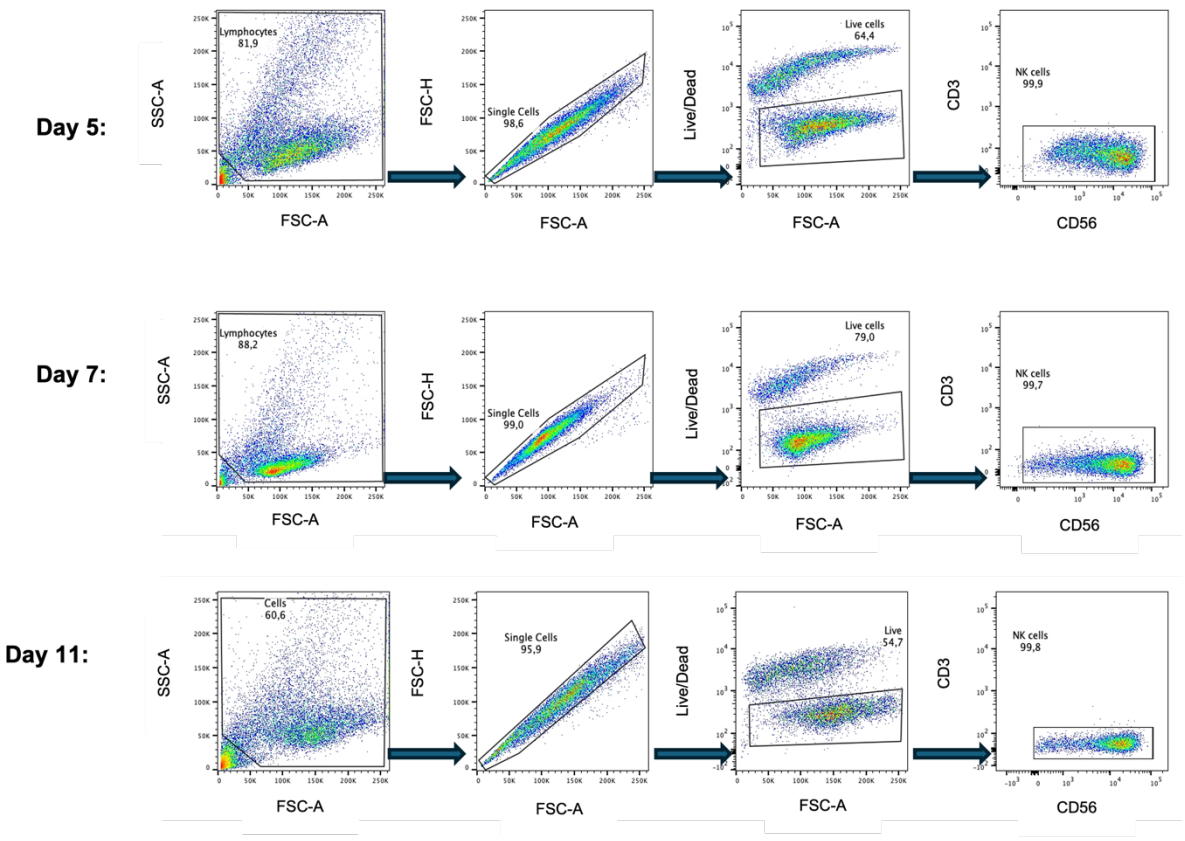

Figure 5.5. Representative flow cytometry plots depicting exNK cell phenotype on days 5, 7, and 11 of the expansion process. A small subset of exNK cells was removed on days 5, 7 and 11 of the expansion and stained for viability and the extracellular markers CD3 and CD56 to assess the purity of the culture and the increase in expression of CD56 which is known to occur because of feeder cell-based expansion.

5.3 exNK cells remain highly functional in the immune suppressive POD1 environment

To determine whether *ex vivo* expansion can render NK cells functionally resistant to the suppressive postoperative environment, we employed an *in vitro* whole blood co-culture system designed and optimized by another PhD candidate in the Auer lab (Mistry et al. 2026, manuscript under review). In short, NK cells were labelled with CFSE fluorescent dye and co-cultured with whole blood collected from BL surgical cancer patients. The co-culture was stimulated with IL-2/12 and the IFN-γ response was measured after 24 hours of stimulation. The CFSE labelling of the exNK cells made it possible to decipher the patient's own NK cells within the whole blood (referred to as endogenous or "endo" NK cells) from the exNK cells that were placed in the blood. The entire procedure was repeated with freshly collected POD1 blood from the same patient. A schematic overview of this assay is presented in Figure 5.6A and a representative gating strategy for delineating endogenous NK cells from exNK cells is shown in Figure 5.6B. Our lab has demonstrated that the dysfunctional phenotype exhibited by endogenous NK cells on POD1 becomes imparted on healthy (unexpanded) NK cells using this model (Mistry et al. 2026, manuscript under review). Representative flow cytometry plots depicting the IFN-γ response of the endogenous BL, endogenous POD1, and exNK cells co-cultured with POD1 blood are shown in Figure 5.7A. The production of IFN-γ by the exNK cells when in POD1 blood was considerably higher than both the endogenous BL and POD1 NK cells (Fig. 5.7B). Although the exNK cells showed a trend towards reduced function when co-cultured with POD1 whole blood (62.88 $\pm$8.36% IFN-γ+) compared to BL whole blood (average 81.9 $\pm$15.63% IFN-γ+) in the IL-2/12 stimulated condition (p=0.08) (Fig. 5.7C), they appeared to be suppressed to a lesser degree than the endogenous POD1 NK cells. Fig 5.7D compares endogenous POD1 NK cell dysfunction

with exNK cell dysfunction, relative to BL. There is a visible trend showing that exNK cells were suppressed to a lesser degree than the patient's own NK cells on POD1, though this was not statistically significant (p=0.13). Furthermore, we found that both BL (p=0.0009) and POD1 (p=0.016) endogenous NK cells had an improved IFN-γ response when in the presence of exNK cells (Fig. 5.7E). Since this was true for both BL and POD1 NK cells, we can deduce that the effect of the exNK cells is not surgery specific. Nonetheless, this result challenges the hypothesis that POD1 NK cells are irreversibly suppressed. Interestingly, preliminary data indicated that this partial rescuing effect was solely induced by exNK cells and not donor-matched unexpanded NK cells (Supp. Fig. 3).

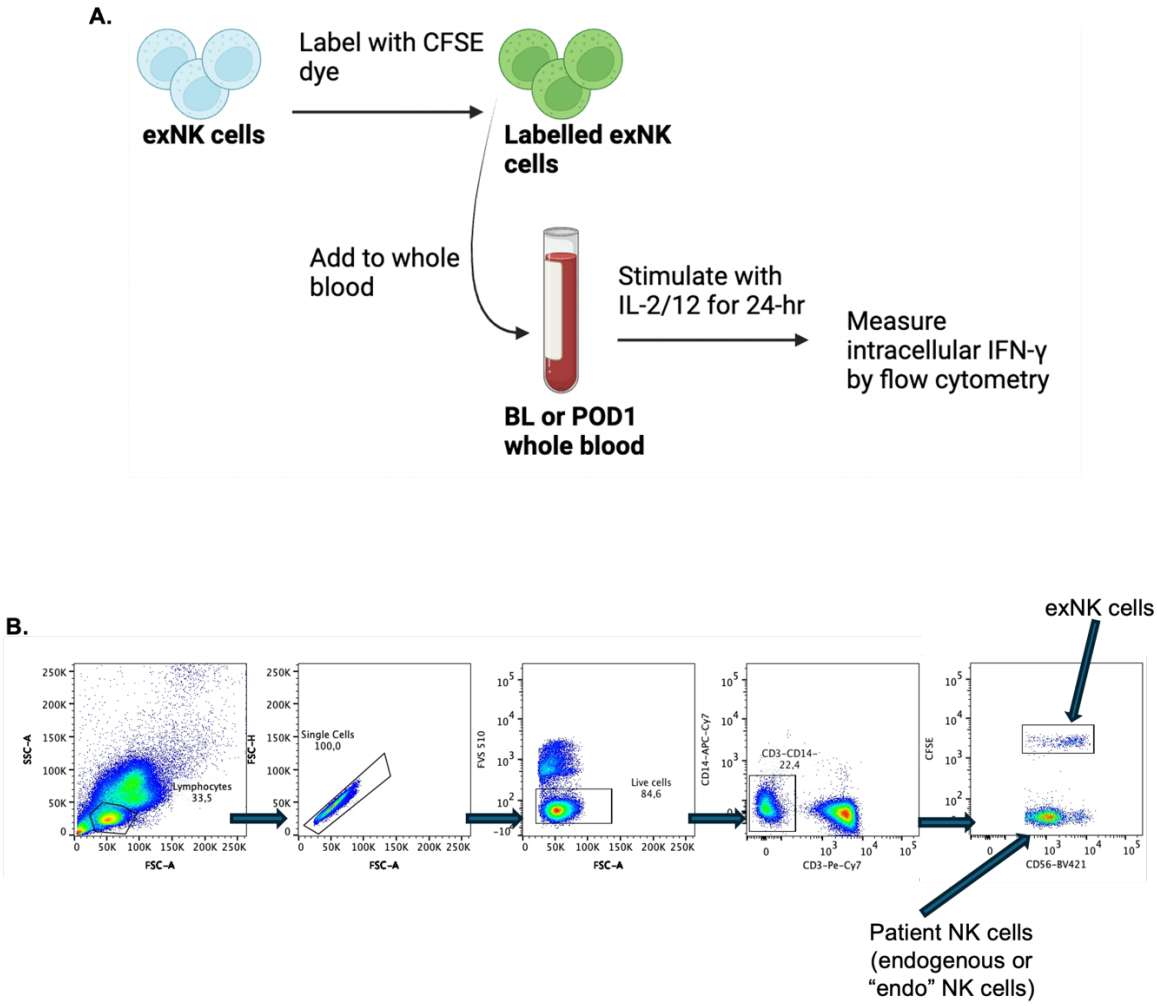

Figure 5.6. Outline of the whole blood co-culture assay. A. Expanded NK cells cryopreserved at day 7 of the expansion were thawed, rested overnight in 100U/mL IL-2, and labelled with CFSE dye prior to co-culture with BL or POD1 whole blood for 24 hours ± IL-2/12 stimulation (400U/mL; 20ng/mL). Measurement of intracellular IFN-γ by flow cytometry was the functional readout. **B.** Representative gating strategy to identify the endogenous NK cells (the NK cells present within the BL or POD1 whole blood) and the CFSE+CD56+ exNK cells. Schematic in panel A made with BioRender.

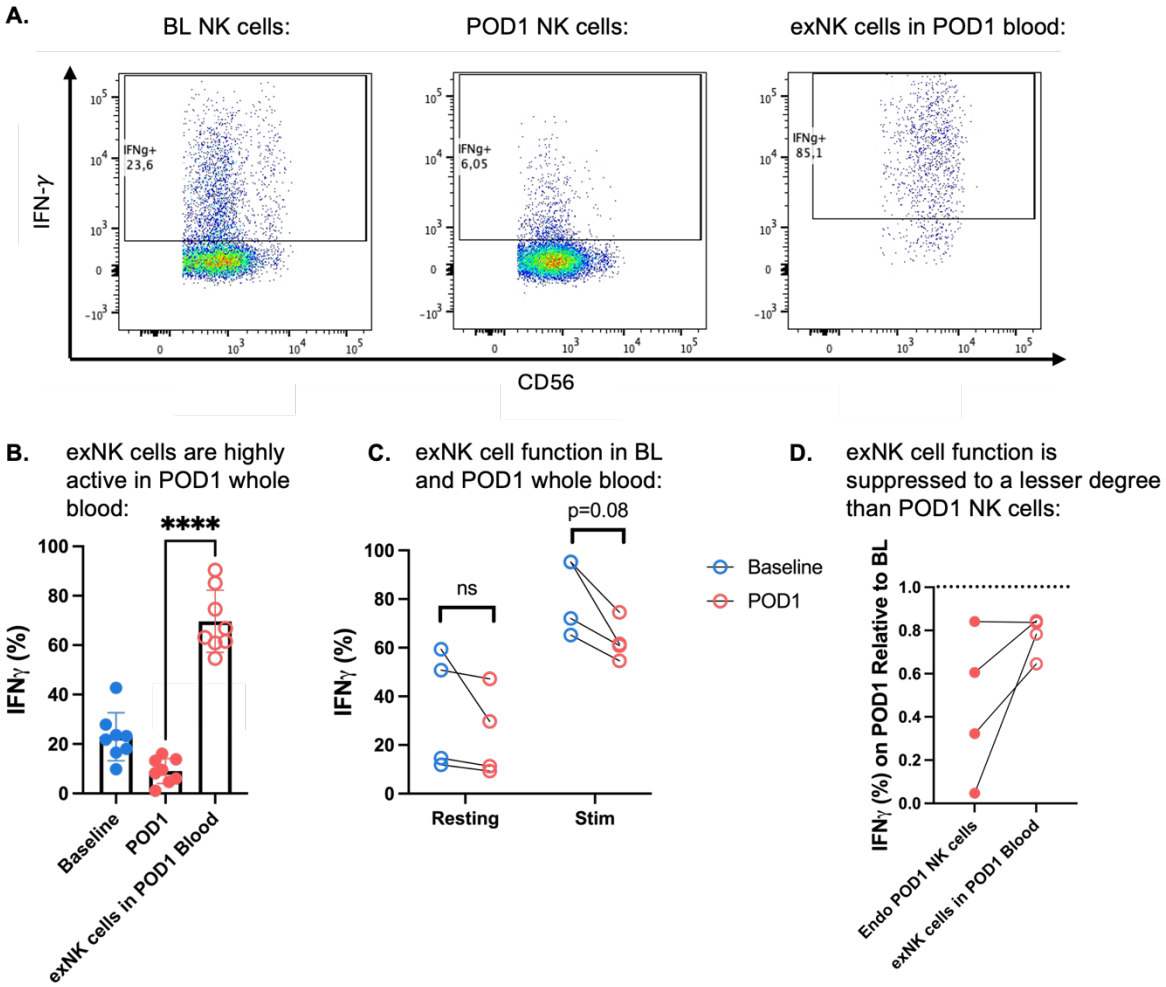
A.
BL NK cells:
POD1 NK cells:
exNK cells in POD1 blood:
IFN-γ
CD56
IFNg+ 23,6
IFNg+ 6,05
IFNg+ 85,1
B.
exNK cells are highly active in POD1 whole blood:
IFNγ (%)
****
Baseline
POD1
exNK cells in POD1 Blood
C.
exNK cell function in BL and POD1 whole blood:
p=0.08
ns
IFNγ (%)
Resting
Stim
Baseline
POD1
D.
exNK cell function is suppressed to a lesser degree than POD1 NK cells:
IFNγ (%) on POD1 Relative to BL
Endo POD1 NK cells
exNK cells in POD1 Blood
E.
BL and POD1 endogenous NK cells are functionally improved in the presence of exNK cells:
IFNγ (%)+ Endogenous NK cells
***
*
Baseline
POD1
Endo NK cells
Endo NK cells in the presence of exNK cells

Figure 5.7. exNK cells are highly functional in POD1 whole blood. A) Representative flow cytometry plots depicting IFN-γ production by endogenous BL NK cells, endogenous POD1 NK cells, and exNK cells exposed to POD1 whole blood and **B)** compiled data from n=8 BL and POD1 samples. **C)** Percent IFN-γ+ exNK cells in BL and POD1 whole blood $\pm$ IL-2/12 stimulation (400U/mL; 20ng/mL) (n=4). **D)** Comparison of endogenous POD1 NK cell dysfunction versus exNK cell dysfunction within POD1 whole blood. Both are normalized to BL, indicated by the dotted line. **E)** Endogenous BL and POD1 NK cell IFN-γ production $\pm$ co-culture with exNK cells, stimulated with IL-2/12 n=4. An unpaired two-tailed t-test was performed in **(B)** and paired two-tailed t-tests were performed for all other analyses to determine statistical significance with Holm-Šídák correction for multiple comparisons where relevant. ns: not significant; *p<0.05; **p<0.01; ***p<0.001; ****p<0.0001. Normality was confirmed using the Shapiro-Wilk test.

5.4 Adopting an *in vivo* model to test the functional ability of exNK cells under surgical stress

To investigate the exNK cells as a perioperative adoptive cell therapy, we began preliminary experiments for an *in vivo* model. As a proof-of-concept, we tested the *in vivo* efficacy of pooled BL, POD1, and healthy NK cells to control tumour burden. This was done by assessing engraftment prevention in a xenograft mouse model using OVCAR8 cells expressing luciferase (OVCAR8-Luc). We chose to use NCG mice for this study. These mice have a NOD genetic background, which significantly reduces their innate immunity. They have a *Prkdc* knockout which generates a SCID-like phenotype, and an *Il2rg* knockout which decreases NK cell production[221]. We received OVCAR8-Luc cells from the Ashkar lab at McMaster University. Briefly, mice were injected ip on day 0 with OVCAR8-Luc cells and either BL, POD1, or healthy NK cells pooled from 3 donors, along with a dose of 10,000U of carrier-free recombinant human IL-2 shown in the schematic in Fig. 5.8A. Tumour burden was quantified by IVIS™ Spectrum (Perkin Elmer), with average radiance measurements quantified by Living Image™ Software within a defined ROI, consistent across all mice from each experimental group. Tumour burden was visibly higher across all groups on day 10 post-injection compared to day 6, indicating establishment and growth of the injected OVCAR8-Luc cells (Fig. 5.8B). In general, the presence of NK cells was associated with reduced tumour burden on both day 6 and day 10 post-injection compared to the vehicle treated group, with healthy NK cells functioning modestly better than the rest. The average tumour burden in the BL NK cell and POD1 NK cell treated groups were not significantly different from each other (Fig. 5.8B). IVIS images depicting tumour burden on day 6 post-injection are shown in Figure. 5.8C.

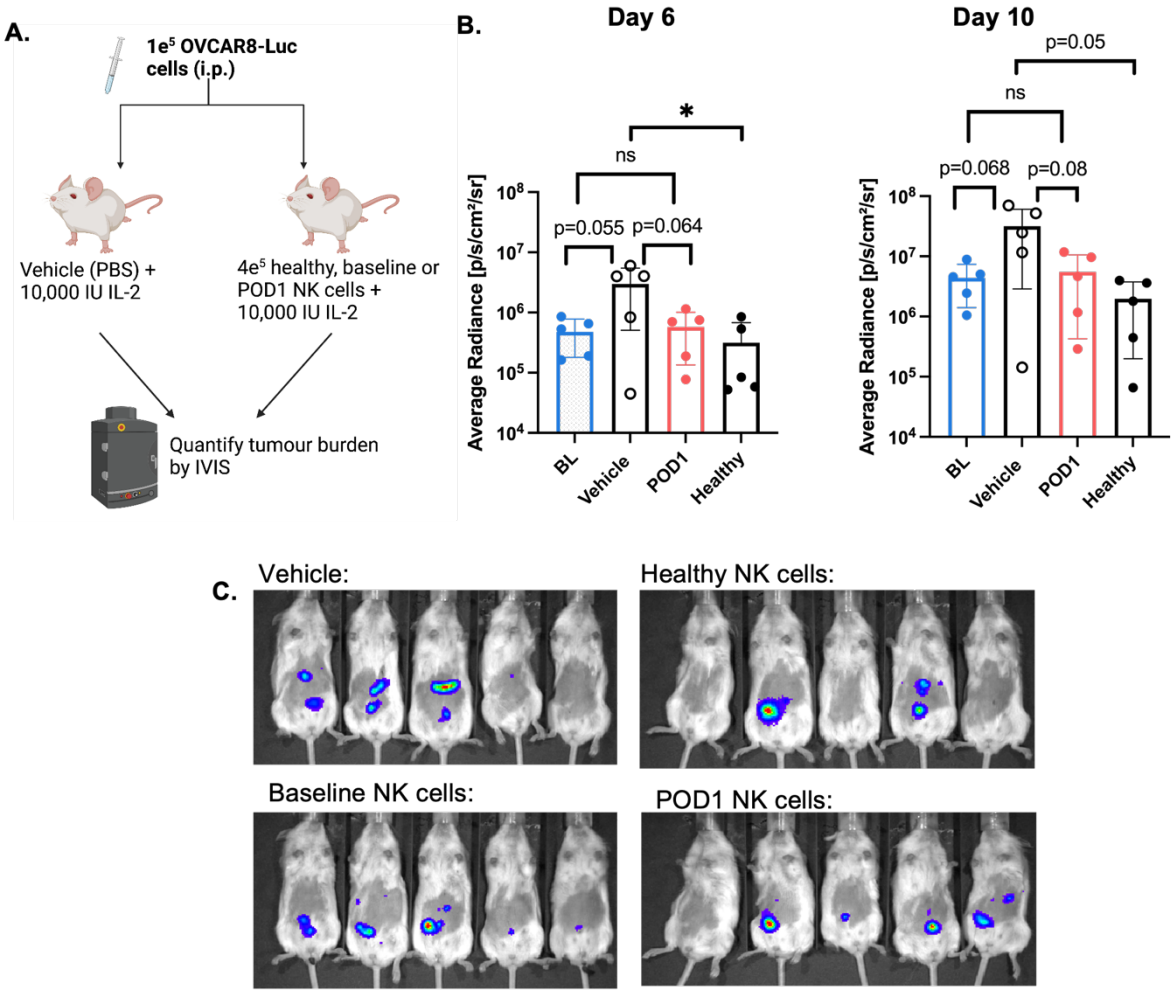

Figure 5.8. OVCAR8-luc xenograft mouse model to assess the *in vivo* efficacy of baseline and POD1 NK cells. A. NCG mice were administered 1e^5 OVCAR8 cells expressing luciferase (OVCAR8-Luc). At the same time, the mice received 4e^5 NK cells along with 10,000 U of IL-2. All injections were intraperitoneal (ip). The NK cells were isolated and frozen from healthy or patient-matched baseline and POD1 samples pooled from 3-4 donors per group. The vehicle control group received an ip injection of PBS with 10,000U of IL-2. N=5 mice/group. Injections were done on day 0 and mice were imaged by IVIS on days 6 and 10 post-injection. **B.** Average radiance measurements on days 6 and 10. **C.** IVIS images on day 6. Unpaired two-tailed t-tests were performed to determine statistical significance between treatment groups. ns: not significant; *p<0.05. Normality was confirmed using the Anderson-Darling, D'Agostino-Pearson, Shapiro-Wilk, and Kolmogorov-Smirnov tests. Schematic in panel A made with BioRender.

Next, we tested the use of exNK cells in this model. For this iteration of the experiment, we tested a modified injection timeline in which OVCAR8-Luc cells were administered two days prior to ip delivery of the exNK cells along with a dose of 10,000U of carrier-free recombinant human IL-2. Based on the IVIS images collected on day 7 post exNK injection and the corresponding average radiance measurements shown in Fig. 5.9A and B, respectively, it is apparent that the exNK cells confer better protection against tumour burden when administered at the same time as the OVCAR8-Luc cells, suggesting that they are preventing engraftment which sustains a reduced tumour burden over time. Despite this discrepancy between the two injection timelines, both exNK cell treated groups had less tumour burden on day 7 post exNK cell injection compared to the vehicle groups. Following day 7 imaging, the mice were sacrificed and a peritoneal wash was performed (PBS + 3%FBS + 1mM EDTA). The cells collected from the peritoneal wash were stained for the human NK cell surface markers CD45 and CD56. We detected a clear population of live exNK cells within the peritoneal wash (Fig. 5.9C). Taken together, this data indicates that exNK cells can control tumour burden in this model and remain viable within the peritoneal cavity for 7 days.

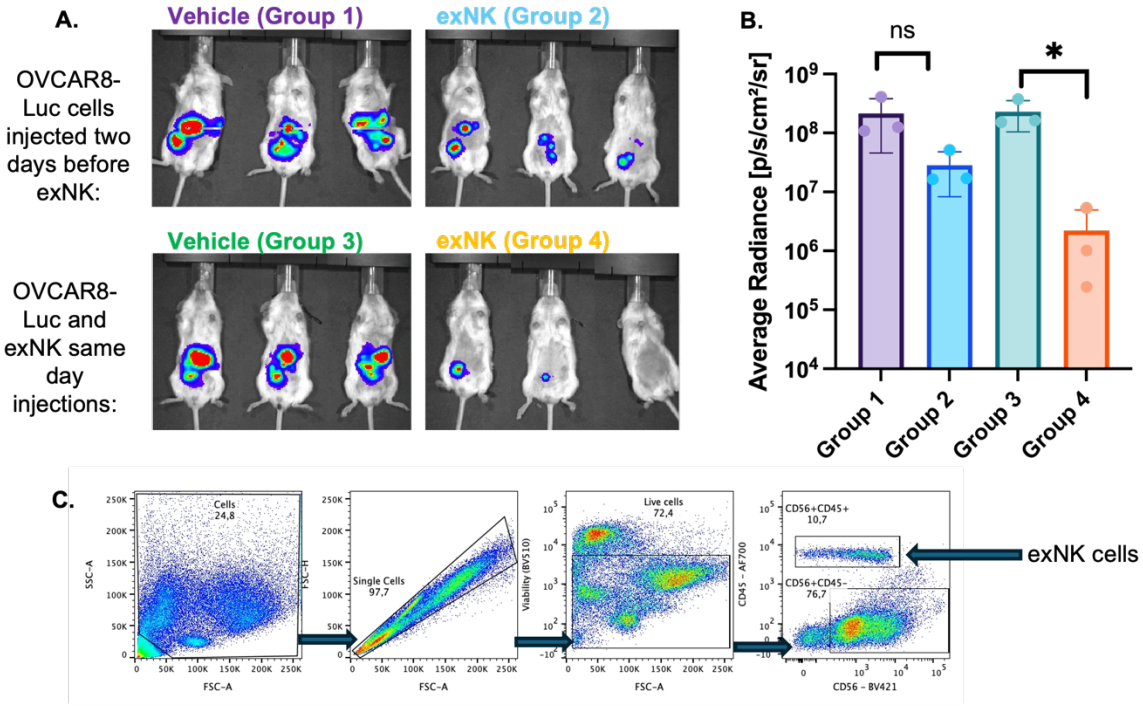

Figure 5.9. exNK cells have the capacity to control tumour burden *in vivo*. NCG mice were administered 1e^5 OVCAR8 cells expressing luciferase (OVCAR8-Luc) either 2 days prior (day -2: Groups 1 and 2) or at the same time (day 0: Groups 3 and 4) as receiving 4e^5 exNK cells or vehicle (PBS) by intraperitoneal (ip) injection. Both vehicle and exNK-treated mice received a dose of 10,000U of IL-2. The exNK cells were used on day 7 of expansion, generated from NK cells collected from 1 healthy donor. N=3 mice/group. **A.** IVIS images on day 7 post exNK cell or vehicle treatment. **B.** Corresponding average radiance measurements on day 7. **C.** Representative flow cytometry gating strategy showing human CD45$^+$CD56$^+$ cells detected in the peritoneal wash (PBS+3%FBS+1mM EDTA), collected on day 7. Unpaired two-tailed t-tests were performed to determine statistical significance between treatment groups. ns: not significant; *p<0.05. Normality was confirmed using the Shapiro-Wilk and Kolmogorov-Smirnov tests.

Following the optimization and establishment of the model detailed above, we sought to incorporate surgical stress. NCG mice received a dose of $1e^5$ OVCAR8-Luc cells ip 2 days prior to undergoing major surgery (laparotomy and left nephrectomy) to allow tumour engraftment prior to exposing them to surgical stress. After closing, the mice received an ip injection of $4e^5$ healthy, unexpanded NK cells combined from two donors along with 10,000U of carrier-free recombinant human IL-2. A schematic outlining the experimental timeline is shown in Fig. 5.10A. Control mice that received both OVCAR8-Luc and NK cells but did not undergo surgery were used as a comparison. IVIS images from all groups taken on postoperative day 7 (POD7) are shown in Fig. 5.10B. Two mice from the surgery group did not survive to POD7. There was no detectable difference in tumour burden between the control and surgically stressed groups. There appears to be a trend in higher tumour burden in the surgically stressed NK-treated group compared to the control NK-treated group, though these results are strongly influenced by two mice (Fig. 5.10C). When comparing the treatments between the control and surgically stressed groups separately, surgery appears to diminish the impact of the NK cells on tumour burden (Fig. 5.10D). Note that the IVIS data presented in Figure 5.10 were collected following acquisition of a new IVIS machine (Vilber Newton 7.0). Interestingly, we were only able to detect the healthy human NK cells within the peritoneal wash of control mice but not in the mice that underwent surgery (Fig. 5.10E). As such, we were unable to conclude whether the differences in tumour burden were a result of the human NK cells becoming functionally impaired because of surgical stress in these mice, or because the NK cells were simply not retained within the peritoneal cavity. As such, we decided that incorporation of surgical stress into this model required further optimization before the exNK cells could be tested. Future experiments will explore modifications to the

model including the possibility of different routes of administration, different readouts of tumour burden, or using a fully humanized murine model.

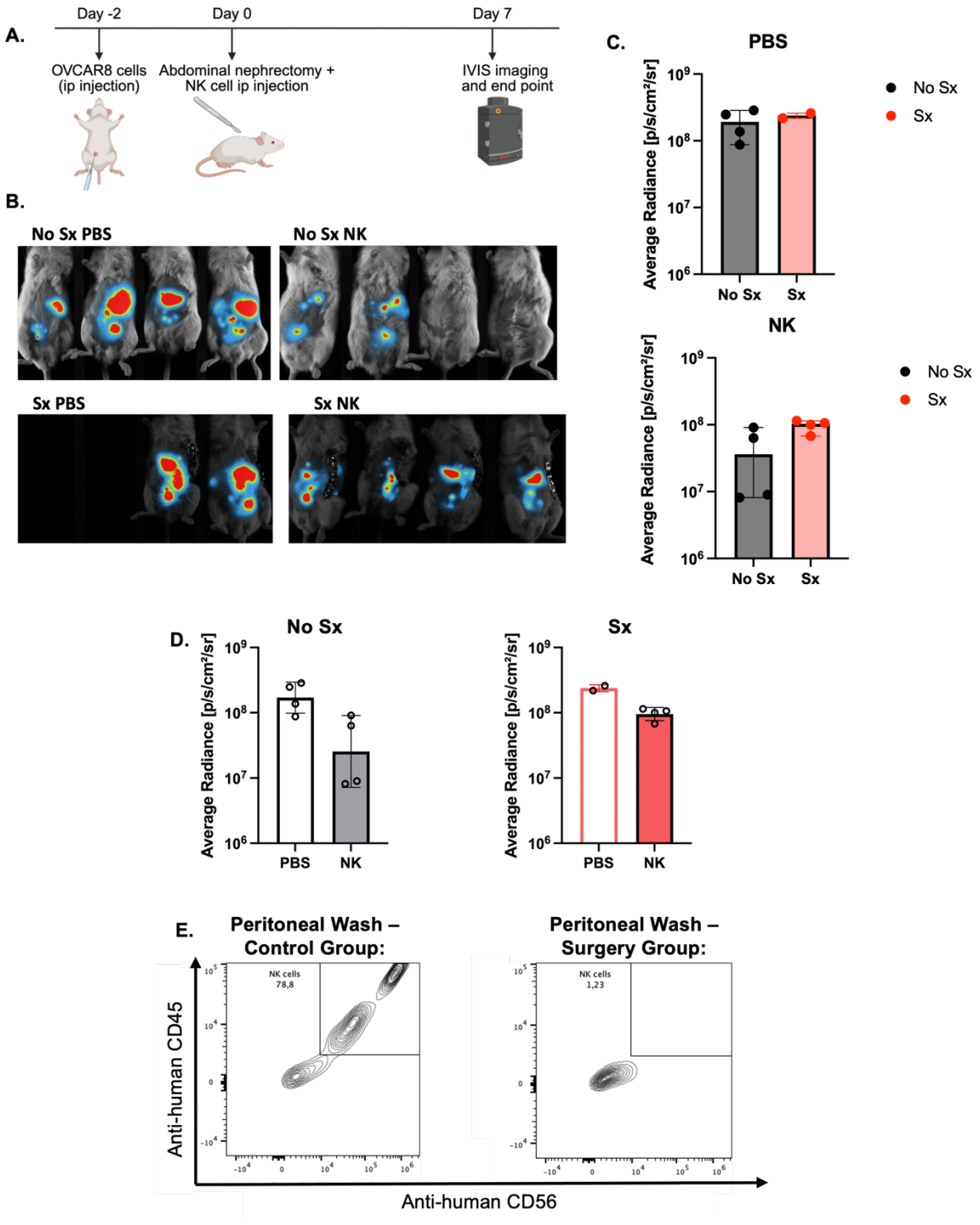
A.
Day -2
Day 0
Day 7
OVCAR8 cells (ip injection)
Abdominal nephrectomy + NK cell ip injection
IVIS imaging and end point
B.
No Sx PBS
No Sx NK
Sx PBS
Sx NK
C.
PBS
Average Radiance [p/s/cm²/sr]
No Sx
Sx
NK
D.
No Sx
Sx
PBS
NK
E.
Peritoneal Wash – Control Group:
Peritoneal Wash – Surgery Group:
NK cells 78,8
NK cells 1,23
Anti-human CD45
Anti-human CD56

Figure 5.10. Incorporation of surgical stress into the OVCAR8-Luc model. A. NCG mice were administered $1e^5$ OVCAR8 cells expressing luciferase (OVCAR8-Luc) two days prior to undergoing surgery (laparotomy with left nephrectomy). Immediately after closing, the mice received $4e^5$ healthy NK cells along with 10,000 U of IL-2. All injections were intraperitoneal (ip). The vehicle control group received an ip injection of PBS with 10,000U of IL-2. N=4 mice/group. Surgery was done on day 0 and mice were imaged by IVIS on POD7. **B.** IVIS imaging on POD7. **C and D.** Average radiance measurements on POD7 comparing control mice (No sx) to surgically stressed mice (Sx) between the PBS and NK cell treated groups, presented in two different ways. **E.** Representative flow cytometry plots showing human $CD45^+CD56^+$ cells detected in the peritoneal wash (PBS+3%FBS+1mM EDTA) from a control mouse (left) and surgically stressed mouse (right). Schematic in panel A made with BioRender.

Chapter Summary:

In all, the results presented here solidify the link between POD1 NK cell function and metabolism. Nutrient supplementation could not rescue POD1 IFN-γ production to BL levels, suggesting that a lack of nutrient availability is unlikely to be the cause of POD1 NK cell dysfunction. Taken together with our metabolic characterization data highlighting that dysfunctional POD1 NK cells have a significantly lower rate of glucose uptake not associated with a change in nutrient transporter expression, we predict that they are intrinsically imprinted with both metabolic and functional defects. To address this hypothesis, we attempted intrinsic metabolic modulation by diverting bioenergetic metabolism away from aerobic glycolysis and towards OxPhos using DCA. While we were unable to see a functional rescue with DCA, we also observed no change in mitochondrial mass or membrane potential. As an alternative approach to intrinsic metabolic modulation, we performed feeder cell-based *ex vivo* expansion of healthy primary NK cells, which generates highly metabolically and functionally active NK cells. For these experiments, we were assessing whether dysfunction could be prevented rather than reversed in the postoperative milieu. We showed that while *ex vivo* expansion could not fully prevent suppression in the postoperative milieu, these cells were not suppressed as severely by surgical stress as the patient's own endogenous NK cells. Together with their markedly higher IFN-γ production in response to IL-2/12 stimulation compared to the patient's NK cells, these findings support their potential as a perioperative adoptive cell therapy. Most importantly, these findings highlight that metabolic reprogramming through *ex vivo* expansion arms NK cells to retain their function under surgical stress, establishing a connection between metabolic activity, function, and the postoperative period. Future aims should thoroughly characterize the metabolic activity of exNK cells and explore methods to

engineer them to retain full functional capacity after surgery, in addition to continuing the development of a murine model to best evaluate their *in vivo* efficacy following surgical stress.

Chapter 6: Discussion

6.1 Summary

The intricate link between immune cell function and metabolism has garnered interest in recent years. While this has largely focused on effector T cells[236], including engineered CAR T cell therapy[237,238], the metabolic activity of primary NK cells has emerged as a distinct focus in the field of immunometabolism. NK cell dysfunction has been linked to metabolic deficiency in many disease states including obesity and cancer[152,158,159]. The perioperative period has long been recognized as an opportunity for residual disease and disseminated tumour cells to take advantage of the immunosuppressive state in the body and form metastases[239]. As such, events occurring within this relatively narrow window can have lasting repercussions on tumour recurrence and metastatic spread. Despite this, surgical resection remains crucial to offering cancer patients the best chance of cure[239]. Given the important role that NK cells play in the anti-tumour immune response, this highlights the largely unmet need to intervene during this critical window to circumvent postoperative NK cell suppression and ultimately improve outcomes for surgical cancer patients[14].

Here we show that NK cell dysfunction spans the different mechanisms of effector function including cytokine production and both granule-mediated and TRAIL-mediated cytotoxicity. Importantly, our results presented in Chapter 3 confirm that POD1 dysfunction persists upon NK cell isolation from whole blood. This is particularly relevant in the study of immune metabolism as it has been extensively reported that the extracellular environment is highly influential on metabolic activity[240]. Our data shows that POD1 NK cells retain their dysfunctional phenotype upon isolation, culture and *ex vivo* stimulation outside of the

postoperative milieu. Hence, we argue that POD1 NK cell dysfunction results from intrinsic reprogramming induced by the surgical insult.

We found that the most prominent dysfunction, measured by IFN-γ production, occurred in response to IL-2/12 stimulation. Accordingly, we characterized the metabolic profile of POD1 NK cells in response to IL-2/12 stimulation to assess metabolism at the peak of effector dysfunction. Our results suggest that the most significant metabolic impairment lies in the capacity of NK cells to undergo OxPhos on POD1, with only a slight reduction in glycolysis. NK cells had a decreased rate of glucose uptake which was not accompanied by a change in expression of nutrient transporters, including GLUT1, after surgery. To elucidate the relationship between NK cell metabolism and function in the postoperative context, we employed several methods of intrinsic and extrinsic metabolic modulation to 1) rescue dysfunctional NK cells or 2) prevent dysfunction. Metabolic modulation has become a promising approach to enhance the function of immune cells, particularly in the context of optimizing adoptive cell therapy for greater efficacy in the TME[235,238]. Within our dataset, nutrient supplementation to support effector function did not rescue POD1 NK cells. Likewise, promoting OxPhos using DCA could not rescue the function of POD1 NK cells, nor induce a change in mitochondrial mass or membrane potential. Finally, we tested feeder cell-based *ex vivo* expansion in the face of postoperative stress. This well-established technique generates both metabolically and functionally active NK cells which are armed to withstand the inhospitable TME[203–205]. Interestingly, not only did healthy donor-derived exNK cells remain highly active in POD1 blood, but their presence also partially rescued endogenous NK cell function.

In short, we have found that human NK cells exhibit a profound deficiency to perform OxPhos after surgery in response to exogenous cytokine stimulation, which is key to

the hyporesponsive phenotype we have established on POD1. A central theme in the interpretation of our data is whether POD1 NK cell functional and metabolic deficiency is caused by the environment in the circulation, or whether there is a cell-intrinsic basis for their dysfunction. While we argue in favour of intrinsic reprogramming, given the complex nature of the postoperative milieu, we acknowledge that this phenomenon is likely caused by a combination of both extrinsic factors as well as intrinsic reprogramming. As such, we consider both angles of this discussion below.

6.2 POD1 NK cell dysfunction spans several levels of effector function and persists after removal from whole blood

We assessed POD1 NK cell function across multiple levels of isolation from the whole blood environment. Reduced IFN-γ production and granzyme B content were detected in POD1 NK cells in both whole blood and following PBMC isolation, while perforin remained relatively unchanged. Granzyme B and perforin are important components of cytolytic granules and arm NK cells to be poised to kill their targets[241]. This discrepancy in the effect of surgery on granzyme B versus perforin content could be related to a mechanism of synthesizing perforin which bypasses loading into cytolytic granules, continuously shuttling perforin to the immune synapse[242,243]. Most importantly, we found that upon isolation from PBMCs, POD1 NK cells have reduced IFN-γ production and an impaired ability to degranulate upon interaction with K562 target cells. Furthermore, we report that the direct cytotoxicity of isolated BL and POD1 NK cells via the major mechanisms of granule-mediated and TRAIL-mediated killing are reduced on POD1. In all, when considering parameters related to cytotoxic function (degranulation and direct cytotoxicity across different mechanisms), we noted that POD1 NK cells were functioning at about 70-80% of

their BL capacity. Conversely, POD1 NK cells were functioning at just over 50% of their BL capacity based on IFN-γ production in response to IL-2/12 stimulation. Therefore, our data indicates global functional impairment on POD1, however the extent of dysfunction differs based on the readout in question. These results formed the basis for characterizing metabolism in response to IL-2/12 stimulation, capturing the peak of POD1 NK cell dysfunction.

Circulating NK cells can be divided into distinct subsets based on their surface expression of CD56 and CD16[244]. While it is widely accepted that there are two subsets ($CD56^{dim}CD16^{bright}$ and $CD56^{bright}CD16^{dim}$) with distinct functional preferences, additional subsets have been reported. Some groups have defined five different NK cell subpopulations within human peripheral blood[245]. Our data consistently shows a clear division of three main subsets which we denoted as $CD56^{bright}$, $CD56^{dim}$ and $CD16^{-}$ throughout our dataset. We have shown that the frequency of the $CD16^{-}$ subset increases in culture with cytokine stimulation, which is a phenomenon reported by other groups[246] and is believed to be caused by the activity of matrix metalloproteinases[247], such as ADAM17[222]. The increase in frequency of the $CD16^{-}$ subset corresponds to a proportional decrease in frequency of the $CD56^{dim}$ subset, supporting the hypothesis that this largely understudied population results from $CD56^{dim}CD16^{bright}$ NK cells shedding CD16 from their surface[247]. These data also disprove the notion that the $CD56^{dim}$ subset is terminally mature and suggests some degree of plasticity between subsets, at least under *in vitro* culture. The importance of considering this population as a distinct NK cell subset has been argued on the basis of its unique functional and phenotypic characteristics[248]. These include high CD27 and low CD57 expression, suggesting that they are immature[245]. Penack et al studied degranulation, measured by surface expression of CD107a, and found that among the NK cells degranulating in response

to leukemia and lymphoma targets, the majority were $CD56^{dim}CD16^{-}$[249]. Within our own dataset, we found that the frequency of the three major NK cell subsets remained constant from BL to POD1, and all subsets showed impaired IFNγ production and degranulation after surgery. Taken together, the $CD16^{-}$ subset likely had a substantial influence on our overall bulk NK cell functional readouts, highlighting the importance of distinguishing it as a unique NK cell subset.

Overall, our results provide compelling evidence that NK cells exhibit intrinsic dysfunction on a cell-per-cell basis after surgery, a phenomenon bestowed upon them by the postoperative milieu. These findings are summarized in Figure 6.1. We argue that exposure to the immunosuppressive POD1 environment within the circulation leaves a lasting imprint on their functional signature which persists long after removal from whole blood. These findings are crucial to our downstream assessment of metabolic activity.

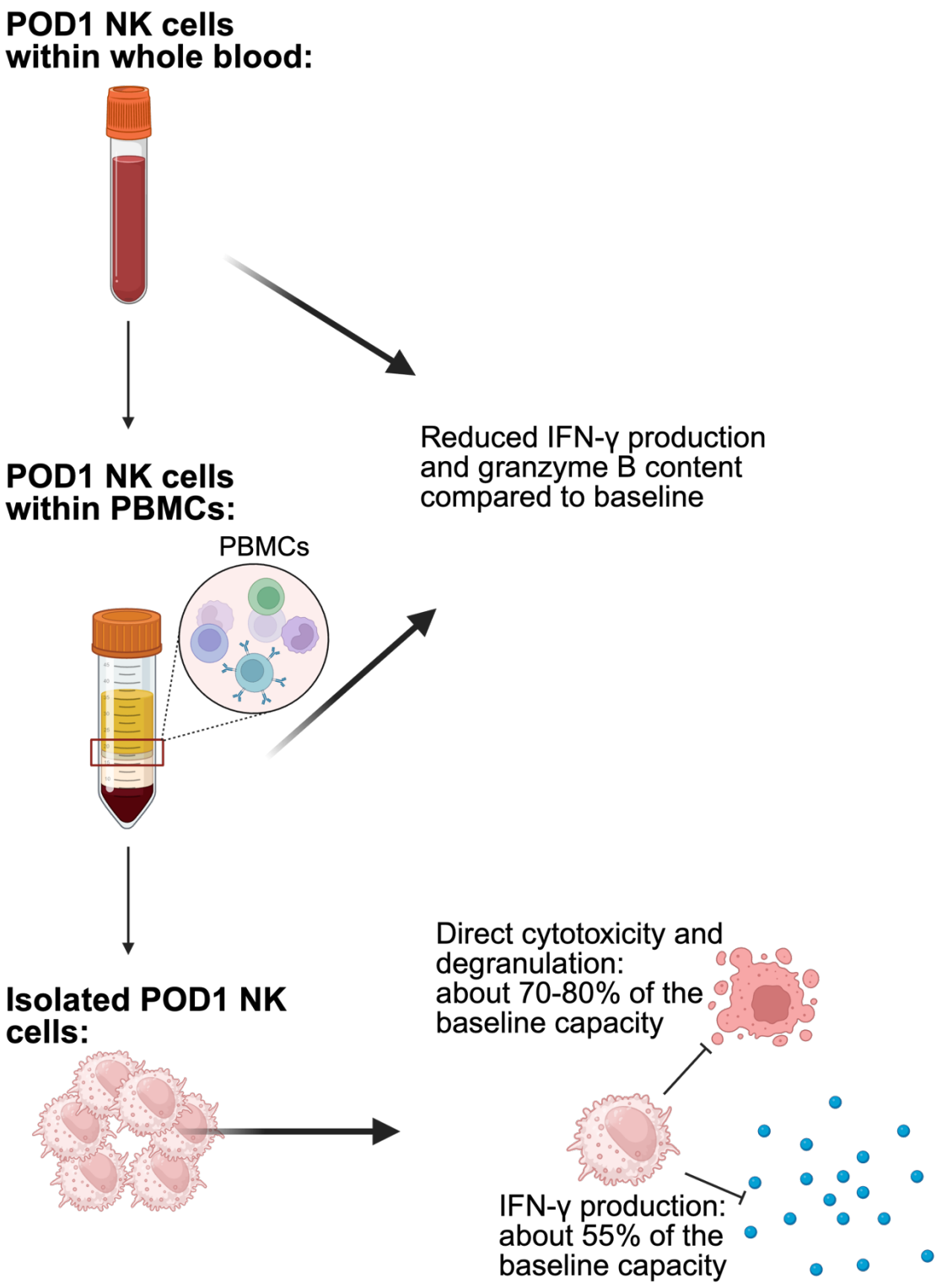

Figure 6.1. Summary of postoperative NK cell dysfunction which persists upon isolation from whole blood.

6.3 Dysfunctional POD1 NK cells have a reduced capacity for OxPhos compared to baseline

Our assessment of real-time metabolic activity clearly points towards a deficiency in OxPhos being at the heart of postoperative NK cell metabolic impairment. As this was measured by Seahorse™, a bulk assay, we were unable to characterize NK cell subsets separately. We report that maximal respiration and spare respiratory capacity, indicative of the cells' ability to respond to a strong energetic demand[250], were significantly reduced on POD1 while glycolytic parameters were not significantly different. Perhaps the most notable finding was that POD1 NK cells exhibited approximately 50% capacity to metabolically respond to a strong energetic demand compared to BL following 24 hours of IL-2/12 stimulation. Taken together with our functional data showing POD1 NK cells producing IFN-γ at about 55% of their BL capacity, these results show that POD1 NK cell dysfunction is directly associated with a proportional decrease in metabolism, solidifying the connection between metabolism and function in NK cells in the perioperative context. Given that NK cell metabolic activity is highly influenced by the type and duration of stimulation[148], measuring metabolism at the end of the 24-hour stimulation period likely influences the metabolic phenotype. NK cells are known to depend on both glycolysis and OxPhos for extended stimulation times of 24 hours or more[251]. Primary NK cells have very low levels of basal metabolic activity at rest[252]. We found that measuring metabolism after just 4 hours of IL-2/12 stimulation (Supp. Fig. 4) resulted in nearly undetectable metabolic activity in both BL and POD1 NK cells, which has also been reported in murine NK cells[148]. This supports our rationale for measuring real-time rates of metabolism following 24 hours of cytokine stimulation.

Our extracellular flux data aligns with our previously reported single cell RNA sequencing data showing that POD1 NK cells have downregulated expression of OxPhos and cellular respiration gene sets[3], which substantially influenced our decision to study POD1 NK cell metabolism. Unfortunately, gene expression data alone does not consider that metabolic networks are highly connected and dynamic, missing critical information about metabolic flux[182]. To generate a flux-based analysis of metabolism from this RNA sequencing dataset, we performed METAFlux to provide an estimation of uptake or release of nutrients in relation to an external reference medium. It is important to consider that these are strictly estimations and only meant to accompany our more direct metabolic readouts. Interestingly, despite the significant downregulation in expression of OxPhos-related genes reported through GSEA, the METAFlux-assigned score indicates that POD1 NK cells take up more O_2 than BL. One important consideration is that the single-cell RNA sequencing analysis was done on resting PBMCs, while most of our direct metabolic readouts were conducted on IL-2/12-stimulated isolated NK cells, which count potentially account for discrepancies between METAFlux estimations and our other metabolic readouts. However, this does not explain why the GSEA results and the METAFlux estimation show opposing results for oxygen consumption/cellular respiration when they were generated from the same dataset. One reason for this discrepancy is that both analyses are measuring fundamentally different things, thereby requiring different assumptions. METAFlux considers expression of rate-limiting enzymes and operates within defined flux constraints, accounting for stoichiometric balance of metabolic reactions[253]. It is also highly influenced by the metabolic model used and the chosen medium conditions. On the other hand, GSEA evaluates expression data globally based on a pre-defined pathway[229] and does not consider whether enzymes are rate-limiting. In all, for the purpose of characterizing the metabolic profile of

POD1 NK cells in this study, we favoured more direct readouts of metabolic flux. However, METAFlux could be a beneficial approach to future studies since it allows for estimations of metabolic flux using gene expression data and would be particularly useful in comparing metabolism across NK cell subsets.

To accompany our real-time metabolic measurements of OxPhos, we assessed parameters related to mitochondrial health including overall mitochondrial mass and membrane potential, which can provide an indication of the metabolic status of a cell[254]. It is generally accepted that healthy mitochondria have intact polarized membrane potentials, resulting in retention of rhodamine dyes, such as TMRM. Zecca et al. showed that dysfunctional tumour-infiltrating NK cells in hepatocellular carcinoma had a higher proportion of mitochondrial membrane depolarization which was associated with reduced glucose uptake in comparison to healthy liver-infiltrating NK cells[255]. Despite this, these readouts must be interpreted with caution, as the mitochondrial mass and membrane potential measured within a cell are highly context dependent. For instance, Ledderose et al. showed that T cell activation with anti-CD3/CD28 stimulation resulted in a steep, immediate decrease in mitochondrial membrane potential[256]. Furthermore, the OxPhos uncoupler FCCP can cause mitochondrial depolarization while simultaneously increasing oxygen consumption in a dose-dependent manner[257]. As such, a drop in membrane potential can also be caused by production of significant amounts of mitochondrial ATP in response to stimulation, and not necessarily only due to poor mitochondrial health. Similarly, an overall high mitochondrial mass does not indicate mitochondrial function. These mitochondria could be damaged and not effectively generate ATP, often due to insufficient clearance of dysfunctional mitochondria through mitophagy[258]. Within our dataset, we observed a significant decrease in membrane potential in both resting and IL-2/12 stimulated POD1 NK

cells compared to BL, but no significant difference in mitochondrial mass. A strong linear correlation between mass and membrane potential would suggest that the mitochondria within the cell are healthy and productive[152]. The linear correlation between mass and membrane potential was strong and significant in BL and POD1 NK cells under both resting and IL-2/12 stimulated conditions. Interestingly, the strength of the correlation decreased slightly with stimulation in BL NK cells, but showed the opposite trend on POD1, suggesting that stimulation affected mitochondrial dynamics differently between our two perioperative timepoints. Most importantly, given that mitochondrial mass remains the same in NK cells after surgery, the decrease in OxPhos that we have observed is not due to a change in total mitochondrial content. One important element that is not captured within this dataset is mitochondrial architecture. This can be assessed through microscopy by measuring elongation, fission and branching as well as evaluating the activity of mitochondrial fusion and fission proteins in relation to mTORC1 signaling[193]. Jheng et al. reported that skeletal muscle cells, when exposed to nutrient excess in the context of obesity, exhibited elevated ROS production and subsequent mitochondrial depolarization. Consequently, the mitochondria adopted a fragmented morphology, which is associated with mitochondrial dysfunction and reduced ATP production[259]. Given that patients experience a period of hyperglycemia after surgery[81], a plausible hypothesis is that the mitochondria within POD1 NK cells are fragmented which is driving their inability to perform OxPhos and efficiently generate ATP, thus contributing to an impaired effector response.

In all, our evidence points towards impaired OxPhos being an essential factor in postoperative NK cell dysfunction. Furthermore, we have strengthened the intricate connection between function and metabolism by directly associating POD1 dysfunction with a corresponding metabolic decrease. Future work should focus on characterizing

mitochondrial dynamics in depth by assessing their architecture. In particular, the relationship between mTORC1 signaling (which we know to be downregulated in NK cells after surgery[3]), mitochondrial dynamics, and OxPhos should be thoroughly characterized in POD1 NK cells as it could be a key mechanistic driver in mediating postoperative NK cell dysfunction. While real-time metabolic measurements provide the most accurate depiction of NK cell metabolic flux, we completed additional elements of metabolic characterization to create a comprehensive overview of the metabolic landscape of POD1 NK cells. We argue that our findings signify a cell-intrinsic nature of POD1 NK cell metabolic impairment.

6.4 Metabolomic characterization suggests a surgery-induced change in amino acid metabolism in NK cells

Metabolomics analysis was done on isolated IL-2/12 stimulated BL and POD1 NK cells. In contrast to metabolite uptake/efflux estimations provided by METAFlux, metabolomics measures direct and absolute concentrations of a targeted list of aqueous metabolites. Even so, the metabolomics data must still be interpreted carefully. Metabolomics provides a static snapshot of metabolite concentrations within a cell at a given time, which can be influenced by multiple factors including uptake/efflux, endogenous synthesis, or rate of metabolism through downstream pathways[260]. Unfortunately, only inosine approached statistical significance, showing a higher abundance in BL NK cells compared to POD1. Inosine is a nucleoside generated from adenosine by adenosine deaminase[170]. It has been shown to improve the function of CD8+ effector T cells, particularly under conditions of glucose restriction[261]. More specifically, the ribose subunit of inosine can enter central carbon metabolism in T cells to support ATP synthesis which fuels effector functions[261]. Furthermore, exposing CAR-T cells to inosine or engineering them to

overexpress adenosine deaminase can increase their stemness and augment their effector functions[262]. As such, a higher abundance of inosine within BL NK cells aligns with them being more functional. Although none of the differences in metabolite concentration between BL and POD1 NK cells reached statistical significance, we still uncovered some notable trends in amino acid abundance within POD1 NK cells. More specifically, many of the metabolites that had an approximately 2-fold increase in concentration or more on POD1 were amino acids, including the essential amino acid tryptophan and its downstream metabolite kynurenic acid. Tryptophan is predominantly metabolized through the kynurenine pathway which leads to the production of NAD+, an important electron acceptor in glycolysis and the TCA cycle. This pathway is activated by inflammation and stress, mainly by IFN-γ and glucocorticoids, and has an influence on immune responses[263]. The metabolite with the highest concentration on BL compared to POD1 was itaconic acid. This well-studied immunometabolite has been shown to affect the TCA cycle by blocking one of its enzymes, succinate dehydrogenase (which is also an enzyme in the ETC), causing a metabolic shift towards aerobic glycolysis and modulating inflammatory responses by macrophages[264]. It has also been shown to assist in the defense against ROS by regulating the Nrf2 pathway. In relation to oxidative stress, a metabolite of interest that showed up as being increased over two-fold on POD1 was cystine. It can be taken up into the cell in exchange for glutamate[265] by the xCT antiporter, which is important for maintaining redox homeostasis[230]. Once inside the cell, cystine becomes reduced to cysteine, which is an important precursor in the production of glutathione – a key antioxidant[266]. Under conditions of oxidative stress, cells require glutathione to neutralize ROS, thereby preventing DNA damage and loss of viability. A high level of intracellular cystine could suggest that the NK cells are taking up more

cystine from their environment to combat potential oxidative stress and/or are unable to metabolize it to generate glutathione, leading to intracellular cystine accumulation.

In addition to looking at the relative abundance of the metabolite hits on BL versus POD1, we also presented significant associations between metabolites through Pearson correlation analysis. Overall, there are notably more significant correlations between metabolites on POD1 than on BL, with the majority being positive correlations. Again, several of these metabolites with significant correlations on POD1 were amino acids. Taken together, we believe this may point towards a change in amino acid metabolism within POD1 NK cells. In mice, NK cells have been shown to rely on the consistent uptake of amino acids through SLC7A5 in response to IL-2/12 stimulation to sustain the constant synthesis and degradation of c-myc, an important transcription factor promoting the expression of glycolytic enzymes and proteins involved in biosynthesis. Loss of c-myc has been shown to be correlated with impaired NK cell function[146,147]. Jenson et al. showed that IL-2 priming upregulated the expression of amino acid transporters in both $CD56^{bright}$ and $CD56^{dim}$ NK cells which was necessary for IFN-γ production and degranulation following engagement of NKG2D[267]. This was found to be regulated by mTORC1 signaling[267]. Furthermore, IL-18 has been shown to increase the expression of CD98/LAT1 in an mTORC1-independent manner, resulting in the uptake of leucine and activation of mTORC1 signaling, supporting increased metabolism, effector function, and proliferation. This response was dependent on intracellular glutamine levels[124]. Taken together, this highlights the critical involvement of amino acids in supporting NK cell function and metabolism, providing a rationale for future experiments studying the implications of surgical stress on amino acid metabolism in dysfunctional POD1 NK cells.

In all, this project focused on understanding differences in bioenergetic metabolism within NK cells that occur after surgery and is associated with their dysfunction. More specifically, harnessing our understanding of these bioenergetic networks to improve the function of POD1 NK cells. While metabolomics contributed to our holistic understanding of POD1 NK cell metabolism, these data could be more beneficial to future studies aimed at delineating the intricate differences in metabolic networks on a more mechanistic level, particularly in relation to the oxidative stress response and amino acid metabolism. This dataset could be expanded by stratifying the results across NK cell subsets and pursuing more flux-based metabolomics analyses, such as stable isotope tracing.

6.5 Challenges in directly comparing metabolism between two perioperative timepoints in primary human NK cells

Faithfully forming a biologically accurate comparison of patient-matched BL and POD1 NK cell metabolism posed several challenges. One of the main limitations of our data was the use of cryopreserved NK cells. Cryopreservation is known to affect cellular metabolism, making freshly isolated cells preferable for metabolic studies[268]. This topic has been thoroughly examined in immunometabolism, as it is a common area of concern especially when using human samples. Luscombe et al. conducted an evaluation of the effects of cryopreservation on the metabolism of PBMCs. Their study assessed the cryopreservation of PBMCs over a duration of up to 70 days, demonstrating an overall decrease in translation the longer the cells were frozen[269]. While they show that cryopreservation caused a metabolic switch, favouring glycolysis over OxPhos and potentially inducing mitochondrial dysfunction, they also highlight that the metabolic increase which occurs in response to activation remained detectable across CD3+ T cell

subpopulations[269]. During our optimization, we considered several possibilities to use fresh NK cells for our extracellular flux assays. One of these included culturing BL NK cells overnight until POD1 NK cells could be collected from the same patient the next day. Supplemental Figure 5 shows the mitochondrial mass and membrane potential in healthy NK cells in culture for 4 and 24 hours (±1 hour). Both mitochondrial parameters were notably higher after 24 hours in culture compared to 4 hours, even without stimulation. Therefore, we could not culture freshly isolated BL NK cells for an additional day and accurately compare their metabolic activity to patient-matched POD1 NK cells. We have clearly demonstrated that POD1 NK cell dysfunction is present in cryopreserved, isolated NK cells. Given our aim to establish a relationship between metabolism and postoperative NK cell dysfunction, we prioritized the assessment of metabolism and function under the same conditions.

A key principle in the study of cellular metabolism is minimizing cell manipulation and assessing metabolic activity under physiologically relevant conditions[270]. Recent advancements have allowed for the evaluation of cellular metabolism within tissue sections, including spatially resolved metabolomics[271] and stable isotope-tracing[272]. Since this approach is not directly applicable to circulating immune cells, the focus has been towards developing techniques to evaluate immune cell metabolism with single-cell resolution, allowing for the assessment of metabolic activity within a heterogenous cell population with minimal manipulation[185]. To address this within our dataset, we pursued SCENITH (single cell energetic metabolism by profiling translation inhibition), which is illustrated in Supplementary Figure 6. Since translation is a highly ATP consuming process, SCENITH is based on the critical assumption that metabolic inhibition results in an immediate and proportional decrease in global translation[186]. Our lab has established that both the phenotypic and functional impact of surgery can be imparted on healthy NK cells through

exposure to suppressive POD1 whole blood (Mistry et al. 2026, manuscript under review). In addition to assessing the metabolism of endogenous POD1 NK cells directly in whole blood, the purpose of pursuing SCENITH was to evaluate whether exposure to POD1 whole blood could change the metabolic signature of exNK cells. A schematic summary of the technique is outlined in Supplemental Figure 6A. As proof-of-concept, we tested the technique in isolated BL and POD1 NK cells. Briefly, IL-2/12 stimulated isolated BL and POD1 NK cells were treated with either oligomycin (1uM), 2-DG (100mM), or both for 30 minutes. Next, O-propargylpuromycin (OPP) was added to the NK cells to terminate translation. OPP incorporation was detected by click chemistry and measured by flow cytometry. As a positive control for translation inhibition, we included a treatment condition with harringtonine, an alkaloid which blocks protein synthesis by impeding peptide bond formation and tRNA binding to the ribosome[273] (Supp. Fig. 6B). Overall, there was a slight but significant decrease in global translation in POD1 NK cells compared to BL NK cells (Supp. Fig. 6C). Interestingly, the metabolic inhibitors oligomycin and 2-DG did not cause a reduction in translation. There was an unexpected trend towards increased global translation with oligomycin treatment in both BL and POD1 NK cells ($p=0.05$) (Supp. Fig. 6D). No significant effect of 2-DG on the global translation of both BL and POD1 NK cells was observed (Supp. Fig. 6E). Luscombe et al. noted a variable impact of oligomycin and 2-DG on translation in NK cells within PBMCs which differed depending on the duration of cryopreservation. They also report “negative inhibition” of translation with 2-DG treatment[269], highlighting the potential limitations of using changes in global translation to make metabolic conclusions regarding primary human NK cells. They also noted the highest degree of non-specific puromycin signal within $CD56^{dim}$ NK cells compared to the other cell types assessed within PBMCs (CD8+ and CD4+ T cell subpopulations and monocytes)[269].

Consequently, we determined that SCENITH would not be a viable approach for us to make conclusions regarding postoperative NK cell metabolism.

While we did not implement SCENITH as a method for assessing NK cell metabolism, we incorporated measurement of global translation as an additional readout in our workflow. More specifically, we gathered information regarding the translational, functional, and metabolic responses to oligomycin and 2-DG treatment. Metabolic inhibition by blocking glycolysis/glycolysis-driven OxPhos using 2-DG or by blocking OxPhos using oligomycin is known to inhibit the function of NK cells[150,274]. We confirmed within our own dataset that both oligomycin and 2-DG strongly impaired the ability of both BL and POD1 NK cells to produce IFN-γ in response to 24 hours of cytokine stimulation. In our assessment of the impact of metabolic inhibition on degranulation following a 4-hour co-culture with K562 target cells, we observed that oligomycin did not affect degranulation, while 2-DG resulted in a decrease. These results confirm that the effect of metabolic inhibition is largely dependent on the type and duration of stimulation, as well as the functional readout in question[274]. The functional impact of metabolic inhibition was consistent across NK cell subsets and between the BL and POD1 timepoints, suggesting that they share the same reliance on glycolysis, OxPhos and glycolysis-driven OxPhos to carry out their effector functions. In addition to their functional impact, oligomycin and 2-DG had a direct metabolic impact, as measured by Seahorse™. Acute injection of oligomycin resulted in an immediate drop in OCR, generating a compensatory increase in ECAR. This could account for the NK cells' resilience against oligomycin measured by their ability to continue translation and degranulation despite blocking the activity of ATP synthase. On the other hand, acute injection of 2-DG resulted in an immediate drop in ECAR with no measurable compensatory increase in OCR. It is important to consider that IFN-γ production

and degranulation occur downstream of distinct signaling pathways within the NK cells. Production of IFN-γ is an energy demanding process in which the cells must respond to cytokine stimulation, triggering transcription, translation and secretion of IFN-γ[125]. Degranulation follows engagement of activation receptors which trigger a phosphorylation cascade downstream of ITAMs leading to mobilization of pre-formed granules[275]. Despite the measured effect of metabolic inhibition on metabolism and IFN-γ production, we did not observe a corresponding decrease in global translation with these two metabolic inhibitors. One possible explanation is that acute metabolic stress is causing an "energy crisis"[150] within the NK cells, potentially activating stress-response signaling pathways which transiently increase translation. We may be measuring translational blockade at the peak of this response before total shutdown. It is also important to consider that the increase in translation being measured may not truly be global. Downstream targets of stress-response signaling pathways include survival genes that the NK cells may express to overcome metabolic stress. This could result in selective increased translation of stress-adaptive transcripts[276,277]. There are also technical considerations that may confound the puromycin signal being detected. For instance, a strong puromycin signal does not necessarily mean that translation is efficient or productive. Puromycin gets incorporated into nascent proteins and blocks further translation. Information regarding potential defects in translation, such as ribosome stalling or incomplete elongation is not detected using this method[278].

In all, we encountered several challenges when devising the best strategy to answer the central question of this project: are postoperative NK cells metabolically impaired? Considering all factors, both logistic and technical, and with full acknowledgement of the criticisms associated with the study of cryopreserved cells, we argue that our approach best fit the constraints of our experimental design. Our aim was to establish a strong link between

POD1 NK cell dysfunction and a change in their metabolism induced by surgical stress, which we have done through the data presented herein.

6.6 NK cell metabolic impairment is caused by intrinsic reprogramming imparted by the immunosuppressive postoperative environment

Our data points towards an intrinsic reprogramming imparted on NK cells by the postoperative environment in the circulation. When considering NK cell metabolism in other contexts of dysfunction, several environmental factors are known to impact metabolism. For example, various factors within the TME including nutrient and oxygen deprivation and high lactate accumulation have been linked to impaired NK cell responses[279]. While there are many similarities between the refractory POD1 NK cell phenotype and NK cells in the TME, the postoperative environment differs in many ways. There are several factors present, both soluble and cell-based, which can impact NK cell function, making it difficult to narrow down one specific mechanism central to dysfunction. Although outside the scope of this project, our lab has focused specifically on TGF-β signaling in NK cells as a potential soluble driver of postoperative NK cell dysfunction. We have previously established a link between TGF-β and reduced mTORC1 signaling in POD1 NK cells[3]. Moreover, we have shown that blocking TGF-β signaling by inhibiting the activity of ALK5 (TGFβRI) was able to prevent dysfunction from occurring in healthy NK cells exposed to suppressive POD1 plasma. The connection between TGF-β, mTORC1 and impaired NK cell function and metabolism has been well-established[30,34,152]. Future directions for the study of postoperative NK cell metabolism should focus on delineating this relationship in the postoperative

context. This can be done by assessing whether blocking TGF-β signaling has a protective effect on metabolism in NK cells exposed to the POD1 environment.

For this project, we considered nutrient availability as an extrinsic variable in the postoperative setting. As mentioned, following trauma to the body, patients are subject to what is called the "metabolic stress response"[81]. This is directly linked to the endocrine response to surgery and occurs largely because of an increase in stress hormones[280]. In short, patients are in a catabolic and hyperglycemic state, which means that the amount of glucose that circulating NK cells are exposed to would transiently increase because of surgical stress[280]. Another consideration is that the glucose level in which the cells are exposed to *in vitro* is significantly higher than a clinically recognized high glucose level[281]. As such, reduced availability of glucose is likely not the cause of POD1 NK cell dysfunction, but rather their inability to efficiently uptake and metabolize the glucose available to them. This was validated by the inability of glucose supplementation to have a functionally rescuing effect on POD1 NK cells, though the response was varied across patients within our dataset. We also tested whether supplementing the culture media with additional arginine or glutamine, two amino acids critical to NK cell function[147,163], could have a rescuing effect on POD1 NK cells. Contrary to glucose, plasma arginine and glutamine levels are known to decrease after surgery[282,283]. Arginine metabolism plays a crucial role in regulating immune responses[163,164], and decreased levels of circulating arginine have been identified as a predictor of mortality in critically injured trauma patients[164]. We have shown that depletion of arginine by activity of ARG1 in sxMDSCs is a major source of their suppressive activity on NK cells[4]. Similarly, glutamine has been found to be a crucial amino acid in governing NK cell function and metabolism not by driving glutaminolysis, but rather through maintenance of c-Myc levels to sustain transcription of glycolytic enzymes[147]. Intracellular

glutamine is exchanged for the import of large neutral amino acids such as leucine, which are important in sustaining NK function and proliferation[124]. Like glucose supplementation, additional arginine or glutamine did not have a functionally rescuing effect on POD1 NK cells. In general, nutrient availability has been shown to have a varied effect on NK cell function. For instance, while increased glucose consumption is known to occur in response to stimulation, inhibition of glucose uptake through facilitative glucose transporters does not impact cytotoxicity or serial killing in NK cells[82]. Although counterintuitive, nutrient excess, particularly glucose, can negatively impact NK cell effector functions. NK cells exposed to glucose concentrations comparable to what is seen in uncontrolled diabetes (~35-45mM) has been shown to impair cytolytic function[284]. In all, we conclude that the approach of supplementing POD1 NK cells with a surplus of nutrients does not rescue their function. This indirectly suggests that a lack of nutrient availability is not responsible for POD1 NK cell functional and metabolic impairment, supporting our hypothesis for an intrinsic basis of dysfunction. As such, we pursued more specific approaches tailored at intrinsically modifying the metabolic activity of NK cells to efficiently generate ATP.

6.7 Metabolic modulation to rescue the function of POD1 NK cells

Treatment with the PDHK inhibitor sodium dichloroacetate (DCA) cannot rescue POD1 NK cell function:

In keeping with our argument that impaired OxPhos is crucial to POD1 NK cell dysfunction, we sought to rescue function by modulating OxPhos. This approach has been well-reported in the context of powering the mitochondria in NK and T cell-based adoptive cell therapies to better withstand the inhospitable TME[235]. There are different ways that this can be achieved such as through blocking the activity of mitochondrial fission enzymes[285],

boosting mitochondrial biogenesis by promoting the expression of PGC1α[199], and by knocking out negative-regulators of activity such as *CISH*[235], which has been shown to improve *in vivo* efficacy and increase the rate of OxPhos in CAR-NK cells[286]. The method in which we chose to boost OxPhos in our POD1 NK cells was through treatment with DCA. This compound has been reported to impair tumour cell proliferation by blocking the activity of PDHK, inducing OxPhos and decreasing aerobic glycolysis[287]. DCA has also been shown to sensitize tumour cells to NK cells through upregulation of stress-induced ligands, a phenomenon that was dependent on the expression of p53[233]. More recently, DCA has been shown to enhance the antitumour immune response by promoting the complete oxidation of glucose, generating ATP more efficiently to sustain effector activity[198]. Contrary to what has been reported with NK92 cells and CAR-T cells, DCA did not have a functionally rescuing effect on whole blood POD1 NK cells when used at a similar concentration as previously reported[197,198]. Given that DCA had a negative impact on IFN-γ production in isolated NK cells with no impact on viability, it is unlikely that increasing the concentration of DCA in whole blood would have changed the result. We also evaluated the corresponding effect of DCA on whole blood NK cell metabolism indirectly by assessing mitochondrial mass and membrane potential ± DCA treatment. We found that DCA did not significantly affect the mitochondrial mass and membrane potential of whole blood POD1 NK cells compared to the vehicle control. In all, we did not see a restorative effect of DCA on function or metabolism in whole blood POD1 NK cells. There are some potential explanations for this result. First, our treatment conditions differed based on what has been previously published. Frisch et al. evaluated the use of DCA to redirect glucose flux in the context of *ex vivo* expansion of both human and murine T cells[197]. When treating the T cells with DCA throughout the duration of expansion, an initial activation period of 24 hours without any DCA treatment was done.

This allowed the cells to undergo an initial upregulation in glycolysis which was found to be necessary for the DCA to exert metabolic and functional benefit to the T cells[197]. There were additional factors such as *in vivo* efficacy and persistence which responded positively to DCA but are not applicable in our context[197,198]. Second, to our knowledge, the effect of DCA has not yet been evaluated in primary human NK cells. It is possible that the rescuing effect of DCA reported in NK92 cells in the context of hepatocellular carcinoma[198] does not translate to primary human NK cells. Finally, given that OxPhos is inherently a major source of ROS, which is known to contribute to NK cell exhaustion[288], the use of DCA likely requires substantial fine-tuning to find the optimal culture conditions which simultaneously boost metabolism and improve effector function without inducing oxidative stress. It is also unclear whether POD1 NK cells are adequately equipped to combat potential oxidative stress. Therefore, future experiments should evaluate the use of DCA treatment in combination with supporting antioxidant defenses, such as through supplementing with glutathione[288], to properly arm the NK cells to deal with harmful byproducts of elevated OxPhos. While we did not observe a rescuing effect of DCA on POD1 NK cells in the culture conditions assessed, we also noted no change in mitochondrial parameters. Therefore, we conclude that this form of metabolic modulation is not effective in rescuing POD1 NK cells. However, we cannot determine whether the concept of boosting OxPhos to rescue function is viable or not from these findings alone. As such, we shifted our focus on other methods, placing an emphasis on prevention of dysfunction rather than functional rescue.

Ex vivo expansion – a promising approach to generate metabolically and functionally resilient NK cells

The process of feeder cell-based *ex vivo* expansion has been widely reported to generate large numbers of highly active NK cells[200,203–205,289]. The *ex vivo* expansion process inherently reprograms NK cells to be resistant to proliferative senescence, and to be highly metabolically active and flexible in their choice of carbon fuel source[171]. We assessed whether *ex vivo* expansion could render healthy NK cells resistant to the immunosuppressive whole blood environment on POD1. To do this, we employed our lab's whole blood *in vitro* co-culture model of surgical stress. We uncovered critical findings regarding the function of exNK cells in the postoperative context. ExNK cells have a very strong level of activity in whole blood compared to the patient's endogenous NK cells, regardless of the perioperative timepoint. While they do exhibit functional suppression in POD1 whole blood compared to BL, the degree to which they are suppressed is less than that of the endogenous NK cells. A significant finding was that the presence of exNK cells augmented the function of endogenous NK cells at BL and partially rescued the function of POD1 NK cells. Because there was functional improvement at both perioperative timepoints, the effect is not surgery specific. It is important to consider that the conditions of this co-culture are static and do not directly represent the dynamic environment that the cells experience in circulation. Given the inherently strong response of the exNK cells to IL-2/12 stimulation, it is possible that they are creating a highly inflammatory environment that is hyperactivating the endogenous NK cells. This may not be representative of what would occur therapeutically, since patients can undergo lymphodepletion prior to allogeneic NK cell therapy[290]. However, we can use these results to infer specific mechanisms that may be driving this functional improvement. Since this was done in whole blood, the strong production of IFN-γ by the exNK cells may be stimulating other cells including macrophages[291] and dendritic cells[292] to produce cytokines, such as IL-12, which are known to trigger IFN-γ production in NK cells. Nonetheless, based

on our data we would expect that no amount of pro-inflammatory cytokine presence would stimulate hyporesponsive POD1 NK cells. As such, this result challenges the hypothesis that the effects of surgical stress on NK cell function are irreversible. Future aims should investigate whether there are corresponding metabolic changes occurring in both the endogenous and exNK cells within the whole blood co-culture assay. One major challenge that remains is how to accurately address this point. One main reason for pursuing SCENITH was to have a method of assessing the effect of POD1 blood on exNK cell metabolism, however we were unable to use this approach for the reasons described earlier. Re-isolating the exNK cells from the whole blood environment for extracellular flux analysis is not logistically feasible and would potentially result in over manipulation of the cells and significant cell loss, thereby not truly reflecting their metabolic state. In summary, determining whether exNK cells are metabolically affected by the postoperative milieu is a complicated endeavour, particularly when attempting to do so using human samples. Consequently, instead of continuing to study the exNK cells solely *in vitro*, we chose to pursue an *in vivo* model to gain a better understanding of their functionality in a therapeutic context.

6.8 Human expanded NK cells show perioperative therapeutic potential *in vivo*

To devise a way of testing the exNK cells *in vivo* we began optimization of a model that closely follows a previously published model using OVCAR8-Luc cells[171,204]. Similar models have been used to test adoptive NK and CAR-T cell-based therapies[197,198,293,294]. Prior to testing the *in vivo* efficacy of our exNK cells, we optimized the model using primary human NK cells derived from surgical cancer patients. Overall, primary NK cells prevented engraftment of OVCAR8-Luc cells compared with the vehicle control. Healthy donor NK

cells exhibited the strongest *in vivo* efficacy compared to BL or POD1 NK cells. Following optimization, we began testing the exNK cells using this model. Although they were successful in preventing engraftment of OVCAR8-Luc cells, a proper donor-matched comparison between unexpanded and expanded NK cells is necessary to determine whether *ex vivo* expansion enhances the *in vivo* efficacy of NK cells in this model. We noted that the difference between the vehicle and exNK cell-treated groups was significant only when the OVCAR8-Luc cells and exNK cells were administered simultaneously, rather than when the OVCAR8-Luc cells were left to establish for 2 days prior to injection of the exNK cells. This suggests that the prevention of engraftment of the OVCAR8-Luc cells is a major determinant of exNK cell *in vivo* efficacy. Notably, the exNK cells were detectable and viable within the peritoneal wash 7 days post-injection, highlighting their *in vivo* persistence. A significant challenge when working on this model was to accurately find a way to incorporate surgical stress. The first step was to confirm whether subjecting the mice to surgical stress could affect the *in vivo* efficacy of unexpanded human NK cells. Unfortunately, we were unable to clearly detect human cells in the peritoneal wash from the surgically stressed cohort 7 days after surgery. Consequently, we could not determine whether differences in tumour burden were caused by dysfunction of the healthy NK cells imparted by surgical stress on the mouse or simply because the NK cells were not retained in the peritoneal cavity. Future iterations of this model should evaluate whether the route of administration (iv versus ip) for both tumour and/or NK cells impacts the localization of the NK cells following surgery. One critical assumption of this model is that murine surgical stress can impart dysfunction on human NK cells. Moreover, this model requires the use of severely immunocompromised NCG mice to permit the establishment of the human OVCAR8-Luc cell line. Therefore, the physiological response to surgical stress does not faithfully depict what occurs in an immunocompetent

mouse, primarily the expansion of suppressive myeloid cells. One option that is being explored to overcome these limitations is the use of a fully humanized mouse model. It has been shown that exNK cells adoptively transferred by iv injection were able to survive and proliferate for 21 days in autologous humanized mice[295]. Our lab has begun preliminary experiments using CD34+ Humanized NSG-FLT3-IL15 mice (The Jackson Laboratory) which contain high levels of human CD3+ T cells, CD33+ myeloid cells, $CD16^{-}/CD56^{dim}$ NK cells and dendritic cells[296]. Initial experiments will evaluate whether exposing these mice to surgical stress has a similar impact on the humanized immune system as what is known to occur in surgical cancer patients. Once this has been established, we will move forward with testing the *in vivo* efficacy of exNK cells in this model. While the development of a fully humanized murine model of surgical stress requires significant optimization, it represents a promising next step in this work.

6.9 Concluding remarks

NK cell effector function and metabolic activity are intricately intertwined. Here we show that human NK cells possess an intrinsic metabolic deficiency that is central to their broad function impairment, which persists long after removal from the postoperative milieu. At the forefront of this phenomenon is a profound inability to perform OxPhos in response to cytokine stimulation. Given the importance in OxPhos in sustaining elevated rates of activity and protecting immune cells from exhaustion, this deficiency in OxPhos could be the key to postoperative NK cell dysfunction. Whether surgical stress imparts a metabolic defect in the NK cells, causing functional impairment, or whether reduced metabolic activity and associated dysfunction is a reactive response to the postoperative environment has yet to be determined. In all, our data defines the metabolic signature of dysfunctional POD1 NK cells,

providing novel metabolic characterization of NK cells within the unique postoperative setting. Given the well-established method of sustaining metabolic activity to fuel effector function, metabolically arming NK cells to remain highly active is a promising approach to the development of an adoptive cell therapy tailored for the postoperative period. Of the metabolic interventions tested here, *ex vivo* expansion was the only approach that partially overcame postoperative suppression, suggesting that comprehensively reprogramming NK cell metabolism before surgery is more effective than attempting to rescue it afterwards. Since surgery is fundamental to offering patients the best chance of cure, this work has the potential to impact the long-term prognoses of cancer patients undergoing surgical resection of their tumour.

References

1. Angka, L. et al. Natural Killer Cell IFNγ Secretion is Profoundly Suppressed Following Colorectal Cancer Surgery. Annals of Surgical Oncology 25, 3747–3754 (2018).
2. Angka, L. et al. A Translational Randomized Trial of Perioperative Arginine Immunonutrition on Natural Killer Cell Function in Colorectal Cancer Surgery Patients. Ann. Surg. Oncol. 29, 7410–7420 (2022).
3. Market, M. et al. Preventing Surgery-Induced NK Cell Dysfunction Using Anti-TGF-β Immunotherapeutics. International Journal of Molecular Sciences 23, 14608 (2022).
4. Angka, L. et al. Perioperative arginine prevents metastases by accelerating natural killer cell recovery after surgery. Molecular Therapy 30, 3270–3283 (2022).
5. Tai, L.-H. et al. Preventing postoperative metastatic disease by inhibiting surgery-induced dysfunction in natural killer cells. Cancer Res 73, 97–107 (2013).
6. Tai, L.-H. et al. Phosphodiesterase-5 inhibition reduces postoperative metastatic disease by targeting surgery-induced myeloid derived suppressor cell-dependent inhibition of Natural Killer cell cytotoxicity. Oncoimmunology 7, e1431082 (2018).
7. Niavarani, S. R. et al. Lipid accumulation impairs natural killer cell cytotoxicity and tumor control in the postoperative period. BMC Cancer 19, 823 (2019).
8. Seth, R. et al. Surgical stress promotes the development of cancer metastases by a coagulation-dependent mechanism involving natural killer cells in a murine model. Annals of Surgery 258, 158–168 (2013).
9. Angka, L. et al. Dysfunctional natural killer cells in the aftermath of cancer surgery. International Journal of Molecular Sciences 18, (2017).
10. Van Der Bij, G. J. et al. The perioperative period is an underutilized window of therapeutic opportunity in patients with colorectal cancer. Annals of Surgery 249, 727–734 (2009).
11. Pollock, R. E., Lotzová, E. & Stanford, S. D. Mechanism of Surgical Stress Impairment of Human Perioperative Natural Killer Cell Cytotoxicity. Archives of Surgery 126, 338–342 (1991).
12. Halsted, W. S. THE RESULTS OF RADICAL OPERATIONS FOR THE CURE OF CARCINOMA OF THE BREAST.*. Annals of Surgery 46, 1 (1907).
13. Demicheli, R., Valagussa, P. & Bonadonna, G. Does surgery modify growth kinetics of breast cancer micrometastases? Br J Cancer 85, 490–492 (2001).
14. van der Bij, G. J. et al. The Perioperative Period is an Underutilized Window of Therapeutic Opportunity in Patients With Colorectal Cancer. Annals of Surgery 249, 727–734 (2009).
15. Coffey, J. et al. Excisional surgery for cancer cure: therapy at a cost. 9.
16. Tohme, S., Simmons, R. L. & Tsung, A. Surgery for Cancer: A Trigger for Metastases. Cancer Res 77, 1548–1552 (2017).

17. Chen, Z. et al. Surgical stress and cancer progression: the twisted tango. Mol. Cancer 18, 132 (2019).
18. Benish, M. & Ben-Eliyahu, S. Surgery as a Double-Edged Sword: A Clinically Feasible Approach to Overcome the Metastasis-Promoting Effects of Surgery by Blunting Stress and Prostaglandin Responses. Cancers 2, 1929–1951 (2010).
19. Yamaguchi, K., Takagi, Y., Aoki, S., Futamura, M. & Saji, S. Significant Detection of Circulating Cancer Cells in the Blood by Reverse Transcriptase–Polymerase Chain Reaction During Colorectal Cancer Resection. Annals of Surgery 232, 58 (2000).
20. Patel, H. et al. Clearance of Circulating Tumor Cells After Excision of Primary Colorectal Cancer. Ann Surg 235, 226–231 (2002).
21. Holmgren, L., O'Reilly, M. S. & Folkman, J. Dormancy of micrometastases: balanced proliferation and apoptosis in the presence of angiogenesis suppression. Nat Med 1, 149–153 (1995).
22. Meng, S. et al. Circulating Tumor Cells in Patients with Breast Cancer Dormancy. Clin Cancer Res 10, 8152–8162 (2004).
23. Haldar, R. et al. Perioperative escape from dormancy of spontaneous micro-metastases: A role for malignant secretion of IL-6, IL-8, and VEGF, through adrenergic and prostaglandin signaling. Brain Behav Immun 109, 175–187 (2023).
24. Decker, D. et al. Abdominal surgical interventions: local and systemic consequences for the immune system--a prospective study on elective gastrointestinal surgery. J Surg Res 126, 12–18 (2005).
25. Castell, J. V. et al. Interleukin-6 is the major regulator of acute phase protein synthesis in adult human hepatocytes. FEBS Letters 242, 237–239 (1989).
26. Gorelik, E. Augmentation of the Antimetastatic Effect of Anticoagulant Drugs by Immunostimulation in Mice. Cancer Res 47, 809–815 (1987).
27. Palumbo, J. S. et al. Platelets and fibrin(ogen) increase metastatic potential by impeding natural killer cell–mediated elimination of tumor cells. Blood 105, 178–185 (2005).
28. Liang, H. et al. Hydroxyethyl starch 200/0.5 decreases circulating tumor cells of colorectal cancer patients and reduces metastatic potential of colon cancer cell line through inhibiting platelets activation. Med Oncol 32, 151 (2015).
29. Park, I.-K., Shultz, L. D., Letterio, J. J. & Gorham, J. D. TGF-β1 Inhibits T-bet Induction by IFN-γ in Murine CD4 + T Cells through the Protein Tyrosine Phosphatase Src Homology Region 2 Domain-Containing Phosphatase-1 . The Journal of Immunology 175, 5666–5674 (2005).
30. Viel, S. et al. TGF-β inhibits the activation and functions of NK cells by repressing the mTOR pathway. Science Signaling 9, (2016).
31. Yang, L. et al. Abrogation of TGFβ Signaling in Mammary Carcinomas Recruits Gr-1+CD11b+ Myeloid Cells that Promote Metastasis. Cancer Cell 13, 23–35 (2008).
32. Zhou, C. et al. A targeted transforming growth factor-beta (TGF-β) blocker (2018).pdf. 9, 23102–23113 (2018).

33. Perrot, C. Y., Javelaud, D. & Mauviel, A. Overlapping activities of TGF-β and Hedgehog signaling in cancer: Therapeutic targets for cancer treatment. Pharmacology and Therapeutics 137, 183–199 (2013).

34. Slattery, K. & Gardiner, C. M. NK Cell Metabolism and TGFβ – Implications for Immunotherapy. Frontiers in Immunology 10, 1–14 (2019).

35. Zaiatz-Bittencourt, V., Finlay, D. K. & Gardiner, C. M. Canonical TGF-β Signaling Pathway Represses Human NK Cell Metabolism. The Journal of Immunology 200, 3934–3941 (2018).

36. Ortaldo, J. R. et al. Mechanistic studies of transforming growth factor-beta inhibition of IL-2-dependent activation of CD3- large granular lymphocyte functions. Regulation of IL-2R beta (p75) signal transduction. Journal of immunology (Baltimore, Md. : 1950) 146, 3791–8 (1991).

37. MALYGIN, A. M., MERI, S. & TIMONEN, T. Regulation of Natural Killer Cell Activity by Transforming Growth Factor-β and Prostaglandin E2. Scandinavian Journal of Immunology 37, 71–76 (1993).

38. Gutierrez, T., Hornigold, R. & Pearce, A. The systemic response to surgery. Surgery (Oxford) 29, 93–96 (2011).

39. Sousa, D. M. et al. Profiling the Adrenergic System in Breast Cancer and the Development of Metastasis. Cancers 14, 5518 (2022).

40. Moretti, S. et al. β-adrenoceptors are upregulated in human melanoma and their activation releases pro-tumorigenic cytokines and metalloproteases in melanoma cell lines. Laboratory Investigation 93, 279–290 (2013).

41. Creed, S. J. et al. β2-adrenoceptor signaling regulates invadopodia formation to enhance tumor cell invasion. Breast Cancer Res 17, 145 (2015).

42. Rosenne, E. et al. In vivo suppression of NK cell cytotoxicity by stress and surgery in F344 rats: Glucocorticoids have a minor role compared to catecholamines and prostaglandins. Brain Behav Immun 37, 207–219 (2014).

43. Thaker, P. H. et al. Chronic stress promotes tumor growth and angiogenesis in a mouse model of ovarian carcinoma. Nat Med 12, 939–944 (2006).

44. Bernabé, D. G., Tamae, A. C., Biasoli, É. R. & Oliveira, S. H. P. Stress hormones increase cell proliferation and regulates interleukin-6 secretion in human oral squamous cell carcinoma cells. Brain, Behavior, and Immunity 25, 574–583 (2011).

45. Roth-Isigkeit, A. K. & Schmucker, P. Postoperative dissociation of blood levels of cortisol and adrenocorticotropin after coronary artery bypass grafting surgery. Steroids 62, 695–699 (1997).

46. Hypothalamic–pituitary–adrenal axis and stress. in Handbook of Clinical Neurology vol. 175 55–64 (Elsevier, 2020).

47. Prete, A. et al. The cortisol stress response induced by surgery: A systematic review and meta-analysis. Clin Endocrinol (Oxf) 89, 554–567 (2018).

48. Liyanarachchi, K., Ross, R. & Debono, M. Human studies on hypothalamo-pituitary-adrenal (HPA) axis. Best Practice & Research Clinical Endocrinology & Metabolism 31, 459–473 (2017).

49. Yeager, M. P. et al. Cortisol antiinflammatory effects are maximal at postoperative plasma concentrations*. Critical Care Medicine 33, 1507 (2005).

50. Cho, Y. M. et al. Dissociation between Plasma Adrenocorticotropin and Serum Cortisol Level during the Early Postoperative Period after Gastrectomy. Hormone Research 53, 246–250 (2000).

51. Judd, A. M. et al. Possible Function of IL-6 and TNF as Intraadrenal Factors in the Regulation of Adrenal Steroid Secretion. Annals of the New York Academy of Sciences 917, 628–637 (2000).

52. Leijte, G. P. et al. Increased Plasma Levels of Danger-Associated Molecular Patterns Are Associated With Immune Suppression and Postoperative Infections in Patients Undergoing Cytoreductive Surgery and Hyperthermic Intraperitoneal Chemotherapy. Front. Immunol. 9, 663 (2018).

53. Peiseler, M. & Kubes, P. Macrophages play an essential role in trauma-induced sterile inflammation and tissue repair. Eur J Trauma Emerg Surg 44, 335–349 (2018).

54. Zindel, J. & Kubes, P. DAMPs, PAMPs, and LAMPs in Immunity and Sterile Inflammation. Annu. Rev. Pathol. 15, 493–518 (2020).

55. McDonald, B. et al. Intravascular Danger Signals Guide Neutrophils to Sites of Sterile Inflammation. Science 330, 362–366 (2010).

56. Rettig, T. C. D. et al. Postoperative Interleukin-6 Level and Early Detection of Complications After Elective Major Abdominal Surgery. Annals of Surgery 263, 1207–1212 (2016).

57. Ziprin, P., Ridgway, P. F., Pfistermüller, K. L. M., Peck, D. H. & Darzi, A. W. ICAM-1 Mediated Tumor-Mesothelial Cell Adhesion is Modulated by IL-6 and TNF-α: A Potential Mechanism by Which Surgical Trauma Increases Peritoneal Metastases. Cell Communication & Adhesion 10, 141–154 (2003).

58. Murdoch, C., Muthana, M., Coffelt, S. B. & Lewis, C. E. The role of myeloid cells in the promotion of tumour angiogenesis. Nat Rev Cancer 8, 618–631 (2008).

59. Kato, M. et al. Elevated plasma levels of interleukin-6, interleukin-8, and granulocyte colony-stimulating factor during and after major abdominal surgery. Journal of Clinical Anesthesia 9, 293–298 (1997).

60. Scheller, J., Chalaris, A., Schmidt-Arras, D. & Rose-John, S. The pro- and anti-inflammatory properties of the cytokine interleukin-6. Biochimica et Biophysica Acta (BBA) - Molecular Cell Research 1813, 878–888 (2011).

61. Benish, M. et al. Perioperative use of beta-blockers and COX-2 inhibitors may improve immune competence and reduce the risk of tumor metastasis. Ann Surg Oncol 15, 2042–2052 (2008).

62. Wang, D. & DuBois, R. N. Eicosanoids and cancer. Nat Rev Cancer 10, 181–193 (2010).

63. Joshi, P. C., Zhou, X., Cuchens, M. & Jones, Q. Prostaglandin E2 suppressed IL-15-mediated human NK cell function through down-regulation of common gamma-chain. J Immunol 166, 885–891 (2001).

64. Torrance, H. D. T. et al. Post-operative immune suppression is mediated via reversible, Interleukin-10 dependent pathways in circulating monocytes following major abdominal surgery. PLOS ONE 13, e0203795 (2018).

65. Alazawi, W., Pirmadjid, N., Lahiri, R. & Bhattacharya, S. Inflammatory and Immune Responses to Surgery and Their Clinical Impact. Annals of Surgery 264, 73–80 (2016).

66. Gentile, L. F. et al. Persistent inflammation and immunosuppression: A common syndrome and new horizon for surgical intensive care. Journal of Trauma and Acute Care Surgery 72, 1491–1501 (2012).

67. Tang, F. et al. Targeting Myeloid-Derived Suppressor Cells for Premetastatic Niche Disruption After Tumor Resection. Ann Surg Oncol 28, 4030–4048 (2021).

68. Market, M., Baxter, K. E., Angka, L., Kennedy, M. A. & Auer, R. C. The potential for cancer immunotherapy in targeting surgery-induced natural killer cell dysfunction. Cancers 11, 1–23 (2019).

69. Ma, X., Wang, M., Yin, T., Zhao, Y. & Wei, X. Myeloid-Derived Suppressor Cells Promote Metastasis in Breast Cancer After the Stress of Operative Removal of the Primary Cancer. Frontiers in Oncology 9, 1–11 (2019).

70. Wang, J. et al. The influence of myeloid-derived suppressor cells on angiogenesis and tumor growth after cancer surgery. International Journal of Cancer 138, 2688–2699 (2016).

71. Wang, J. et al. Surgery-induced monocytic myeloid-derived suppressor cells expand regulatory T cells in lung cancer. Oncotarget 8, 17050–17058 (2017).

72. Ananth, A. A. et al. Surgical stress abrogates pre-existing protective T cell mediated anti-tumor immunity leading to postoperative cancer recurrence. PLoS ONE 11, (2016).

73. Tai, L. H. et al. Preventing postoperative metastatic disease by inhibiting surgery-induced dysfunction in natural killer cells. Cancer Research 73, 97–107 (2013).

74. Li, H., Han, Y., Guo, Q., Zhang, M. & Cao, X. Cancer-Expanded Myeloid-Derived Suppressor Cells Induce Anergy of NK Cells through Membrane-Bound TGF-β1. The Journal of Immunology 182, 240–249 (2009).

75. Cassetta, L. et al. Differential expansion of circulating human MDSC subsets in patients with cancer, infection and inflammation. J Immunother Cancer 8, e001223 (2020).

76. Cassetta, L. et al. Deciphering myeloid-derived suppressor cells: isolation and markers in humans, mice and non-human primates. Cancer Immunol Immunother 68, 687–697 (2019).

77. Gabrilovich, D. I. & Nagaraj, S. Myeloid-derived suppressor cells as regulators of the immune system. Nature Reviews Immunology 9, 162–174 (2009).

78. Cuthbertson, D. P. POST-SHOCK METABOLIC RESPONSE. The Lancet 239, 433–437 (1942).

79. Clark, A., Imran, J., Madni, T. & Wolf, S. E. Nutrition and metabolism in burn patients. Burns & Trauma 5, (2017).

80. Reid, C. L. & Campbell, I. T. Nutritional and metabolic support in trauma, sepsis and critical illness. Current Anaesthesia & Critical Care 15, 336–349 (2004).

81. MacColl, H., Morton, S. & Vasireddy, A. The metabolic response to trauma. Surgery (Oxford) 42, 373–377 (2024).

82. Picard, L. K., Littwitz-Salomon, E., Waldmann, H. & Watzl, C. Inhibition of Glucose Uptake Blocks Proliferation but Not Cytotoxic Activity of NK Cells. Cells 11, 3489 (2022).

83. Market, M., Baxter, K. E., Angka, L., Kennedy, M. A. & Auer, R. C. The Potential for Cancer Immunotherapy in Targeting Surgery-Induced Natural Killer Cell Dysfunction. Cancers (Basel) 11, E2 (2018).

84. Cooper, M. A., Fehniger, T. A. & Caligiuri, M. A. The biology of human natural killer-cell subsets. Trends in Immunology 22, 633–640 (2001).

85. Vivier, E., Tomasello, E., Baratin, M., Walzer, T. & Ugolini, S. Functions of natural killer cells. Nature Immunology 9, 503–510 (2008).

86. Waldhauer, I. & Steinle, A. NK cells and cancer immunosurveillance. Oncogene 27, 5932–5943 (2008).

87. Paust, S., Senman, B. & Von Andrian, U. H. Adaptive immune responses mediated by natural killer cells. Immunological Reviews 235, 286–296 (2010).

88. Liu, H. et al. Role of NKG2D and its ligands in cancer immunotherapy. American journal of cancer research 9, 2064–2078 (2019).

89. Lanier, L. L. NK cell recognition. Annual Review of Immunology 23, 225–274 (2005).

90. Kruse, P. H., Matta, J., Ugolini, S. & Vivier, E. Natural cytotoxicity receptors and their ligands. Immunology & Cell Biology 92, 221–229 (2014).

91. Vivier, E., Nunès, J. A. & Vély, F. Natural Killer Cell Signaling Pathways. Science 306, 1517–1519 (2004).

92. Sivori, S. et al. NKp46 is the major triggering receptor involved in the natural cytotoxicity of fresh or cultured human NK cells. Correlation between surface density of NKp46 and natural cytotoxicity against autologous, allogeneic or xenogeneic target cells. European Journal of Immunology 29, 1656–1666 (1999).

93. Ferlazzo, G. et al. Human Dendritic Cells Activate Resting Natural Killer (NK) Cells and Are Recognized via the NKp30 Receptor by Activated NK Cells. The Journal of Experimental Medicine 195, 343–351 (2002).

94. Hu, X., Chen, J., Wang, L. & Ivashkiv, L. B. Crosstalk among Jak-STAT, Toll-like receptor, and ITAM-dependent pathways in macrophage activation. J Leukoc Biol. 82, 237–243 (2007).

95. Watzl, C. & Long, E. O. Signal Transduction During Activation and Inhibition of Natural Killer Cells. CP in Immunology 90, (2010).

96. Bauer, S. et al. Activation of NK Cells and T Cells by NKG2D, a Receptor for Stress-Inducible MICA. Science 285, 727–729 (1999).

97. Saito, H., Osaki, T. & Ikeguchi, M. Decreased NKG2D expression on NK cells correlates with impaired NK cell function in patients with gastric cancer. Gastric Cancer 15, 27–33 (2012).

98. Zhang, J., Basher, F. & Wu, J. D. NKG2D Ligands in Tumor Immunity: Two Sides of a Coin. Front. Immunol. 6, (2015).

99. Coudert, J. D. et al. Altered NKG2D function in NK cells induced by chronic exposure to NKG2D ligand–expressing tumor cells. Blood 106, 1711–1717 (2005).

100. Horng, T., Bezbradica, J. S. & Medzhitov, R. NKG2D signaling is coupled to the interleukin 15 receptor signaling pathway. Nat Immunol 8, 1345–1352 (2007).

101. Burshtyn, D. N. et al. Recruitment of Tyrosine Phosphatase HCP by the Killer Cell Inhibitory Receptor. Immunity 4, 77–85 (1996).

102. Long, E. O. Negative signaling by inhibitory receptors: the NK cell paradigm. Immunological Reviews 224, 70–84 (2008).

103. Horton, N. C. & Mathew, P. A. NKp44 and Natural Cytotoxicity Receptors as Damage-Associated Molecular Pattern Recognition Receptors. Front. Immunol. 6, (2015).

104. Bhatnagar, N. et al. FcγRIII (CD16)-mediated ADCC by NK cells is regulated by monocytes and FcγRII (CD32). European Journal of Immunology 44, 3368–3379 (2014).

105. Lo Nigro, C. et al. NK-mediated antibody-dependent cell-mediated cytotoxicity in solid tumors: biological evidence and clinical perspectives. Ann Transl Med 7, 105 (2019).

106. Kellner, C. et al. Tumor cell lysis and synergistically enhanced antibody-dependent cell-mediated cytotoxicity by NKG2D engagement with a bispecific immunoligand targeting the HER2 antigen. Biological Chemistry 403, 545–556 (2022).

107. Hsieh, Y.-T. et al. Characterization of FcγRIIIA effector cells used in in vitro ADCC bioassay: Comparison of primary NK cells with engineered NK-92 and Jurkat T cells. Journal of Immunological Methods 441, 56–66 (2017).

108. Benavente, M. C. R. et al. Distinct CD16a features on human NK cells observed by flow cytometry correlate with increased ADCC. Sci Rep 14, 7938 (2024).

109. Lisovsky, I. et al. Differential contribution of education through KIR2DL1, KIR2DL3, and KIR3DL1 to antibody-dependent (AD) NK cell activation and ADCC. J Leukoc Biol. 105, 551–563 (2019).

110. Smyth, M. J. et al. Activation of NK cell cytotoxicity. Molecular Immunology 42, 501–510 (2005).

111. Liu, D. et al. Integrin-Dependent Organization and Bidirectional Vesicular Traffic at Cytotoxic Immune Synapses. Immunity 31, 99–109 (2009).

112. Perez, O. D., Mitchell, D., Jager, G. C. & Nolan, G. P. LFA-1 signaling through p44/42 is coupled to perforin degranulation in CD56+CD8+ natural killer cells. Blood 104, 1083–1093 (2004).

113. Kurowska, M. et al. Terminal transport of lytic granules to the immune synapse is mediated by the kinesin-1/Slp3/Rab27a complex. Blood 119, 3879–3889 (2012).

114. Liu, D., Martina, J. A., Wu, X. S., Hammer III, J. A. & Long, E. O. Two modes of lytic granule fusion during degranulation by natural killer cells. Immunology & Cell Biology 89, 728–738 (2011).

115. Marcet-Palacios, M. et al. Vesicle-associated membrane protein 7 (VAMP-7) is essential for target cell killing in a natural killer cell line. Biochemical and Biophysical Research Communications 366, 617–623 (2008).

116. Takeda, K. et al. Involvement of tumor necrosis factor-related apoptosis-inducing ligand in surveillance of tumor metastasis by liver natural killer cells. Nat Med 7, 94–100 (2001).

117. Smyth, M. J. et al. Tumor Necrosis Factor–Related Apoptosis-Inducing Ligand (Trail) Contributes to Interferon γ–Dependent Natural Killer Cell Protection from Tumor Metastasis. J Exp Med 193, 661–670 (2001).

118. Dickens, L. S. et al. A Death Effector Domain Chain DISC Model Reveals a Crucial Role for Caspase-8 Chain Assembly in Mediating Apoptotic Cell Death. Molecular Cell 47, 291–305 (2012).

119. Mirandola, P. et al. Activated human NK and CD8+ T cells express both TNF-related apoptosis-inducing ligand (TRAIL) and TRAIL receptors but are resistant to TRAIL-mediated cytotoxicity. Blood 104, 2418–2424 (2004).

120. Prager, I. & Watzl, C. Mechanisms of natural killer cell-mediated cellular cytotoxicity. Journal of Leukocyte Biology 105, 1319–1329 (2019).

121. Wajant, H. & Moosmayer, D. Di□erential activation of TRAIL-R1 and -2 by soluble and membrane TRAIL allows selective surface antigen-directed activation of TRAIL-R2 by a soluble TRAIL derivative.

122. Romee, R. et al. Cytokine activation induces human memory-like NK cells. Blood 120, 4751–4760 (2012).

123. Hunter, C. A., Gabriel, K. E., Radzanowski, T., Neyer, L. E. & Remington, J. S. Type I interferons enhance production of IFN-γ by NK cells. Immunology Letters 59, 1–5 (1997).

124. Almutairi, S. M. et al. Interleukin-18 up-regulates amino acid transporters and facilitates amino acid–induced mTORC1 activation in natural killer cells. Journal of Biological Chemistry 294, 4644–4655 (2019).

125. Gotthardt, D., Trifinopoulos, J., Sexl, V. & Putz, E. M. JAK/STAT Cytokine Signaling at the Crossroad of NK Cell Development and Maturation. Front. Immunol. 10, (2019).

126. Stabile, H. et al. JAK / STAT signaling in regulation of innate lymphoid cells: The gods before the guardians. Immunological Reviews 286, 148–159 (2018).

127. Wang, K. S., Frank, D. A. & Ritz, J. Interleukin-2 enhances the response of natural killer cells to interleukin-12 through up-regulation of the interleukin-12 receptor and STAT4. Blood 95, 3183–3190 (2000).

128. Voss, S. D., Sondel, P. M. & Robb, R. J. Characterization of the interleukin 2 receptors (IL-2R) expressed on human natural killer cells activated in vivo by IL-2: association of the p64 IL-2R gamma chain with the IL-2R beta chain in functional intermediate-affinity IL-2R. J Exp Med 176, 531–541 (1992).

129. Eckelhart, E. et al. A novel Ncr1-Cre mouse reveals the essential role of STAT5 for NK-cell survival and development. Blood 117, 1565–1573 (2011).

130. de Jong, J. L., Farner, N. L., Widmer, M. B., Giri, J. G. & Sondel, P. M. Interaction of IL-15 with the shared IL-2 receptor and c subunits. The IL-15// c receptor-ligand complex is less stable than the IL-2// c receptor-ligand complex.

131. Ikeda, H., Old, L. J. & Schreiber, R. D. The roles of IFNγ in protection against tumor development and cancer immunoediting. Cytokine and Growth Factor Reviews 13, 95–109 (2002).

132. Imai, K., Matsuyama, S., Miyake, S., Suga, K. & Nakachi, K. Natural cytotoxic activity of peripheral-blood lymphocytes and cancer incidence: an 11-year follow-up study of a general population. The Lancet 356, 1795–1799 (2000).

133. Tai, L. H. et al. Perioperative influenza vaccination reduces postoperative metastatic disease by reversing surgery-induced dysfunction in natural killer cells. Clinical Cancer Research 19, 5104–5115 (2013).

134. Gardiner, C. M. NK cell metabolism. J Leukoc Biol 105, 1235–1242 (2019).

135. Donnelly, R. P. & Finlay, D. K. Glucose, glycolysis and lymphocyte responses. Molecular Immunology 68, 513–519 (2015).

136. Wang, Z. et al. Glycolysis and Oxidative Phosphorylation Play Critical Roles in Natural Killer Cell Receptor-Mediated Natural Killer Cell Functions. Front. Immunol. 11, (2020).

137. Traba, J., Miozzo, P., Akkaya, B., Pierce, S. K. & Akkaya, M. An Optimized Protocol to Analyze Glycolysis and Mitochondrial Respiration in Lymphocytes. J Vis Exp 54918 (2016) doi:10.3791/54918.

138. Extracellular Flux Analysis to Monitor Glycolytic Rates and Mitochondrial Oxygen Consumption. in Methods in Enzymology vol. 542 125–149 (Academic Press, 2014).

139. Lum, J. J. et al. The transcription factor HIF-1α plays a critical role in the growth factor-dependent regulation of both aerobic and anaerobic glycolysis. Genes Dev. 21, 1037–1049 (2007).

140. Liberti, M. V. & Locasale, J. W. The Warburg Effect: How Does it Benefit Cancer Cells? Trends in Biochemical Sciences 41, 211–218 (2016).

141. Sokolov, S. S., Balakireva, A. V., Markova, O. V. & Severin, F. F. Negative feedback of glycolysis and oxidative phosphorylation: Mechanisms of and reasons for it. Biochemistry Moscow 80, 559–564 (2015).

142. Mookerjee, S. A., Nicholls, D. G. & Brand, M. D. Determining Maximum Glycolytic Capacity Using Extracellular Flux Measurements. PLOS ONE 11, e0152016 (2016).

143. Lu, W. et al. Novel Role of NOX in Supporting Aerobic Glycolysis in Cancer Cells with Mitochondrial Dysfunction and as a Potential Target for Cancer Therapy. PLOS Biology 10, e1001326 (2012).

144. Mookerjee, S. A., Gerencser, A. A., Nicholls, D. G. & Brand, M. D. Quantifying intracellular rates of glycolytic and oxidative ATP production and consumption using extracellular flux measurements. Journal of Biological Chemistry 292, 7189–7207 (2017).

145. Assmann, N. et al. Srebp-controlled glucose metabolism is essential for NK cell functional responses. Nat Immunol 18, 1197–1206 (2017).

146. Littwitz-Salomon, E. et al. Metabolic requirements of NK cells during the acute response against retroviral infection. Nat Commun 12, 5376 (2021).

147. Loftus, R. M. et al. Amino acid-dependent cMyc expression is essential for NK cell metabolic and functional responses in mice. Nat Commun 9, 2341 (2018).

148. Keppel, M. P., Saucier, N., Mah, A. Y., Vogel, T. P. & Cooper, M. A. Activation-Specific Metabolic Requirements for NK Cell IFN-γ Production. J.I. 194, 1954–1962 (2015).

149. Slattery, K. & Gardiner, C. M. NK Cell Metabolism and TGFβ – Implications for Immunotherapy. Front. Immunol. 10, 2915 (2019).

150. Keating, S. E. et al. Metabolic Reprogramming Supports IFN-γ Production by CD56 ^{bright} NK Cells. J.I. 196, 2552–2560 (2016).

151. Donnelly, R. P. et al. mTORC1-Dependent Metabolic Reprogramming Is a Prerequisite for NK Cell Effector Function. J.I. 193, 4477–4484 (2014).

152. Slattery, K. et al. TGFβ drives NK cell metabolic dysfunction in human metastatic breast cancer. J Immunother Cancer 9, e002044 (2021).

153. Viel, S., Besson, L., Marotel, M., Walzer, T. & Marçais, A. Regulation of mTOR metabolic fitness and effector functions by cytokines in natural killer cells. Cancers 9, 1–12 (2017).

154. Thomson, A. W., Turnquist, H. R. & Raimondi, G. Immunoregulatory functions of mTOR inhibition. Nat Rev Immunol 9, 324–337 (2009).

155. Marzec, M. et al. IL-2– and IL-15–induced activation of the rapamycin-sensitive mTORC1 pathway in malignant CD4ƨ T lymphocytes. 111, 9 (2008).

156. Marçais, A. et al. The metabolic checkpoint kinase mTOR is essential for IL-15 signaling during the development and activation of NK cells. Nat Immunol 15, 749–757 (2014).

157. Kobayashi, T. et al. Increased lipid metabolism impairs NK cell function and mediates adaptation to the lymphoma environment. Blood 136, 3004–3017 (2020).

158. Michelet, X. et al. Metabolic reprogramming of natural killer cells in obesity limits antitumor responses. Nat Immunol 19, 1330–1340 (2018).

159. Slattery, K. et al. Uptake of lipids from ascites drives NK cell metabolic dysfunction in ovarian cancer. S c i e n c e Imm u n o l o g y (2025).

160. Scott, K. E. N. & Cleveland, J. L. Lactate Wreaks Havoc on Tumor-Infiltrating T and NK Cells. Cell Metabolism 24, 649–650 (2016).

161. Harmon, C. et al. Lactate-Mediated Acidification of Tumor Microenvironment Induces Apoptosis of Liver-Resident NK Cells in Colorectal Liver Metastasis. Cancer Immunology Research 7, 335–346 (2019).

162. Husain, Z., Huang, Y., Seth, P. & Sukhatme, V. P. Tumor-Derived Lactate Modifies Antitumor Immune Response: Effect on Myeloid-Derived Suppressor Cells and NK Cells. The Journal of Immunology 191, 1486–1495 (2013).

163. Martí I Líndez, A.-A. & Reith, W. Arginine-dependent immune responses. Cell. Mol. Life Sci. 78, 5303–5324 (2021).

164. Costa, B. P. et al. Argininemia and plasma arginine bioavailability – predictive factors of mortality in the severe trauma patients? Nutr Metab (Lond) 13, 60 (2016).

165. Finlay, D. K. et al. PDK1 regulation of mTOR and hypoxia-inducible factor 1 integrate metabolism and migration of CD8+ T cells. J Exp Med 209, 2441–2453 (2012).

166. Ni, J. et al. Single-Cell RNA Sequencing of Tumor-Infiltrating NK Cells Reveals that Inhibition of Transcription Factor HIF-1α Unleashes NK Cell Activity. Immunity 52, 1075-1087.e8 (2020).

167. Lim, S. A. et al. Hypoxia-Driven HIF-1α Activation Reprograms Pre-Activated NK Cells towards Highly Potent Effector Phenotypes via ERK/STAT3 Pathways. Cancers 13, 1904 (2021).

168. Chambers, A. M. & Matosevic, S. Immunometabolic Dysfunction of Natural Killer Cells Mediated by the Hypoxia-CD73 Axis in Solid Tumors. Front. Mol. Biosci. 6, 60 (2019).

169. Li, J. et al. CD39/CD73 upregulation on myeloid-derived suppressor cells via TGF-β-mTOR-HIF-1 signaling in patients with non-small cell lung cancer. OncoImmunology 6, e1320011 (2017).

170. Chambers, A. M. et al. Adenosinergic Signaling Alters Natural Killer Cell Functional Responses. Front. Immunol. 9, 2533 (2018).

171. Poznanski, S. M. et al. Metabolic flexibility determines human NK cell functional fate in the tumor microenvironment. Cell Metabolism 33, 1205-1220.e5 (2021).

172. Traba, J., Waldmann, T. A. & Anton, O. M. Analysis of Human Natural Killer Cell Metabolism. (2021).

173. Nath, S. & Villadsen, J. Oxidative phosphorylation revisited. Biotech & Bioengineering 112, 429–437 (2015).

174. Yoo, I., Ahn, I., Lee, J. & Lee, N. Extracellular flux assay (Seahorse assay): Diverse applications in metabolic research across biological disciplines. Molecules and Cells 47, 100095 (2024).

175. Chacko, B. K. et al. Methods for defining distinct bioenergetic profiles in platelets, lymphocytes, monocytes, and neutrophils, and the oxidative burst from human blood. Laboratory Investigation 93, 690–700 (2013).

176. Yadava, N. & Nicholls, D. G. Spare Respiratory Capacity Rather Than Oxidative Stress Regulates Glutamate Excitotoxicity after Partial Respiratory Inhibition of Mitochondrial Complex I with Rotenone. J. Neurosci. 27, 7310–7317 (2007).

177. Jang, C., Chen, L. & Rabinowitz, J. D. Metabolomics and Isotope Tracing. Cell 173, 822–837 (2018).

178. Floegel, A. et al. Identification of Serum Metabolites Associated With Risk of Type 2 Diabetes Using a Targeted Metabolomic Approach. Diabetes 62, 639–648 (2013).

179. Andrisic, L. et al. Short overview on metabolomics approach to study pathophysiology of oxidative stress in cancer. Redox Biology 14, 47–58 (2018).

180. Zenobi, R. Single-Cell Metabolomics: Analytical and Biological Perspectives. Science 342, 1243259 (2013).

181. Johnson, C. H., Ivanisevic, J. & Siuzdak, G. Metabolomics: beyond biomarkers and towards mechanisms. Nat Rev Mol Cell Biol 17, 451–459 (2016).

182. Huang, Y. et al. Characterizing cancer metabolism from bulk and single-cell RNA-seq data using METAFlux. Nat Commun 14, 4883 (2023).

183. Liu, Y., Beyer, A. & Aebersold, R. On the Dependency of Cellular Protein Levels on mRNA Abundance. Cell 165, 535–550 (2016).

184. Wang, Y. et al. Proteotoxic stress response drives T cell exhaustion and immune evasion. Nature https://doi.org/10.1038/s41586-025-09539-1 (2025) doi:10.1038/s41586-025-09539-1.

185. Ahl, P. J. et al. Met-Flow, a strategy for single-cell metabolic analysis highlights dynamic changes in immune subpopulations. Commun Biol 3, 305 (2020).

186. Argüello, R. J. et al. SCENITH: A Flow Cytometry-Based Method to Functionally Profile Energy Metabolism with Single-Cell Resolution. Cell Metabolism 32, 1063-1075.e7 (2020).

187. Seahorse XF Cell Mito Stress Test Kit User Guide. 20.

188. Seahorse XF Glycolysis Stress Test Kit User Guide. 22.

189. Vrieling, F. et al. In-depth immunometabolic profiling by measuring single-cell protein translation inhibition via bioorthogonal noncanonical amino acid tagging (SCENITH-BONCAT). Preprint at https://doi.org/10.1101/2023.08.03.551800 (2023).

190. Zorova, L. D. et al. Mitochondrial membrane potential. Analytical Biochemistry 552, 50–59 (2018).

191. Zheng, X. et al. Mitochondrial fragmentation limits NK cell-based tumor immunosurveillance. Nat Immunol 20, 1656–1667 (2019).

192. Indo, H. P. et al. Evidence of ROS generation by mitochondria in cells with impaired electron transport chain and mitochondrial DNA damage. Mitochondrion 7, 106–118 (2007).

193. Morita, M. et al. mTOR Controls Mitochondrial Dynamics and Cell Survival via MTFP1. Molecular Cell 67, 922-935.e5 (2017).

194. Terrén, I. et al. IL-12/15/18-induced cell death and mitochondrial dynamics of human NK cells. Front. Immunol. 14, 1211839 (2023).

195. Michelakis, E. D., Webster, L. & Mackey, J. R. Dichloroacetate (DCA) as a potential metabolic-targeting therapy for cancer. Br J Cancer 99, 989–994 (2008).

196. Neuroprotective Effects and Therapeutic Potential of Dichloroacetate: Targeting Metabolic Disorders in Nervous System Diseases. https://www.tandfonline.com/doi/epdf/10.2147/IJN.S439728?needAccess=true doi:10.2147/IJN.S439728.

197. Frisch, A. T. et al. Redirecting glucose flux during in vitro expansion generates epigenetically and metabolically superior T cells for cancer immunotherapy. Cell Metabolism 37, 870-885.e8 (2025).

198. Yang, X. et al. Targeting PDHK1 by DCA to Restore NK Cell Function in Hepatocellular Carcinoma. Molecular Cancer Therapeutics 23, 1731–1742 (2024).

199. Gerbec, Z. J. et al. Conditional Deletion of PGC-1α Results in Energetic and Functional Defects in NK Cells. iScience 23, 101454 (2020).

200. Nham, T. et al. Ex vivo-expanded NK cells from blood and ascites of ovarian cancer patients are cytotoxic against autologous primary ovarian cancer cells. Cancer Immunol Immunother 67, 575–587 (2018).

201. Wang, X. et al. Membrane-bound interleukin-21 and CD137 ligand induce functional human natural killer cells from peripheral blood mononuclear cells through STAT-3 activation. Clinical and Experimental Immunology 172, 104–112 (2013).

202. Zhu, H. et al. Metabolic Reprograming via Deletion of CISH in Human iPSC-Derived NK Cells Promotes In Vivo Persistence and Enhances Anti-tumor Activity. Cell Stem Cell 27, 224-237.e6 (2020).

203. Granzin, M. et al. Highly efficient IL-21 and feeder cell-driven ex vivo expansion of human NK cells with therapeutic activity in a xenograft mouse model of melanoma. OncoImmunology 5, e1219007 (2016).

204. Poznanski, S. M. et al. Expanded CD56 ^{superbright} CD16 $^{+}$ NK Cells from Ovarian Cancer Patients Are Cytotoxic against Autologous Tumor in a Patient-Derived Xenograft Murine Model. Cancer Immunol Res 6, 1174–1185 (2018).

205. Yang, Y. et al. Superior Expansion and Cytotoxicity of Human Primary NK and CAR-NK Cells from Various Sources via Enriched Metabolic Pathways. Molecular Therapy - Methods & Clinical Development 18, 428–445 (2020).

206. Berrien-Elliott, M. M. et al. Systemic IL-15 promotes allogeneic cell rejection in patients treated with natural killer cell adoptive therapy. Blood 139, 1177–1183 (2022).

207. Berrien-Elliott, M. M., Jacobs, M. T. & Fehniger, T. A. Allogeneic natural killer cell therapy. Blood 141, 856–868 (2023).

208. Wang, Z. et al. Augmented anti-tumor activity of NK-92 cells expressing chimeric receptors of TGF-βR II and NKG2D. Cancer Immunol Immunother 66, 537–548 (2017).

209. Foltz, J., Moseman, J., Thakkar, A., Chakravarti, N. & Lee, D. TGFβ Imprinting During Activation Promotes Natural Killer Cell Cytokine Hypersecretion. Cancers 10, 423 (2018).

210. Pereira, M. de S. F., Sezgin, Y., Thakkar, A. & Lee, D. A. Tgfβ-Imprinting Decrease CD38 Expression and Lead to Metabolic Reprogramming on Primary NK Cell. Blood 136, 4 (2020).

211. Ni, J., Miller, M., Stojanovic, A., Garbi, N. & Cerwenka, A. Sustained effector function of IL-12/15/18–preactivated NK cells against established tumors. J Exp Med 209, 2351–2365 (2012).

212. Cooper, M. A. et al. Cytokine-induced memory-like natural killer cells. Proc. Natl. Acad. Sci. U.S.A. 106, 1915–1919 (2009).

213. Sartain, M. & Clara, S. The Agilent Metabolomics Dynamic MRM Database and Method.

214. Mazer, S. & Technologies, A. MassHunter Metabolomics Dynamic MRM Database and Method Method Setup Guide.

215. Angka, L. et al. Preventing surgery-induced natural killer cell suppression and metastases by inhibiting PI3K-gamma signaling in myeloid-derived suppressor cells. J Immunother Cancer 14, e013304 (2026).

216. Lee, D. et al. Improving metabolic flux predictions using absolute gene expression data. BMC Syst Biol 6, 73 (2012).

217. Graudenzi, A. et al. Integration of transcriptomic data and metabolic networks in cancer samples reveals highly significant prognostic power. Journal of Biomedical Informatics 87, 37–49 (2018).

218. Robinson, J. L. et al. An atlas of human metabolism. Sci. Signal. 13, eaaz1482 (2020).

219. Cantor, J. R. et al. Physiologic Medium Rewires Cellular Metabolism and Reveals Uric Acid as an Endogenous Inhibitor of UMP Synthase. Cell 169, 258-272.e17 (2017).

220. Glucose Uptake-Glo™ Assay | Glucose Uptake Assay Kit. https://www.promega.ca/products/energy-metabolism/metabolite-detection-assays/glucose-uptake_glo-assay/.

221. NCG Mouse | Charles River. https://www.criver.com/products-services/find-model/ncg-mouse?region=24.

222. Romee, R. et al. NK cell CD16 surface expression and function is regulated by a disintegrin and metalloprotease-17 (ADAM17). Blood 121, 3599–3608 (2013).

223. Kuylenstierna, C. et al. NKG2D performs two functions in invariant NKT cells: Direct TCR-independent activation of NK-like cytolysis and co-stimulation of activation by CD1d. European Journal of Immunology 41, 1913–1923 (2011).

224. Chovatiya, N. et al. Inability of ovarian cancers to upregulate their MHC-class I surface expression marks their aggressiveness and increased susceptibility to NK cell-mediated cytotoxicity. Cancer Immunology, Immunotherapy 71, 2929–2941 (2022).

225. Tolmachev, V. et al. Optimal specific radioactivity of anti-HER2 Affibody molecules enables discrimination between xenografts with high and low HER2 expression levels. Eur J Nucl Med Mol Imaging 38, 531–539 (2011).

226. The tumor suppressive effect and apoptotic mechanism of TRAIL gene-containing recombinant NDV in TRAIL-resistant colorectal cancer HT-29 cells and TRAIL-nonresistant HCT116 cells, with each cell bearing a mouse model - Jung - 2023 - Cancer Medicine - Wiley Online Library. https://onlinelibrary.wiley.com/doi/full/10.1002/cam4.6622.

227. MitoTracker® Mitochondrion-Selective Probes.

228. Poznanski, S. M., Barra, N. G., Ashkar, A. A. & Schertzer, J. D. Immunometabolism of T cells and NK cells: metabolic control of effector and regulatory function. Inflamm. Res. 67, 813–828 (2018).

229. Subramanian, A. et al. Gene set enrichment analysis: A knowledge-based approach for interpreting genome-wide expression profiles. Proceedings of the National Academy of Sciences 102, 15545–15550 (2005).

230. Cystine–glutamate antiporter xCT deficiency suppresses tumor growth while preserving antitumor immunity. https://www.pnas.org/doi/10.1073/pnas.1814932116 doi:10.1073/pnas.1814932116.

231. 11875 - RPMI 1640 - CA. https://www.thermofisher.com/ca/en/home/technical-resources/media-formulation.114.html.

232. Garcia-Martin, M. O. et al. Modulation of the Antitumor Response to Metformin, Caffeine, and Sodium Dichloroacetate by the Hypoxic Microenvironment in Lung Cancer Cells. International Journal of Molecular Sciences 26, (2025).

233. Belkahla, S. et al. The metabolism of cells regulates their sensitivity to NK cells depending on p53 status. Sci Rep 12, 3234 (2022).

234. Stockwin, L. H. et al. Sodium dichloroacetate selectively targets cells with defects in the mitochondrial ETC. International Journal of Cancer 127, 2510–2519 (2010).

235. Verhezen, T., Wouters, A., Smits, E. & De Waele, J. Powering immunity: mitochondrial dynamics in natural killer cells. Trends in Molecular Medicine S1471491425001066 (2025) doi:10.1016/j.molmed.2025.04.004.

236. Buck, M. D., O'Sullivan, D. & Pearce, E. L. T cell metabolism drives immunity. J Exp Med 212, 1345–1360 (2015).

237. Hatae, R. et al. Enhancing CAR-T cell metabolism to overcome hypoxic conditions in the brain tumor microenvironment. JCI Insight 9, e177141.

238. McPhedran, S. J., Carleton, G. A. & Lum, J. J. Metabolic engineering for optimized CAR-T cell therapy. Nat Metab 6, 396–408 (2024).

239. Hiller, J. G., Perry, N. J., Poulogiannis, G., Riedel, B. & Sloan, E. K. Perioperative events influence cancer recurrence risk after surgery. Nat. Rev. Clin. Oncol. 15, 205–218 (2018).

240. Lagziel, S., Gottlieb, E. & Shlomi, T. Mind your media. Nat Metab 2, 1369–1372 (2020).

241. Krzewski, K., Gil-Krzewska, A., Nguyen, V., Peruzzi, G. & Coligan, J. E. LAMP1/CD107a is required for efficient perforin delivery to lytic granules and NK-cell cytotoxicity. Blood 121, 4672–4683 (2013).

242. Lesteberg, K., Orange, J. & Makedonas, G. Recycling endosomes in human cytotoxic T lymphocytes constitute an auxiliary intracellular trafficking pathway for newly synthesized perforin. Immunol Res 65, 1031–1045 (2017).

243. Makedonas, G. et al. Rapid Up-Regulation and Granule-Independent Transport of Perforin to the Immunological Synapse Define a Novel Mechanism of Antigen-Specific CD8+ T Cell Cytotoxic Activity. The Journal of Immunology 182, 5560–5569 (2009).

244. Smith, S. L. et al. Diversity of peripheral blood human NK cells identified by single-cell RNA sequencing. Blood Adv 4, 1388–1406 (2020).

245. Poli, A. et al. CD56bright natural killer (NK) cells: an important NK cell subset. Immunology 126, 458–465 (2009).

246. Tsukerman, P. et al. Expansion of CD16 positive and negative human NK cells in response to tumor stimulation. European Journal of Immunology 44, 1517–1525 (2014).

247. Grzywacz, B., Kataria, N. & Verneris, M. R. CD56dimCD16+ NK cells downregulate CD16 following target cell induced activation of matrix metalloproteinases. Leukemia 21, 356–359 (2007).

248. Zimmer, J. $CD56^{dim}$ $CD16^{dim}$ Natural Killer (NK) Cells: The Forgotten Population. HemaSphere 4, e348 (2020).

249. Penack, O. et al. CD56dimCD16neg cells are responsible for natural cytotoxicity against tumor targets. Leukemia 19, 835–840 (2005).

250. Tumino, N. et al. The tumor microenvironment drives NK cell metabolic dysfunction leading to impaired antitumor activity. International Journal of Cancer 152, 1698–1706 (2023).

251. Gardiner, C. M. & Finlay, D. K. What Fuels Natural Killers? Metabolism and NK Cell Responses. Front. Immunol. 8, (2017).

252. O'Brien, K. L. & Finlay, D. K. Immunometabolism and natural killer cell responses. Nat Rev Immunol 19, 282–290 (2019).

253. Colijn, C. et al. Interpreting Expression Data with Metabolic Flux Models: Predicting Mycobacterium tuberculosis Mycolic Acid Production. PLOS Computational Biology 5, e1000489 (2009).

254. Rambold, A. S. & Pearce, E. L. Mitochondrial Dynamics at the Interface of Immune Cell Metabolism and Function. Trends in Immunology 39, 6–18 (2018).

255. Zecca, A. et al. Targeting Stress Sensor Kinases in Hepatocellular Carcinoma-Infiltrating Human NK Cells as a Novel Immunotherapeutic Strategy for Liver Cancer. Front. Immunol. 13, 875072 (2022).

256. Ledderose, C. et al. Mitochondria Are Gate-keepers of T Cell Function by Producing the ATP That Drives Purinergic Signaling *. Journal of Biological Chemistry 289, 25936–25945 (2014).

257. Brennan, J. P., Berry, R. G., Baghai, M., Duchen, M. R. & Shattock, M. J. FCCP is cardioprotective at concentrations that cause mitochondrial oxidation without detectable depolarisation. Cardiovasc Res 72, 322–330 (2006).

258. Kwong, C.-T. J. & Kaplan, M. J. Mitochondrial dysfunction in myeloid cells: a central deficit in autoimmune diseases. Trends in Immunology 46, 717–727 (2025).

259. Jheng, H.-F. et al. Mitochondrial Fission Contributes to Mitochondrial Dysfunction and Insulin Resistance in Skeletal Muscle. Molecular and Cellular Biology 32, 309–319 (2012).

260. Sauer, U. Metabolic networks in motion: 13C-based flux analysis. Mol Syst Biol 2, MSB4100109 (2006).

261. Wang, T. et al. Inosine is an alternative carbon source for CD8+-T-cell function under glucose restriction. Nat Metab 2, 635–647 (2020).

262. Klysz, D. D. et al. Inosine induces stemness features in CAR-T cells and enhances potency. Cancer Cell 42, 266-282.e8 (2024).

263. Kanova, M. & Kohout, P. Tryptophan: A Unique Role in the Critically Ill. International Journal of Molecular Sciences 22, 11714 (2021).

264. Ma, K. et al. Itaconic Acid: A Regulator of Immune Responses and Inflammatory Metabolism. CIMB 47, 534 (2025).

265. Bassi, M. et al. Identification and characterisation of human xCT that co-expresses, with 4F2 heavy chain, the amino acid transport activity system xc–. Pflügers Arch - Eur J Physiol 442, 286–296 (2001).

266. Sato, H. et al. Redox Imbalance in Cystine/Glutamate Transporter-deficient Mice *. Journal of Biological Chemistry 280, 37423–37429 (2005).

267. Jensen, H., Potempa, M., Gotthardt, D. & Lanier, L. L. IL-2-induced expression of the amino acid transporters SLC1A5 and CD98 is a prerequisite for NKG2D-mediated activation of human NK cells. J Immunol 199, 1967–1972 (2017).

268. Masson, J. J. R. et al. The Multiparametric Analysis of Mitochondrial Dynamics in T Cells from Cryopreserved Peripheral Blood Mononuclear Cells (PBMCs). in Immunometabolism (ed. Mishra, S.) vol. 2184 215–224 (Springer US, New York, NY, 2020).

269. Luscombe, C., Jones, E., Gregorova, M., Jones, N. & Rivino, L. Impact of cryopreservation on immune cell metabolism as measured by SCENITH. https://dx.doi.org/10.1093/oxfimm/iqae015.

270. Makowski, L., Chaib, M. & Rathmell, J. C. Immunometabolism: From basic mechanisms to translation. Immunological Reviews 295, 5–14 (2020).

271. Wang, Z. et al. Spatial-resolved metabolomics reveals tissue-specific metabolic reprogramming in diabetic nephropathy by using mass spectrometry imaging. Acta Pharmaceutica Sinica B 11, 3665–3677 (2021).

272. Wang, L. et al. Spatially resolved isotope tracing reveals tissue metabolic activity. Nat Methods 19, 223–230 (2022).

273. Fresno, M., Jiménez, A. & Vázquez, D. Inhibition of Translation in Eukaryotic Systems by Harringtonine. European Journal of Biochemistry 72, 323–330 (1977).

274. Terrén, I. et al. Metabolic changes of Interleukin-12/15/18-stimulated human NK cells. Sci Rep 11, 6472 (2021).

275. Krzewski, K. & Coligan, J. E. Human NK cell lytic granules and regulation of their exocytosis. Front. Immun. 3, (2012).

276. Cláudio, N., Dalet, A., Gatti, E. & Pierre, P. Mapping the crossroads of immune activation and cellular stress response pathways. EMBO J 32, 1214–1224 (2013).

277. Moseley, P. Stress proteins and the immune response. Immunopharmacology 48, 299–302 (2000).

278. Marciano, R., Leprivier, G. & Rotblat, B. Puromycin labeling does not allow protein synthesis to be measured in energy-starved cells. Cell Death Dis 9, 39 (2018).

279. Terrén, I., Orrantia, A., Vitallé, J., Zenarruzabeitia, O. & Borrego, F. NK Cell Metabolism and Tumor Microenvironment. Front. Immunol. 10, (2019).

280. Desborough, J. P. The stress response to trauma and surgery. BJA: British Journal of Anaesthesia 85, 109–117 (2000).

281. Duncan, A. E. & Soltesz, E. Role of Intraoperative and Postoperative Blood Glucose Concentrations in Predicting Outcomes after Cardiac Surgery. PERIOPERATIVE MEDICINE 112, (2010).

282. Pribis, J. P., Zhu, X., Vodovotz, Y. & Ochoa, J. B. Systemic Arginine Depletion After a Murine Model of Surgery or Trauma. JPEN J Parenter Enteral Nutr 36, 53–59 (2012).

283. Viggiano, E. et al. Plasma glutamine decreases immediately after surgery and is related to incisiveness. J. Cell. Physiol. 227, 1988–1991 (2012).

284. Whalen, M. M. Inhibition of Human Natural Killer Cell Function in vitro by Glucose Concentrations Seen in Poorly Controlled Diabetes. Cellular Physiology and Biochemistry 7, 53–60 (2008).

285. Aishwarya, R. et al. Pleiotropic effects of mdivi-1 in altering mitochondrial dynamics, respiration, and autophagy in cardiomyocytes. Redox Biology 36, 101660 (2020).

286. Daher, M. et al. Targeting a cytokine checkpoint enhances the fitness of armored cord blood CAR-NK cells. Blood 137, 624–636 (2021).

287. Meng, G. et al. Targeting aerobic glycolysis by dichloroacetate improves Newcastle disease virus-mediated viro-immunotherapy in hepatocellular carcinoma. Br J Cancer 122, 111–120 (2020).

288. Guerra, L. et al. Glutathione is critical for NK cell-mediated immunity. Cell Reports 45, (2026).

289. Jung, D. et al. Ex vivo expanded allogeneic natural killer cells have potent cytolytic activity against cancer cells through different receptor-ligand interactions. J Exp Clin Cancer Res 40, 333 (2021).

290. Geller, M. A. et al. A phase II study of allogeneic natural killer cell therapy to treat patients with recurrent ovarian and breast cancer. Cytotherapy 13, 98–107 (2011).

291. Ma, J. et al. Regulation of macrophage activation. CMLS, Cell. Mol. Life Sci. 60, 2334–2346 (2003).

292. Nakahara, T. et al. Engagement of human monocyte-derived dendritic cells into interleukin (IL)-12 producers by IL-1beta + interferon (IFN)-gamma. Clin Exp Immunol 139, 476–482 (2005).

293. Jo, D.-H. et al. Entinostat, a histone deacetylase inhibitor, enhances CAR-NK cell anti-tumor activity by sustaining CAR expression. Front. Immunol. 16, (2025).

294. Marin, D. et al. Safety, efficacy and determinants of response of allogeneic CD19-specific CAR-NK cells in CD19+ B cell tumors: a phase 1/2 trial. Nat Med 30, 772–784 (2024).

295. Vahedi, F. et al. Ex Vivo Expanded Human NK Cells Survive and Proliferate in Humanized Mice with Autologous Human Immune Cells. Sci Rep 7, 12083 (2017).

296. CD34+ Humanized NSG-FLT3-IL15. https://www.jax.org/jax-mice-and-services/preclinical-research-services/humanized-mice/cd34/nsg-flt3-il15.

Appendix I: Supplementary Data

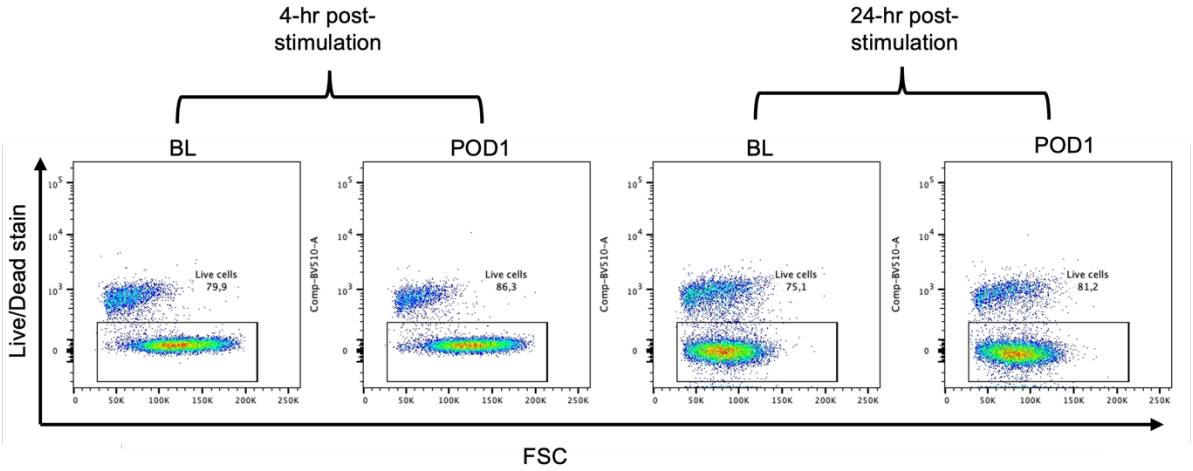

Supplemental Figure 1. Representative flow plots depicting NK cell viability both 4 hours and 24 hours into the IL-2/12 stimulation period.

Appendix I: Supplementary Data

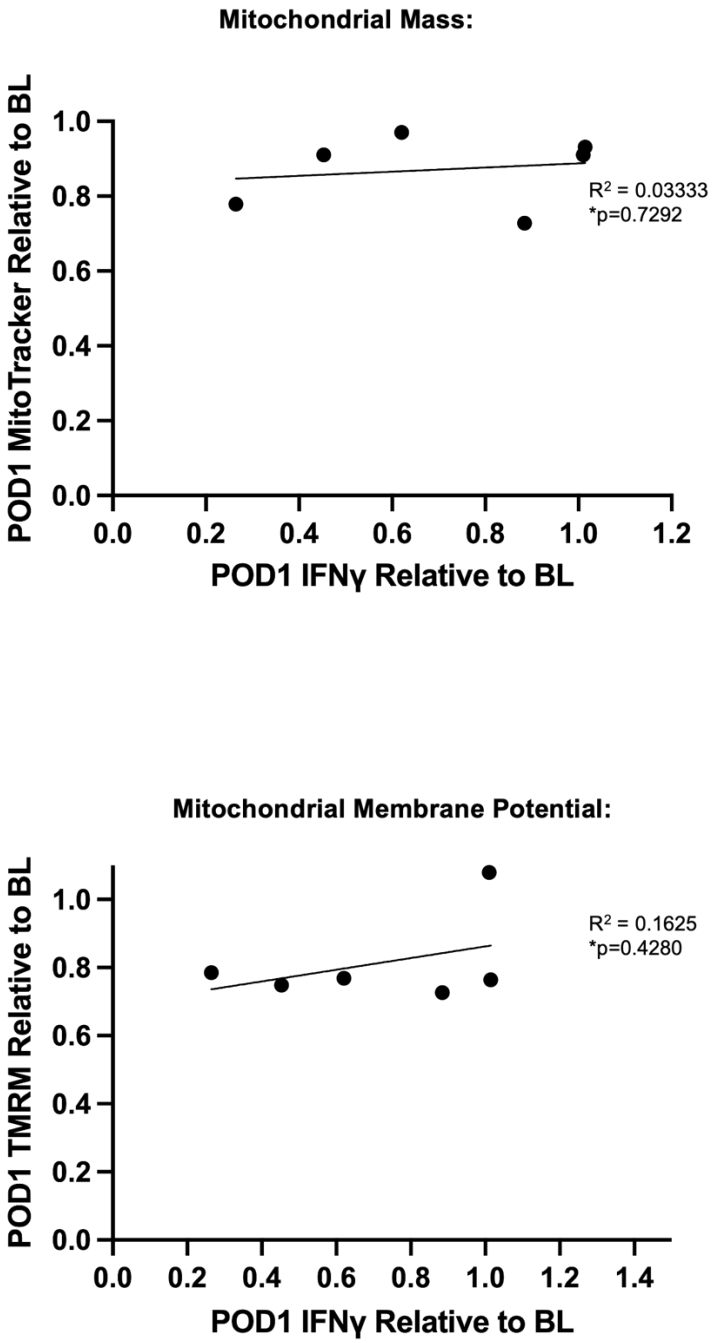

Supplemental Figure 2. There is no correlation between reduction in IFN-γ production and mitochondrial mass or membrane potential in POD1 NK cells.

Appendix I: Supplementary Data

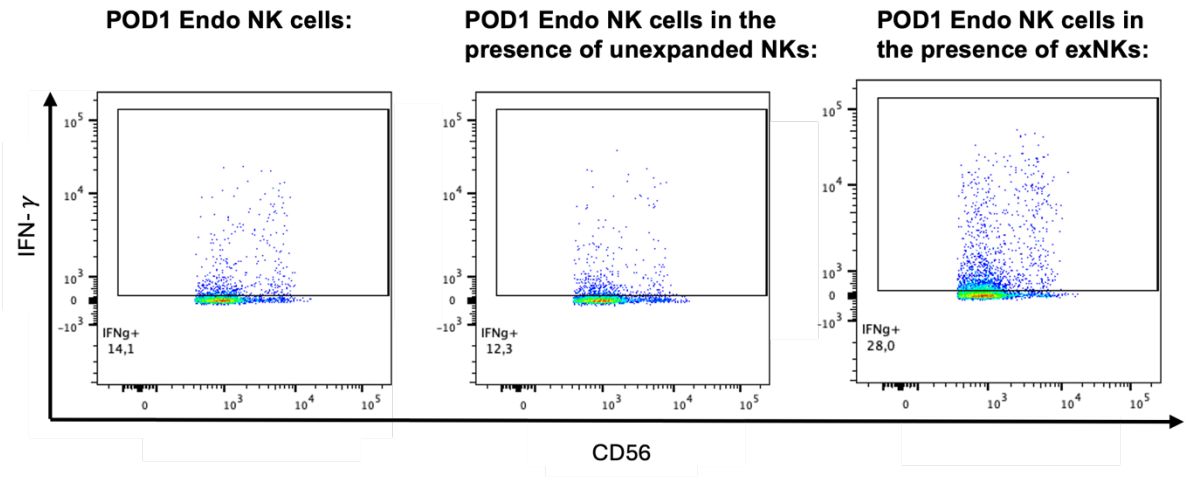

Supplemental Figure 3. The presence of exNK cells, but not unexpanded NK cells from the same donor, improves the function of POD1 NK cells

Appendix I: Supplementary Data

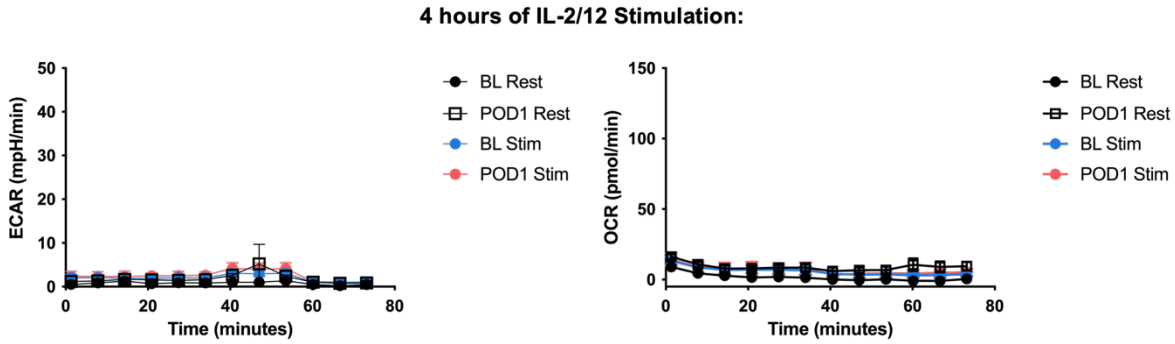

Supplemental Figure 4. Representative ECAR and OCR plots from a glycolytic stress test done following 4 hours of IL-2/12 stimulation. Isolated NK cells have very low levels of metabolic activity after 4 hours of IL-2/12 stimulation.

Appendix I: Supplementary Data

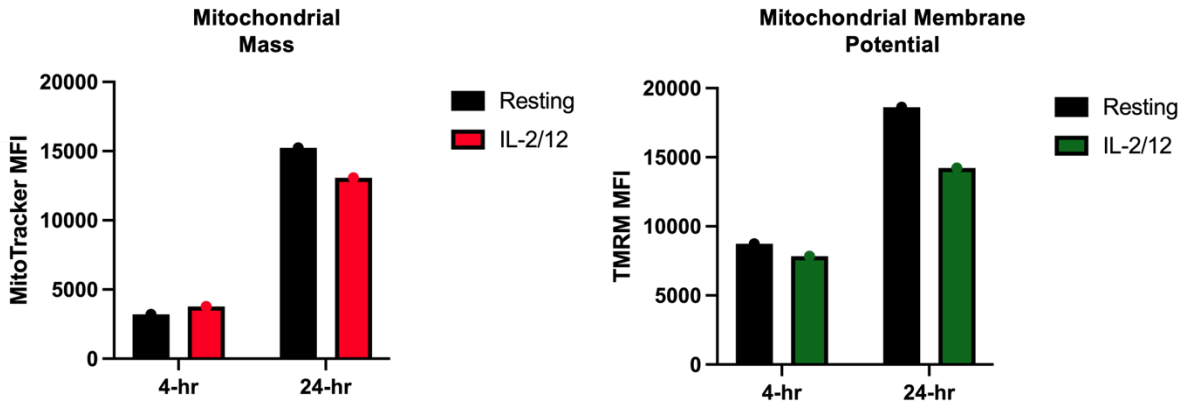

Supplemental Figure 5. Mitochondrial mass and membrane potential increase in healthy resting NK cells overnight in maintenance IL-2.

Appendix I: Supplementary Data

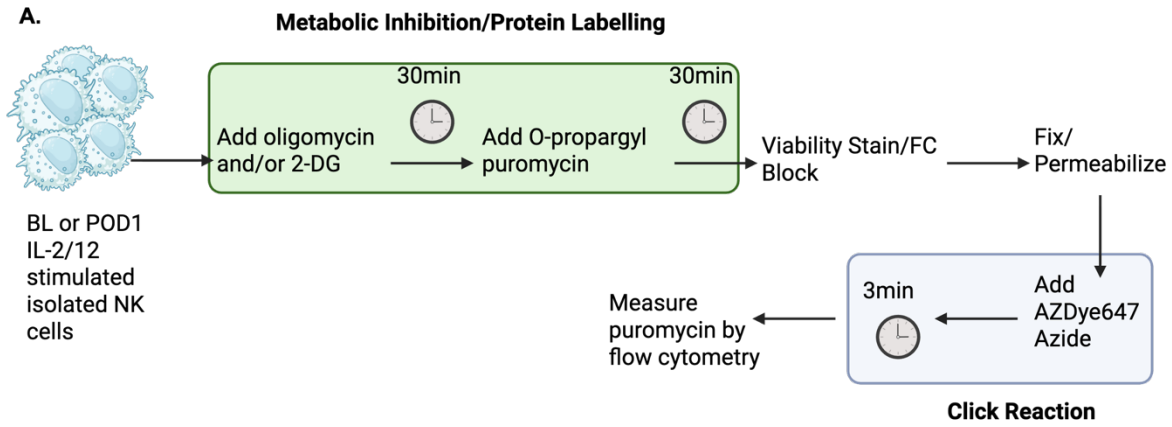

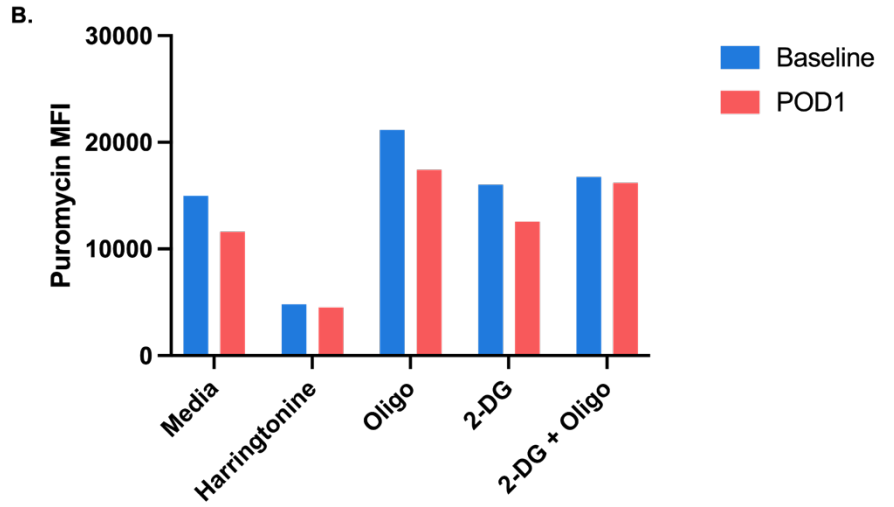

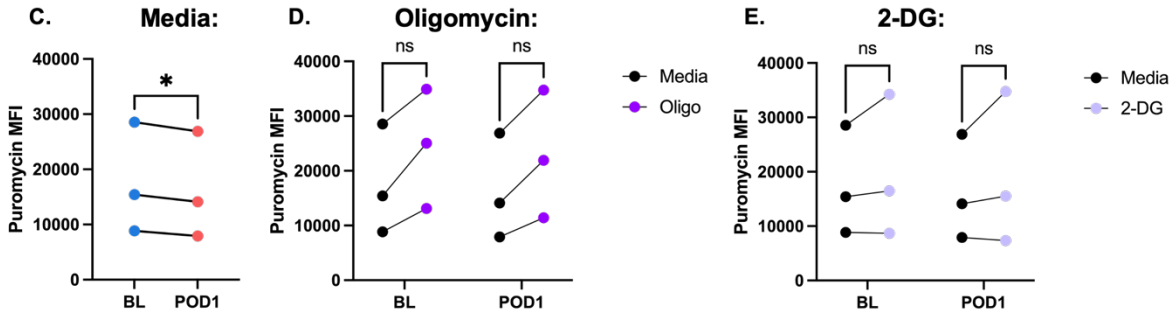

Supplemental Figure 6. SCENITH in isolated NK cells. A/B) Cryopreserved patient-matched BL and POD1 NK cells were thawed, rested for 1 hr, and stimulated for 24 hours with IL-2/12 (400U/mL; 20ng/mL)**.** Following the stimulation, NK cells were treated with either 1uM oligomycin, 100mM 2-DG, a combination of 2-DG and oligomycin (same concentration as the single treatment conditions), 5uM Harringtonine (positive control and inhibitor of translation), or media for 30min. NK cells were then treated with 10uM o-propargyl puromycin (OPP) for 30min, without washing off the inhibitors. Cells were then stained for viability and NK cell markers (CD16 and CD56). Intracellular staining for puromycin was done via click reaction. Briefly, NK cells were fixed and permeabilized prior to incubating with 'click buffer' for 40min at room temperature. Click buffer solution is comprised of 1mM Copper (II) sulfate pentahydrate, 10mM Sodium ascorbate, THPTA, and 2uM AzDye 647 Azide Plus (azide conjugated to Alexa Fluor 647 to allow detection by flow cytometry) in PBS. The translational response of the isolated NK cells following SCENITH was measured by puromycin signal in the **(C)** media, **(D)** oligomycin (1uM) and **(E)** 2-DG (10mM) treatment conditions. Paired two-tailed t-tests. *$p<0.05$, ns: not significant. Normality was confirmed using the Shapiro-Wilk test.

Appendix II: Patient Demographics

Supplemental Table 1. Overview of cancer patient demographics. Combined data (age, sex, cancer type, stage, and blood loss estimates) for all cancer patients included in this study. Data is presented as median with 95% confidence intervals (italicized). Blood loss estimations were not indicated for all patients.

Category	**Total**	**Male**	**Female**
Number of patients	87	58	29
Median Age (years)	66 *(65-68)*	66.5 *(65-68)*	66 *(62-74)*
Median Surgery Length	3h (*3h-3h30min*)	3h7min (*3h-3h45min*)	2h50min (*1hr30min-3hr30min*)
Cancer Type			
Colorectal	17	9	8
Prostate	29	29	-
Renal	8	3	5
Bladder	4	3	1
Gynecologic	5	-	5
Pancreatic	9	7	2
Liver metastasis	6	2	4
Gastric	2	1	1
Soft tissue	4	2	2
Thoracic	2	2	-
Gallbladder	1	-	1
Stage			
T0	4	4	-
T1	13	7	6
T2	26	19	7
T3	29	22	7
T4	13	6	7
Unknown	2	1	1
Median Estimated Blood Loss	150mL (100-250mL) Data from 44 patients	100mL *(100-200mL)* Data from 34 patients	250mL (*100-800mL*) Data from 10 patients

Supplemental Table 2. Overview of healthy donors. Age and sex of the individual healthy donors used in this study.

Healthy Donor #	Age	Sex
1	76	Male
2	70	Female
3	26	Female
4	29	Male

Appendix III: Full list of metabolite hits generated through metabolomics in IL-2/12 isolated BL and POD1 NK cells (n=3).

Metabolite Name	Below threshold?	P value	Mean of Baseline (nM/10^5 cells)	Mean of POD1 (nM/10^5 cells)	Difference	SE of difference	t ratio	df	Adjusted P Value
Adenine	No	0.008834	1.732	1.638	0.09429	0.008921	10.57	2	0.606096
Adenosine	No	0.336248	1.282	0.9322	0.3498	0.2787	1.255	2	>0.999999
Adenosine 3-5-cyclic monophosphate	No	0.206522	3.451	2.154	1.297	0.7035	1.844	2	>0.999999
Adenosine 5-diphosphate	No	0.318098	1009	857.8	151.4	114.9	1.318	2	>0.999999
Adenosine 5-monophosphate	No	0.404357	1826	1539	286.9	273.6	1.049	2	>0.999999
Adenosine 5-triphosphate	No	0.790028	276.5	256.4	20.15	66.34	0.3037	2	>0.999999
Adipic acid	No	0.386	0.4311	0.5069	-0.07578	0.06889	1.1	2	>0.999999
Alanine/Sarcosine	No	0.091027	231.6	205.9	25.62	8.307	3.084	2	0.999946
alpha-Ketoglutaric acid	No	0.493049	1.096	0.8223	0.2738	0.3292	0.8317	2	>0.999999
Aminoadipic acid	No	0.474493	1.898	4.104	-2.206	2.526	0.8735	2	>0.999999
Arginine	No	0.379182	1145	1844	-699.8	624.9	1.12	2	>0.999999
Asparagine	No	0.530447	144.6	187.9	-43.33	57.61	0.7521	2	>0.999999
Aspartic Acid	No	0.535796	758.6	1009	-250.9	338.5	0.7412	2	>0.999999
beta-Hydroxy Butyric acid	No	0.473146	86.97	76.53	10.44	11.91	0.8766	2	>0.999999
Bisphosphoglyceric acid	No	0.324799	4994	3485	1510	1166	1.295	2	>0.999999
Carnosine	No	0.542144	2.278	2.302	-0.02414	0.03315	0.7283	2	>0.999999
Citric acid / Isocitric acid	No	0.847014	266.3	282.8	-16.46	75.21	0.2189	2	>0.999999
Citrulline	No	0.544282	2.018	2.837	-0.8189	1.131	0.724	2	>0.999999
Creatine	No	0.954882	140.9	142.5	-1.553	24.31	0.06387	2	>0.999999
Creatinine	No	0.433044	23.36	39.41	-16.06	16.5	0.9734	2	>0.999999
Cystine	No	0.388823	16.09	44.01	-27.92	25.56	1.092	2	>0.999999
Cytidine	No	0.551304	4.724	3.051	1.672	2.355	0.71	2	>0.999999
Cytidine 5-diphosphate	No	0.896174	60.55	62.13	-1.58	10.7	0.1476	2	>0.999999
Cytidine 5-monophosphate	No	0.948576	16.33	16.51	-0.1813	2.489	0.07282	2	>0.999999
Cytidine 5-triphosphate	No	0.392892	28.14	31.96	-3.811	3.527	1.08	2	>0.999999
Deoxy-ribose	No	0.490688	43.21	41.67	1.542	1.842	0.837	2	>0.999999
Deoxyuridine	No	0.363319	0.2249	1.379	-1.154	0.9887	1.168	2	>0.999999
Dihydroxyacetone phosphate	No	0.142233	63.91	33.35	30.56	12.95	2.36	2	>0.999999
Erythronic acid	No	0.453136	32.38	51.25	-18.88	20.43	0.9237	2	>0.999999
Fructose 1,6-biphosphate	No	0.100599	32.7	23.21	9.488	3.261	2.91	2	0.99998
Gluconic acid	No	0.552481	44.4	35.7	8.703	12.3	0.7077	2	>0.999999
Glucose 6-phosphate	No	0.42167	15.23	8.452	6.779	6.762	1.003	2	>0.999999
Glutamic acid	No	0.889953	10528	10356	172.4	1101	0.1566	2	>0.999999
Glutamine	No	0.42265	6100	9419	-3320	3320	1	2	>0.999999
Glutathione (oxidized)	No	0.462124	230.6	142.6	87.98	97.5	0.9023	2	>0.999999
Glutathione (reduced)	No	0.864165	16.24	13.8	2.44	12.59	0.1939	2	>0.999999
Glyceric acid	No	0.395862	102.6	127.7	-25.19	23.49	1.072	2	>0.999999
Guanine	No	0.877723	2.4	2.085	0.3149	1.807	0.1742	2	>0.999999
Guanosine	No	0.159809	1.595	1.064	0.5308	0.2422	2.191	2	>0.999999
Gutanosine 5-triphosphate	No	0.553127	119.6	101.3	18.37	26	0.7064	2	>0.999999
Hexoses	No	0.364111	14714	30038	-15324	13151	1.165	2	>0.999999
Histidine	No	0.36882	11.6	18.01	-6.404	5.564	1.151	2	>0.999999
Hydroxyglutaric acid	No	0.505316	7.402	9.148	-1.746	2.169	0.805	2	>0.999999
Hypoxanthine	No	0.283734	28268	21790	6478	4463	1.452	2	>0.999999
Inosine	No	0.212801	24.49	13.2	11.29	6.253	1.805	2	>0.999999
Inosine 5-monophosphate	No	0.170237	166.6	118.8	47.81	22.74	2.103	2	>0.999999
Isoleucine	No	0.428386	430.7	814.7	-384	389.7	0.9852	2	>0.999999
Itaconic acid	No	0.390179	4.679	0.2192	4.46	4.098	1.088	2	>0.999999
Kynurenic acid	No	0.436452	0.1474	0.3315	-0.184	0.1908	0.9648	2	>0.999999
Kynurenine	No	0.546328	2.816	4.536	-1.72	2.389	0.7199	2	>0.999999
Lactic acid	No	0.57845	4422	5726	-1304	1983	0.6574	2	>0.999999
Leucine	No	0.410637	777.6	1583	-805	780.3	1.032	2	>0.999999
Malic acid	No	0.805475	53.42	58.61	-5.186	18.49	0.2805	2	>0.999999
Malonic acid	No	0.211302	23.44	24.8	-1.357	0.7477	1.814	2	>0.999999
Methionine	No	0.36047	0	1.957	-1.957	1.664	1.176	2	>0.999999
N-Acetylalanine	No	0.086733	0.4656	0.319	0.1466	0.04624	3.171	2	0.99992
N-Acetylcarnosine	No	0.765164	0.0769	0.108	-0.03109	0.091	0.3417	2	>0.999999
N-Acetylglutamic acid	No	0.153559	1.498	0.9568	0.541	0.2406	2.248	2	>0.999999
N-Acetylneuraminic acid	No	0.789493	56.95	66.3	-9.347	30.69	0.3045	2	>0.999999
N-Acetylserine	No	0.141596	5.018	2.259	2.759	1.166	2.367	2	>0.999999
N-Carbamyl-aspartic acid	No	0.469194	810.5	559.3	251.2	283.6	0.8858	2	>0.999999
N-Carbamyl-glutamic acid	No	0.483283	2.371	1.391	0.9801	1.148	0.8535	2	>0.999999
Nicotinamide adenine dinucleotide	No	0.579061	28.22	29.61	-1.392	2.121	0.6563	2	>0.999999
Nicotinamide riboside	No	0.746254	0.3208	0.2838	0.03701	0.09976	0.371	2	>0.999999
O-hydroxybenzoic acid	No	0.914413	289.4	286.9	2.568	21.14	0.1215	2	>0.999999
O-Phosphorylethanolamine	No	0.365425	6975	6178	797.1	686.5	1.161	2	>0.999999
Orotic acid	No	0.169904	0.7421	0.5013	0.2407	0.1143	2.105	2	>0.999999
Pantothenic acid	No	0.432158	10.4	21.59	-11.19	11.47	0.9756	2	>0.999999
Pentose Alcohol	No	0.344376	6.216	5.701	0.5147	0.4192	1.228	2	>0.999999
Pentoses	No	0.358105	85.63	105.4	-19.73	16.66	1.184	2	>0.999999
Phenylalanine	No	0.411651	110.6	248	-137.4	133.5	1.029	2	>0.999999
Phosphoenolpyruvic acid	No	0.660929	0.5408	0.4392	0.1016	0.1994	0.5097	2	>0.999999
Phosphoglyceric acid	No	0.277423	4.645	2.692	1.953	1.321	1.478	2	>0.999999
Proline	No	0.388896	78.94	125.2	-46.22	42.33	1.092	2	>0.999999
Pyridinedicarboxylic acid	No	0.475066	4.565	0.6992	3.866	4.433	0.8722	2	>0.999999

Appendix III Continued: Full list of metabolite hits generated through metabolomics in IL-2/12 isolated BL and POD1 NK cells (n=3).

Pyridoxal	No	0.643333	0.5801	0.7439	-0.1637	0.3032	0.5399	2	>0.999999
Pyridoxal 5 phosphate	No	0.277348	10.94	7.848	3.096	2.094	1.479	2	>0.999999
Pyridoxine	No	0.408997	4.876	13.04	-8.169	7.885	1.036	2	>0.999999
Pyroglutamic acid	No	0.385871	692.1	1366	-673.9	612.4	1.1	2	>0.999999
Pyruvic acid	No	0.372725	5.228	3.036	2.192	1.924	1.139	2	>0.999999
Quinic acid	No	0.383876	6.985	4.244	2.742	2.478	1.106	2	>0.999999
Ribose 5-phosphate	No	0.344386	8.219	5.332	2.887	2.351	1.228	2	>0.999999
Ribulose 5-phosphate	No	0.42366	8.548	5.354	3.194	3.202	0.9974	2	>0.999999
Serine	No	0.786016	236.7	255.4	-18.72	60.42	0.3098	2	>0.999999
Succinic acid	No	0.401313	163.9	243.5	-79.67	75.37	1.057	2	>0.999999
Taurine	No	0.989313	2854	2860	-5.855	387.4	0.01511	2	>0.999999
Thiamine	No	0.459857	15.21	18.82	-3.607	3.973	0.9077	2	>0.999999
Threonine	No	0.471295	267.3	436.8	-169.5	192.4	0.8809	2	>0.999999
Thymidine	No	0.228058	0.3776	1.382	-1.004	0.5847	1.717	2	>0.999999
Thymine	No	0.634354	0.3354	0.3038	0.03162	0.05691	0.5556	2	>0.999999
trans-4-Hydroxy-proline	No	0.635853	65.91	60.96	4.946	8.945	0.5529	2	>0.999999
Tryptophan	No	0.498623	164.2	390.5	-226.2	276.1	0.8195	2	>0.999999
Tyrosine	No	0.427991	167.2	340.8	-173.5	176	0.9862	2	>0.999999
UDP-Glucose /Galactose	No	0.180283	166.5	132.6	33.93	16.76	2.024	2	>0.999999
UDP-Glucuronic Acid	No	0.341259	3.558	2.912	0.6461	0.5218	1.238	2	>0.999999
Uracil	No	0.647114	11.53	6.99	4.54	8.511	0.5334	2	>0.999999
Uric acid	No	0.461436	81.52	202	-120.5	133.3	0.9039	2	>0.999999
Uridine	No	0.867861	12.04	10.45	1.59	8.432	0.1885	2	>0.999999
Uridine 5-diphosphate	No	0.527212	31.48	26.48	5.005	6.596	0.7588	2	>0.999999
Uridine 5-monophosphate	No	0.671577	90.85	84.01	6.848	13.93	0.4917	2	>0.999999
Uridine 5-triphosphate	No	0.872733	233.3	230.7	2.589	14.27	0.1815	2	>0.999999
Valine(/Betaine)	No	0.416539	501	1030	-529.4	521	1.016	2	>0.999999
Xanthine	No	0.405277	46.79	117.9	-71.13	67.99	1.046	2	>0.999999
Xanthosine	No	0.73424	2.292	2.47	-0.1776	0.4555	0.3899	2	>0.999999
Xylulose-5-phosphate	No	0.734159	2.255	2.524	-0.269	0.6897	0.39	2	>0.999999

Curriculum Vitae

Education

PhD in Microbiology and Immunology Candidate
Ottawa Hospital Research Institute; University of Ottawa, ON
September 2020-Present

- Completing thesis in the lab of Dr. Rebecca Auer, Centre for Innovative Cancer Research, Ottawa Hospital Research Institute
- Permission to write obtained December 2025

Honours Bachelor of Science in Biochemistry with option in Microbiology and Immunology
University of Ottawa, ON
2015-2020

- Completed in April 2020
- Graduated with Summa Cum Laude distinction

Employment

Junior Regulatory Compliance and Enforcement Officer (Co-op) May-Aug. 2019
Health Canada, Ottawa, ON

- Screened a variety of drug establishment license applications submitted to Health Canada by pharmaceutical companies. Responsible for ensuring they were completed in accordance with Health Canada regulations
- Corresponded by email on a regular basis with representatives from pharmaceutical companies to answer their regulatory questions and clarify discrepancies in their applications
- Completed an issue analysis pertaining to licensing cell banks used to produce biologics

Food Safety Research Assistant (Co-op) Sept. -Dec. 2018
Canadian Food Inspection Agency, Ottawa, ON

- Optimized a protocol for the synthesis of gold nanoparticles and conducted colorimetric assays to test the nanoparticles' ability to detect bacteria
- Planned experiments and interpreted data by consulting scientific literature
- Monitored lab freezers and incubators, and maintained experimental documentation for quality assurance purposes

Clinical Research Coordinator (Co-op) Jan. -Aug. 2018
Ottawa Hospital Research Institute, Ottawa, ON

- Completed co-op term in the lab of Dr. Rebecca Auer at the Centre for Innovative Cancer Research
- Obtained informed consent from eligible patients for clinical trials pertaining to novel cancer therapies
- Processed patient blood samples and collected tissue samples from the hospital pathology lab to be stored and used for experiments
- Organized and maintained important study documentation including signed consent forms and correspondence with the local research ethics board

Summer Student Research Assistant May-Aug. 2017
University of Ottawa, ON

- Volunteered as a summer student in the lab of Dr. Natalie Goto with the Faculty of Science

- Studied the impact of a mutation on a particular protein's ability to perform its biological function through a series of biochemical experiments and analyses
- Devised a modified protocol to optimize purification of the mutated protein

Lifeguard/Swim Instructor (pools) Oct. 2015-Jan. 2017
Brewer Pool, City of Ottawa Aquatics Department

- Developed valuable teaching skills by instructing swimming lessons for children ages 3-12 years
- Showed leadership while working with other lifeguards to respond to situations that occur in an aquatic setting

Senior Camp Counsellor June-Aug. 2016
Brewer Pool, City of Ottawa Aquatics Department

- Established leadership skills by managing aquatic activities for children
- Demonstrated responsibility by ensuring that proper care and attention was given to all children, which included those with medical conditions or special needs

Awards and Achievements

1. **Doctoral Admission Scholarship ($45,000)**, 2020-2026. University of Ottawa, ON
2. **Best Poster Presentation Winner 2nd Place ($200)**, OHRI Research Day 2025, Ottawa, ON
3. **Ontario Graduate Scholarship ($15,000)**, 2024-2025. University of Ottawa, ON
4. **Ontario Graduate Scholarship ($15,000)**, 2023-2024. University of Ottawa, ON
5. **Best Poster Presentation Winner 4th Place ($75),** BMI Seminar Day 2024, **University of Ottawa, ON**
6. **Best Poster Presentation Winner 2nd Place ($200)**, OHRI Research Day 2022, Ottawa, ON
7. **Queen Elizabeth II Graduate Scholarship in Science and Technology ($15,000)**, 2021-2022. University of Ottawa, ON
8. **Best Oral Presentation Winner 3rd Place ($75),** BMI Seminar Day 2021, **University of Ottawa, ON**
9. **Canada Graduate Scholarship – Master's ($17,500)**, 2020-2021. University of Ottawa, ON
10. **Faculty Plaque in Biochemistry**-Highest standing in the Honours biochemistry program, 2020. University of Ottawa, ON
11. **Society of Chemical Industry Plaque**-Highest standing in the Honours biochemistry program, 2020. University of Ottawa, ON
12. **Dean's Honour List**, 2015-2020. University of Ottawa, ON
13. **Merit Scholarship ($1,000)**, 2020. University of Ottawa, ON
14. **Renewable Undergraduate Admission Scholarship ($12,000)**, 2015-2020. University of Ottawa, ON

Publications

1. **Scaffidi, Marlena***; Mistry, Henna*; Tanese de Souza, Christiano; Alam, Rafeah; Auer, Rebecca C. (in press). Surgical stress triggers widespread impairment of NK cell cytotoxicity and cytokine release. *Cancer Immunology, Immunotherapy*. Accepted.

2. Market, Marisa; Tennakoon, Gayashan; **Scaffidi, Marlena***; Cook, David; Angka, Leonard; Ng, Juliana; Tanese de Souza, Christiano; Kennedy, Michael A; Vanderhyden, Barbara; Auer, Rebecca C. (2022). Preventing Surgery-induced NK Cell Dysfunction Using Anti-TGFβ Immunotherapeutics. *International Journal of Molecular Sciences*. 23, 14608. Published.

3. Angka, Leonard; Martel, Andre B; Ng, Juliana; Pecarskie, Amanda; Sadiq, Manahil; Jeong, Ahwon; **Scaffidi, Marlena***; Tanese de Souza, Christiano; Kennedy, Michael A; Tadros, Shaheer; Auer, Rebecca C. (2022). A translational randomized trial of perioperative arginine immunonutrition on natural killer cell function in colorectal cancer surgery patients. *Annals of Surgical Oncology.* 29, 7410-7420. Published.

4. Market, Marisa; Tennakoon, Gayashan; Ng, Juliana; **Scaffidi, Marlena***; Tanese de Souza, Christiano; Kennedy, Michael A.; Auer, Rebecca C. (2020). A Method of Assessment of Human Natural Killer Cell Phenotype and Function in Whole Blood. *Frontiers in Immunology*. 11, 963. Published.

Oral and Poster Presentations

1.**Scaffidi M***, Mistry H; Harper M-E; Auer RC. *"The metabolic landscape of dysfunctional natural killer cells following surgical stress."* Ottawa Hospital Research Institute Annual Research Day (November 2025). Oral Presentation.

2.**Scaffidi M***; Mistry H; Tanese de Souza C; Cook D; Poznanski S; Ashkar A; Auer RC. "*Defining natural killer cell metabolism as a mechanism of postoperative dysfunction."* BioCanRx Summit for Cancer Immunotherapy (April 2025). Toronto, ON. Poster Presentation.

3.**Scaffidi M**. "*Characterizing the metabolic profile of natural killer cells in the perioperative period."* uOttawa Faculty of Medicine BMI Seminar Day (February 2025). Ottawa, ON. Oral Presentation.

4.**Scaffidi M***; Mistry H; Cook D; Auer RC. "*Characterizing the metabolic profile of natural killer cells in the perioperative period."* OISB-OHRI Systems Biology Research Half Day (January 2025). Ottawa, ON. Poster Presentation.

5.**Scaffidi M***, Mistry H; Cook D; Angka L; Auer RC. *"Defining the metabolic profile of natural killer cells in the postoperative period."* Canadian Natural Killer Cell Consortium (CanNKC) 2nd Annual Symposium (June 2024). Oral Presentation.

6.**Scaffidi M***. *"Defining the metabolic profile of natural killer cells in the postoperative period."* Ottawa Hospital Research Institute Annual Research Day (November 2023). Oral Presentation.

7. **Scaffidi M***; Mistry H; Tanese de Souza C; Cook D; Poznanski S; Ashkar A; Auer RC. "*Defining natural killer cell metabolism as a mechanism of postoperative dysfunction."* BioCanRx Summit for Cancer Immunotherapy (October 2023). Ottawa, ON. Poster Presentation.

8. **Scaffidi M***; Mistry H; Market M; Tanese de Souza C; Cook D; Ashkar A; Auer RC. *"Defining postoperative natural killer cell metabolism for the development of a novel perioperative adoptive cell therapy."* Canadian Natural Killer Cell Consortium (CanNKC) Inaugural Symposium (May 2023). Hamilton, ON. Poster Presentation.

9. **Scaffidi M***; Market M; Tennakoon G; Angka L; Cook D; Tanese de Souza C; Alam R; Ashkar A; Auer RC. "*Characterizing the relationship between natural killer cell function and metabolism in the postoperative period."* BioCanRx Summit for Cancer Immunotherapy (November 2022). Montreal, QC. Poster Presentation.

10. **Scaffidi M***; Market M; Tennakoon G; Angka L; Cook D; Tanese de Souza C; Alam R; Ashkar A; Auer RC. "*Characterizing the relationship between natural killer cell function and metabolism in the postoperative period."* Canadian Society for Immunology 34th Annual Conference (June 2022). Halifax, NS. Poster Presentation.

11. **Scaffidi M*** and Mistry H. *"Targeting postoperative NK cell dysfunction to prevent metastasis and cancer recurrence."* Canadian Natural Killer Cell Consortium (CanNKC) Seminar (January 2022). Oral Presentation (virtual).

12. **Scaffidi M***; Market M; Haché G; Tennakoon G; Ng J; Kennedy MA; Auer RC.*"Investigating the role of TGFβ signaling in the loss of natural killer cell effector functions following surgical stress"*. General Surgery Research Day (April 2021). Ottawa, ON. Oral Presentation (virtual).

13. Gu F, Liu L, Rogowski J, Duceppe M-O, Karami S, **Scaffidi M***, Chen P, Huang H. *"Colorimetric Identification of Foodborne Pathogen Strains using 'Chemical Nose' Gold Nanoparticles - Proof-of-Concept Study."* Health Canada Science Forum, Shaw Center, Ottawa, ON. January 2019. Poster Presentation.

14. Huang H, Jogowski J, Liu L, Duceppe M-O, Karami S, **Scaffidi M***, Chen P, Gu F. 2019. *"Differentiation and Screening of Foodborne Bacterial Pathogen Strains Using Colorimetric Gold Nanoparticles."* International Association of Food protection Annual Meeting, Kentucky, Louisville, USA, July 2019. Published in J Food Protect, Supplement A, 2019, Vol 82:276, Abstract# P3-89.

Leadership Roles

Member of the CanNKC Symposium Organizing Committee Jan. 2023 – June 2024

- Contributed to planning the logistics of the 1st (2023) and 2nd (2024) annual symposiums
- Participated in applying to funding agencies for financial support
- Contacted potential keynote speakers

Doors Open Ottawa June 1, 2024

- Participated in giving tours of the lab to members of the public interested in learning about cancer research

Café Scientifique Feb. 4, 2024

- Assisted in organizing the first Café Scientifique conducted by the OHRI Cancer Research Program, aimed at informing cancer patients and their families about the research being done there
- Participated in giving tours of the lab to attendees

Member of the OHRI Cancer Research Program Student Committee Sept. 2022-Aug. 2024

- Assisted in planning social events for students in the cancer therapeutics program
- Addressed issues/concerns within the student community

DEGREE Shadowing Program Mentor June 2022

- Introduced the graduate student experience to an undergraduate student via shadowing in the lab for 3 days during the summer
- Demonstrated various lab techniques, and answered specific questions regarding my project and graduate school in general

Member of the BMI Graduate Student Association Sept. 2020-June 2021

- Elected for the Secretary position
- Responsible for recording notes during bi-weekly meetings and attending the Cellular and Molecular Medicine Student Association meetings to ensure communication between councils
- Organized virtual social events for graduate students within the biochemistry and microbiology and immunology programs

Mentor for 4th Year Honours Student Sept. 2020-Apr. 2021 and Sept. 2023 – Apr. 2024

- Provided training to the student on all relevant laboratory techniques and expectations regarding documentation of data
- Guided the student throughout their project by assisting in planning and completing experiments, data analysis, and thesis editing

Volunteer Experience

Let's Talk Science Outreach Sept. 2022-Apr. 2024
University of Ottawa, ON

- Facilitated scientific activities with elementary school children as a way of making STEM more accessible to students

In From the Cold Ministry Nov. 2018-Mar. 2019
Parkdale United Church, Ottawa, ON

- Prepared sandwiches and bread baskets for a monthly meal served to people in need by the Parkdale United Church

Swimming with a Mission Sept. 2018-Mar. 2020
Lowertown Pool, Ottawa, ON

- Taught individual swimming lessons to children with special needs once per week

Cashier at Italian Community Festival May 2017 and 2018
Madonna della Risurrezione Parish, Ottawa, ON

- Sold tickets and food items at the annual Italian community festival
- Monitored cash register